PDMS-based Antimicrobial Surfaces for Healthcare Applications

This thesis is presented to UCL in partial fulfilment of the requirements for the Degree of Doctor of Philosophy

Ekrem Ozkan

Supervised by

Professor Ivan P. Parkin

Materials Chemistry Research Centre

Dr Elaine Allan

Division of Microbial Diseases

2017

DECLARATION

I, Ekrem Ozkan confirm that the work presented in this thesis is my own. Where information has been derived from other sources, I confirm that this has been indicated in the thesis.

ABSTRACT

This thesis describes two types of approaches for reducing the incidence of hospital-acquired infections (HAIs), which are chemical approaches that inactivate bacteria that adhere to the surface i.e. bactericidal activity and physical approaches that inhibit initial bacterial attachment to the surface i.e. anti-biofouling activity. Specifically, the antimicrobial polydimethylsiloxane (PDMS)-based systems detailed in this thesis are: (i) photosensitizer, crystal violet (CV),-coated PDMS for both medical device and hospital touch surface applications, (ii) crystal violet-coated, zinc oxide nanoparticle-encapsulated PDMS for hospital touch surface applications, (iii) superhydrophobic antibacterial copper coated PDMS films *via* aerosol assisted chemical vapour deposition (AACVD) for hospital touch surface applications and (iv) slippery copper-coated PDMS films to prevent biofilm formation on medical devices.

The materials were characterized using techniques including: X-ray diffraction (XRD), scanning electron microscopy (SEM), UV-vis absorbance spectroscopy, water-contact angle measurement and microbiology tests. Functional testing indicated that CV-coated samples were suitable for targeted applications and showed potent light-activated antimicrobial activity when tested against model Gram-positive bacteria, *Staphylococcus aureus*, and Gram-negative bacteria, *Escherichia coli*, associated with hospital-acquired infections, with > 4 log reduction in viable bacterial numbers observed. On the other hand, CVD modified samples demonstrated highly significant antibacterial activity against both bacteria (> 4 log reduction in bacterial numbers) under dark conditions. Moreover, they resulted in a significant reduction in bacterial cell adhesion compared to PDMS and glass controls. However, superhydrophobic materials accumulated biofilm of both bacteria over a 2-day period while slippery materials significantly prevented biofilm formation over the same period. The novel and highly efficacious antibacterial materials reported in this thesis show a very strong potential to be utilized in hospital environments for reducing the incidence of HAIs.

ACKNOWLEDGEMENTS

First and foremost, I would like to start by thanking Prof Ivan Parkin, my first supervisor for giving the opportunity to work with you. Thank you for being not only an excellent supervisor but also great supporter for every struggle in our lives. Thank you for your valuable suggestions, for reading and correcting my manuscripts, and for all the interesting conversations. Thank you for the guidance and advice, both on the project and dissertation.

I would also like to thank Dr. Elaine Allan, my second supervisor, for teaching and helping me patiently everything about my project, for all advices, your support and criticism. Thank you for the interesting discussions and that I could always knock on your door and get almost instant help with solving my problems.

I would also like to extend my thanks to Dr. Steve Firth, who was easy to turn to when I had trouble using SEM. I am also very grateful to people in 308 and 320 who helped me whenever I need them. Thank you for your support and assistant throughout this project period.

I would like to express my gratitude to my dear parents, sister and twin who were always encouraging me especially my mother who took care of us during our hard times.

Finally, I would like to thank my dear wife, Feyza, and my little girl, Eslem Sema who brought joy to my soul. Thank you for always supporting me with your love and sharing my joys and miseries during my programme. This research would not be possible without their love. I love you.

PUBLICATIONS

List of publications associated with this thesis:

1. OZKAN, E., Parkin, I. P. & Allan, E. The antibacterial properties of light-activated polydimethylsiloxane containing crystal violet. *RSC Adv.* (2014). doi:10.1039/C4RA08503E

2. OZKAN, E., Tunali Ozkan, F., Allan, E. & Parkin, I. P. The use of zinc oxide nanoparticles to enhance the antibacterial properties of light-activated polydimethylsiloxane containing crystal violet. *RSC Adv.* (2014). doi:10.1039/C4RA13649G

3. OZKAN, E., Crick, C. C., Taylor, A., Allan, E. & Parkin, I. P. Copper-based water repellent and antibacterial coatings by aerosol assisted chemical vapour deposition. *Chem. Sci.* **7,** 5126–5131 (2016).

4. OZKAN, E., Parkin, I.P. & Allan, E. Extremely durable biofouling-resistant surfaces based on Cu/PDMS composites. (Manuscript in preparation).

CONTENTS

LIST OF FIGURES AND TABLES

Chapter 3 – Synergetic Combination of Zinc Nanoparticle with Crystal Violet as a White-light Activated Antibacterial Paint		

LIST OF ABBREVIATIONS

Aerosol assisted chemical vapour deposition	AACVD
Atomic force microscopy	AFM
Brain-Heart-Infusion	BHI
Contact angle	CA
Centers for Disease Control and Prevention	CDC
Chemical vapour deposition	CVD
Escherichia coli	E. coli
Hospital-acquired infection	HAI
MacConkey agar	MAC
Methicillin resistant-*Staphylococcus aureus*	MRSA
Mannitol salt agar	MSA
Phosphate buffer saline	PBS
Photodynamic therapy	PDT
Reactive oxygen species	ROS
Singlet oxygen	$^1O_2$
Sliding angle	SA
Slippery liquid-infused porous surfaces	SLIPS
Transmission electron microscope	TEM
Ultraviolet-visible	UV-vis
X-ray diffraction	XRD

Chapter 1: HOSPITAL-ACQUIRED INFECTIONS AND STRATEGIES FOR THEIR CONTROL

1.1: An Introduction to Hospital-Acquired Infections

Hospital-acquired infections (HAIs), also known as nosocomial infections, are defined by The United Kingdom (UK) Department of Health (DoH) as "any infection by any infectious agent acquired as a consequence of a person's treatment by the UK National Health Service (NHS) or which is acquired by a health care worker in the course of their NHS duties".[1] They are among the most frequent adverse events in hospitalized patients, affecting healthcare systems worldwide[2]. Since 1980, the incidence of HAIs has been increasing dramatically especially because of the emergence and worldwide spread of multidrug-resistant bacteria resulting from the over and mis-use of antibiotics.[3] Dealing with the control, prevention and successful treatment of these infections within healthcare institutions is an ongoing problem.

HAIs are a leading cause of patient morbidity and mortality, striking between 7-10% of all patients in developed and developing countries. In European countries, more than 4 million patients are affected each year by approximately 4.5 million episodes of HAIs with an average prevalence of 7.1, leading to 16 million extra-days of hospital stay, at least 37 000 attributable deaths. The estimated annual incidence rate of HAIs in the US is 4.5% with approximately 1.7 million affected patients, causing approximately 99 000 deaths. In high-income countries, the prevalence rate of HAIs varies between 5% and 15%, whereas approximately 15-19% of patients are affected by at least one HAI in low-and middle countries. Additionally, annual financial losses due to HAIs are significant, accounting for about € 7 billion in Europe and about $ 6.5 billion in the US.[4]

1.2: Antimicrobial resistance

Antimicrobial agents were developed to combat bacterial infections *ca.* 70 years ago.[5] However, the widespread use of antibiotics to manage and treat bacterial infections have led to the emergence of bacteria that are resistant to antibiotics.[5,6] Antibiotic resistance is the resistance of a microorganism to a certain antibiotic drug that was originally effective to treat the infections resulting from it.[7] The rise of antimicrobial resistance is associated with the inappropriate use of antibiotics (e.g. for viral infections), non-compliance in patients and widespread antibiotic use in animal husbandry.[8] The first major problem in treating infectious diseases with antibiotics was the emergence of vancomycin-resistant *Enterococcus* (VRE) that possess intrinsic resistance to several frequently utilized antibiotics and an ability of acquiring resistance to all currently available antibiotics.[9] Also, more than of 40% of *Staphylococcus aureus* strains collected from hospitals were found to be resistant to the antibiotic methicillin.[10]

As new resistance mechanisms emerge and spread globally, standard methods become ineffective to treat common infectious diseases, leading to prolonged illness, higher health care expenditures and a greater risk of death.[11] According to The Centers for Disease Control and Prevention (CDC, 2013), nearly 2 million patients were affected by antibiotic resistant infections, causing more than 23 000 deaths in the U.S alone. Also, antibiotic-resistant infections cost the U.S healthcare system over \$20 billion per year.[12,13] Consequently, there is an urgent need for a realistic alternative to the prescription antibiotics as well as strategies to prevent HAIs.

1.3: Role of The Environment in the transmission of HAIs

The Centers for Disease Control and Prevention (CDC) has listed contact transmission, direct from body to surface or indirectly through contaminated inanimate objects, as one of the main modes of transmission of microorganisms.[14] [15] Hand hygiene plays a crucial role in preventing the spread of microorganisms[16,17] and it is recommended by the World Health Organization[18] that hands should be cleaned before and after touching a patient and the environmental sites close to the patient (e.g. bed rails) as evidence demonstrates that

such sites can be heavily contaminated with bacteria or bacterial spores.[19–23] In 2004, the NHS National Patient Safety Agency implemented the "clean your hands" campaign to improve healthcare worker hand hygiene to reduce the incidence of HAIs. However, compliance levels among healthcare works are generally poor. In fact, 34 different studies have reported that the average level of compliance with the CDC guidelines among healthcare workers was 40%. Therefore, such low hand hygiene compliance can increase the probability of environmental contamination *via* healthcare workers.[24]

The environment has also been demonstrated to play a crucial role in the spread of infection within a healthcare facility. There is mounting evidence showing a link between poor environmental hygiene and the spread of microorganisms leading to HAIs.[24] The role of the environment in the spread of HAIs is demonstrated in **Fig. 1.1**.
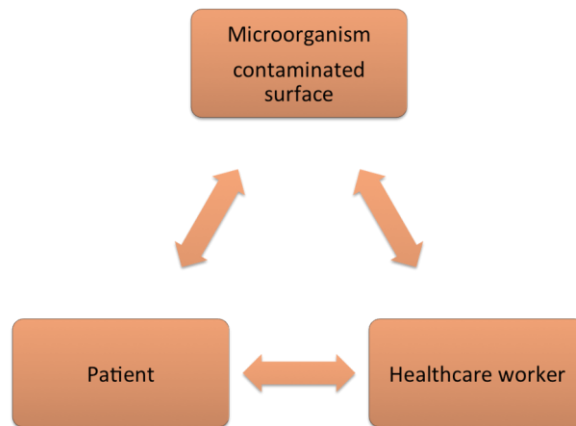
Fig. 1.1 The role of surfaces in the transmission of bacteria.

Infectious microorganisms can be transferred from patient to patient via contact with inanimate surfaces.[25] The most frequently contaminated surfaces are floors, doorknobs, television remote control devices, bed-frame lockers, mattresses, bedside tablets and toilet seats in rooms previously occupied by a colonized or infected patient.[26–29] Moreover, medical devices (e.g. stethoscopes and otoscopes) and different plastic items (e.g. pagers and cell phones) in the hospital are highly prone to bacterial contamination and can serve as reservoirs of nosocomial pathogens and vectors for cross-transmission.[30,31] An estimated 20-40% of HAIs are because of cross-infection by the hands of healthcare staff in contact

with patients or by touching contaminated surfaces. The characteristics and symptoms of some clinically-relevant infections are summarized in **Table 1.1**.

Table 1.1 Examples of organisms causing nosocomial infections.

Organism	Transmission	Symptoms
S. aureus	Contact with a purulent lesion or carrier, unsanitary conditions, overcrowding	Skin, blood, respiratory tract infection, septicaemia and death
Clostridium difficile	Extensive contamination in the environment	Diarrhoea and colitis
Escherichia coli	Person-to-person transmission and ingestion of contaminated food/water	Blood and urinary tract infection
Norovirus	Faecal contaminated vehicle (food or water) and person-to-person transmission	Abdominal pain, nausea, vomiting, headache and chills
Pseudomonas aeruginosa	Contamination from tap water, hospital sinks and different medical devices	Lung and urinary tract infection

1.3.1: Microorganisms commonly responsible for HAIs

Inanimate surfaces are potential reservoirs of pathogenic microbes correlating with the incidence of nosocomial infection. Several important microorganisms, including *Clostridium difficile (C. difficile)*, *Escherichia coli (E.coli)*, methicillin-resistant *Staphylococcus aureus* (MRSA), vancomycin-resistant enterococci (VRE), and *Pseudomonas aeruginosa*, may survive on inanimate surfaces for extended periods of time and can therefore be a source of transmission if no regular preventive surface disinfection is carried out.

Inconsistent results of bacterial survival on dry inanimate surfaces are reported (**Table 1.2**). Overall, Gram-negative species have been demonstrated to survive longer compared to Gram-positive species. Large differences in survival times can be attributed to not only types of species and strains but also variations in experimental conditions such as inoculum size, humidity, the suspending medium, and the surface material (i.e. a longer persistence of bacteria on plastic or steel relative to glass).[32] In addition, environmental factors such as increased humidity (> 70%) and lower temperatures (4-6 ˚C) can improve persistence of bacteria, viruses and fungi.[32]

Table 1.2 Length of survival of common hospital-related pathogens on surfaces and associated infectious dose, where known.[32,33]

Organism	Infectious Dose (If known)	Length of Survival on Surfaces
Staphylococcus aureus	<15CFU/10^6 (oral dose)	7 days - >1 year
Clostridium difficile	1CFU (in mouse models)[34]	5 months
Klebsiella spp.	No experimental evidence	<1 hour – 30 months
E. coli	10 CFU[35]	<1 hour – 16 months
Acinetobacter spp.	No experimental evidence	3 days – 5 months
Pseudomonas aeruginosa	10^8 (oral dose)	6 hours – 16 months

What is important for determining the risk of a patient contracting or spreading a HAI infection is that the longer a nosocomial pathogen can persist on a surface the longer it may be a source of transmission, and therefore endangering a susceptible patient or a healthcare worker.[36,37]

1.4: Common pathogens

1.4.1: Methicillin-resistant *Staphylococcus aureus* (MRSA)

MRSA is resistant to multiple beta-lactam antibiotics including methicillin, penicillin, oxacillin and amoxicillin. It was primarily identified as a nosocomial infection in the US in the late 1960s among older and sicker patients contaminated by healthcare workers.[38]

MRSA is usually transmitted from patient to patient *via* the hands of health-care workers (HCW), but persistence of the pathogen in the environment may also play a role.[39] Thus, MRSA can contaminate the near patient environment including the floor, bedframe, and the patient locker.[40]

MRSA infections are a major cause of morbidity, mortality and cost among inpatients. The incidence has significantly increased twofold to threefold since the late 2000s worldwide.[41] The rate of MRSA infections within the US increased from 46.3/1000 inpatients in 2006 to 66.4/1000 inpatients in 2010, and in the EU there were around 170 000 patients infected by MRSA each year.[42,43]

Legislation and national infection control interventions were put into practice in England in order to reduce rates of MRSA-related infections within hospitals. This has resulted in a decrease in rates of such infections by 85% between April 2003 and March 2011.[44] Whether *S. aureus* is sensitive or resistant, its transmission is clonal and in recent years there has been an increase in the incidence of both sensitive- and resistant S. aureus infections causing skin and soft issue infections.[45]

1.4.2: *Escherichia coli (E. coli)*

E. coli is a Gram-negative, rod shaped bacterium that is commonly found in the intestines of people and animals and is a major constituent of a healthy human intestinal tract.[46] However, it causes problems when entering our bloodstreams or tissues within the body, resulting in up to 40% of septicaemia and 75% meningitis cases.[47] It grows in moist hospital environments and can also be found in solutions, humidifiers, endotracheal tubes, medical

devices and equipment.[46] *E. coli* is the major cause of bloody diarrhea.[48] Additionally, it is responsible for 90% of UTIs[49] and haemolytic uremic syndrome in some people (in particular children under age 5) that destruct red blood cells and results in kidney failure.[50]

Recent studies demonstrated that the incidence of drug-resistant *E. coli* infections in the U.S. doubled from 5.28 incidents per 100,000 patients to 10.5 infections per 100,000 between 2009 and 2014.[51] Also, *E. coli* is the major cause of bacteraemia in the UK. According to Public Health England (PHE) rate of bloodstream infections due to *E.coli* increased by 15.6% from 2010 to 2014.[52]

1.5: Antibacterial surfaces

Regular cleaning of hospital surfaces to control infections caused by pathogenic microorganisms will not guarantee complete elimination. In this context, there are some high-tech approaches gaining attention to develop "self-sterilizing" or "self-sanitising" antibacterial surfaces that were first proposed in 1964 but were not considered as effective controls to minimize the spread of pathogens until years later.[53]

Various reasons may cause surface contamination in a typical healthcare environment. In particular, it may be because of direct transfer through touching from an infected or colonized patient, or from a member of healthcare staff who is carrying the pathogenic microbe on their hands. When a surface has become contaminated, a cyclical problem occurs because this contamination can now be transferred to other surfaces and patients in the vicinity. While appropriate hand washing by healthcare staff can inhibit the further spread of pathogens through hand-surface transmission,[54] it cannot eliminate the surface contamination itself as well as the potential direct transmission by the patient and thus, the cycle will always continue. The effectiveness of traditional approaches to eradicate surface contamination is under debate. A study demonstrated that in the healthcare environment MRSA was detected on 74% of swab samples before cleaning and on 66% of swab samples after cleaning.[55]

In recent years, the NHS has implemented a range of strategies, including mandatory surveillance, legislation, and inspection in order to decrease the number of HAIs. In

particular, significant effort has been devoted to prevent HAIs attributed to MRSA, and *C. difficile* because they have caused multiple fatalities.[56,57] Although the actions have achieved a reduction in HAIs since 2007, fatality rate (~9000 deaths per year) is still tragically high and requires further control measures.[58]

In order to overcome the problems of the cyclical nature mentioned above, antimicrobial surface coatings need to be developed to reduce microbial loads on a surface without outside intervention and therefore reinforce the hygiene regime of a healthcare environment. Such a coating may possibly break the "nosocomial infection loop" that would solve the problem of person-person transmission (**Fig. 1.2**).[59]
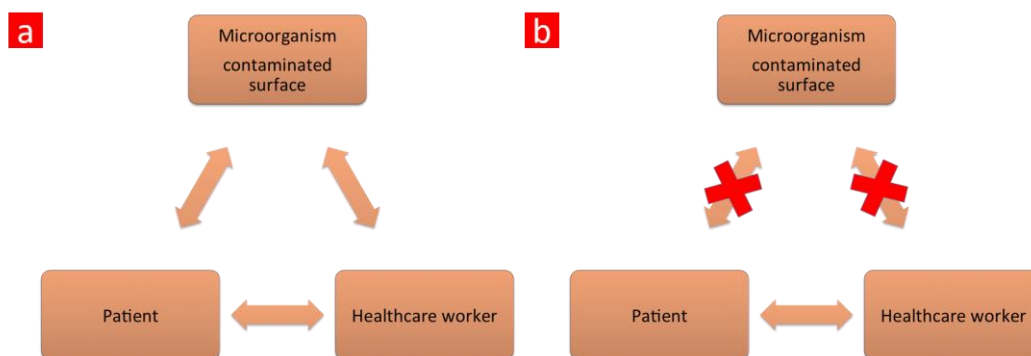
Fig. 1.2 The role of surfaces in the transmission of hospital infection. (a) Cycle of bacterial transfer from surfaces to patients. (b) Disruption of cycle because of the use of an antimicrobial surface.

Antimicrobial surfaces may either (i) inactivate bacteria that do adhere to the surface (i.e. bactericidal activity) using bactericidal nanoparticles or (ii) prevent the attachment of bacteria (*i.e.* anti-biofouling activity) using superhydrophobic and slippery surfaces.

1.5.1: Antibacterial nanomaterials

At the beginning of the 20th century, infectious diseases were the leading cause of death worldwide. However, success in reducing morbidity and mortality from infectious diseases during the last century was attributed mainly to the use of antimicrobial drugs. Nowadays, however, microbial resistance to these drugs has reached a critical point, invalidating the

therapeutic efficiency of major antimicrobial drugs that are currently utilized in clinical settings.[59]

A large number of bacteria are resistant to at least one antibiotic including methicillin-resistant and vancomycin-resistant *Staphylococcus aureus*, vancomycin-resistant *Enterococcus*, *E. coli*, and *Pseudomonas aeruginosa*.[60–63] 40-60% of strains of *S. aureus* in hospitals in the US and UK are resistant to methicillin and most of these strains are also resistant to multiple antibiotics.[62] Antibiotic-resistance bacterial infections lead to prolonged hospital stays, increased mortality and costlier treatments.[61,64]

To overcome this global problem, the use of biocidal nanoparticle agents has emerged as a promising method to both prevent development of bacterial resistance and overcome existing resistance mechanisms including decreased uptake and increased efflux of antibiotic from the bacterial cell[65–67] and biofilm formation.[64,68] It is believed that high surface area to volume ratios and novel chemico-physical features of different nanomaterials are associated with efficient antimicrobial activities.[69] Antibacterial nanoparticles provide many distinctive advantages over conventional antibiotics including acute toxicity reduction, overcoming resistance and lower costs of synthesis methods. Different types of nanoparticles (NPs) (e.g. silver, zinc and copper) overcome bacterial drug resistance since they show simultaneous multi-site attack mechanism against pathogenic microorganisms, therefore making it unlikely that bacterial will develop resistance.[70]

Fig. 1.3 summarizes the multiple mechanisms of antibacterial activity of various NPs. Some antimicrobial mechanisms of nano-materials contain: i) photocatalytic generation of reactive oxygen species (ROS) that lead to damage cellular and viral components, ii) compromise the wall/membrane of bacteria, iii) interrupt energy transduction, and iv) circumvent enzyme activity and DNA synthesis.[64]
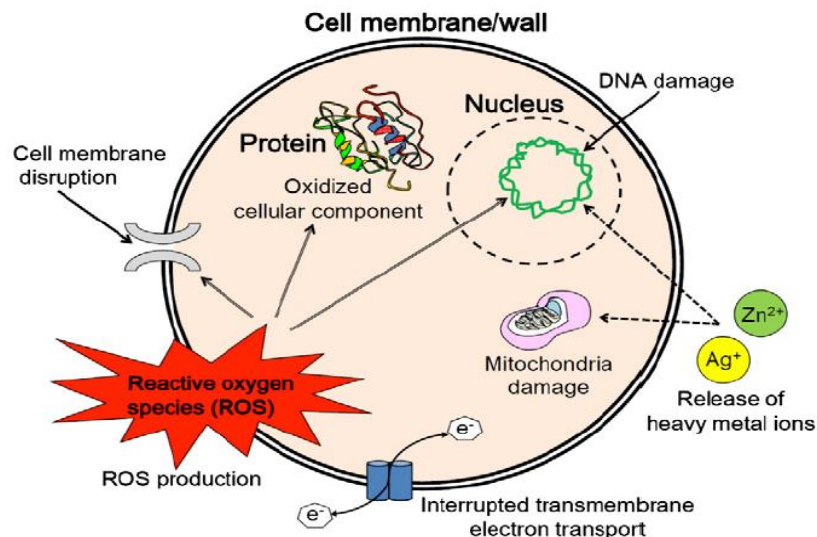
Figure 1.3 Different antimicrobial mechanisms of nanoparticles.[64]

1.5.1.1: Silver-coated surfaces

The use of silver as a therapy for infectious diseases lost its popularity after the discovery of penicillin in the 1940s.[71] However, the limited efficacy of antibiotics against bacteria that recently emerged revived the clinical utilization of silver and its compounds in a range of applications such as wound dressings[72], medical devices and catheters,[73] and textiles.[74] Silver nanoparticles (Ag Nps) have been proven to be strongly bactericidal against a variety of microorganisms including drug-resistant bacteria, fungi and viruses.[75–79] Since Ag NPs use numerous antimicrobial mechanisms to kill bacteria the development of resistance to them is unlikely.[77,78] Their antimicrobial properties are attributed to release of Ag+ ions from the Ag NPs in aqueous solution that exert antimicrobial activity through different mechanisms.[64,78,80]

Firstly, silver ions can interact with sulfur and phosphorus-containing proteins in the bacterial membrane,[75,77–79] causing holes in the membrane that allows cytoplasmic contents to leak out the cell, and sometimes resulting in cell death.[78,79] Also, these interactions allow the ions to penetrate into the cell cytoplasm by passing through the wall and plasma membrane of the cell, where the ions provide additional antimicrobial effects.[75,79]

Once Ag^+ is in the bacterial cell, it shows several more antibacterial effects: (i) Ag+ also attaches to and damages DNA and RNA of microbes,[75,77–79,81] (ii) Ag+ circumvents DNA replication and cell division of microbes,[79,81] and (iii) Ag+ can generate reactive oxygen species (ROS) that shows toxic effects both on bacterial and eukaryotic host cells[78–80]

It was reported that the antimicrobial activity of Ag NPs is inversely dependent upon the nanoparticle size[82,83] and shape.[84] Combination of Ag NPs and antibiotic such as penicillin G, amoxicillin, erythromycin and vancomycin lead to enhanced and synergistic antibacterial activities against Gram-positive and Gram-negative bacteria (e.g., *E. coli* and *S. aureus*).[85–87] On the other hand, prolonged exposure to soluble silver-including materials may generate toxic effects such as organ damages (e.g. liver and kidney), irritation (e.g. eyes and skin) and alteration in blood cell counts.[88] Conversely, some studies suggested that Ag NPs are non-toxic.[89,90] As a result, the use of Ag NPs can be considered as promising antimicrobial compounds that require comprehensive understanding of their potential toxicity.

1.5.1.2: Copper-coated surfaces

Copper (Cu) has been known as an antibacterial agent for centuries and was used to treat ulcers by Hippocrates (Hippocrates, 400 BC). A broad range of microorganisms are susceptible to copper, including *S. aureus, E. coli, C. difficile, E. faecalis, E. faecium, Mycobacterium tuberculosis,* and influenza A H1H1.[91]

Cu NPs have been fabricated using a broad range of techniques including thermal reduction,[92] chemical reduction, vacuum vapour deposition and microwave irradiation techniques.[93] These techniques utilize oxygen-free conditions to prepare the nanoparticles because they rapidly oxidise to Cu^{2+} ions in air or aqueous media.[94] Therefore, it is vital that a technique is developed which can stabilize Cu NPs to inhibit oxidation and agglomeration. Nanoparticles readily agglomerate since they possess a high surface energy that limits effective dispersion into solutions or polymer matrices.[95] Alternative techniques have been carried out to produce Cu NPs in the presence of polymers (e.g. chitosan,[96]

polyethylene glycol[97]) or surfactants (e.g. cetyl trimethyl ammonium bromide) as stabilizers in order to form coatings around the nanoparticle surface.[98]

Copper surfaces have been examined for their use in the healthcare environments in the UK, USA, Chile and Japan.[99–101] For instance, copper-containing taps, door push plates and toilet seats were applied to an acute medical ward in the UK, which resulted in much lower bacterial loads on the surfaces compared to that found on non-copper containing control surfaces.[102]

Although the exact bactericidal mechanism of Cu NPs is not fully understood, it has been demonstrated to be mainly because of disruption of cellular respiration, DNA damage by means of the generation of reactive oxygen and ionic copper species that cause damage to bacterial enzymes and proteins.[103–105]

1.5.1.3: Zinc oxide-coated surfaces

Zinc oxide nanoparticles (ZnO NPs), which are non-toxic to human and biocompatible, have been used as drug carriers, cosmetic ingredients, and medical filling materials.[106,107] In addition, it was found that ZnO NPs exhibited antibacterial property against important food-borne pathogens such as *E. coli* 0157:H7 and enterotoxigenic *E.coli*[108–110] as well as against drug-resistant bacteria (e.g. MRSA).[68] ZnO NPs have benefits compared to Ag NPs such as lower cost, a white appearance and UV-blocking characteristics.[111] It is believed that ZnO NPs destroy lipids and proteins of the bacterial cell membrane, which result in a leakage of intracellular contents and ultimately the death of bacterial cells.[112,113]

ZnO NPs use multiple mechanisms to destroy pathogens and therefore the likelihood that bacteria will develop resistance to them is low. These mechanisms include: (i) ZnO NPs attach strongly to bacterial cell membranes and disturb both the lipids and proteins of membrane, leading to increased membrane permeability and leakage of cytoplasmic contents out of the cell, which result in cell death,[64,68,75] (ii) ZnO NPs can also produce Zn^{2+} ions and ROS (e.g. H_2O_2), which possess harmful effects on the bacterial cell,[65,75] (ii) ZnO coated polyvinyl alcohol (PVA) increases membrane permeability and then penetrates into the cytoplasm of the cell, where it induces oxidative stress.[65,68]

1.5.1.4: Titanium oxide-coated surfaces

Titanium oxide (TiO_2) has been used in a wide range of applications including water sterilization for drinking[114] and self- cleaning windows[115]. TiO_2 is a photocatalyst that needs sub 385 nm radiation due to its high band gap. Hence, TiO_2 absorbs UV light and can store energy in order to efficiently convert carbonatious materials on the surface into carbon dioxide and water. Therefore, it can keep itself clean under UV. Owing to its self-cleaning ability, TiO_2 has been coated onto various types of surfaces such as glass,[116–119] textiles[120,121] and catheters.[122]. Moreover, TiO_2 has much potential to circumvent the spread of hospital pathogens such as *E. coli* and MRSA. For the first time, Matsunaga *et al*. discovered the antimicrobial properties of titanium oxide in 1985. It was reported that after 2 hours ultra-violet (UV) irradiation, platinized TiO_2 was capable of eliminating 10^3 cfu/ml *Saccharomyces cerevisiae* and 10^3 cfu/ml *E. coli* due to its photo-catalytic activity.[123]

Although TiO_2-based materials show remarkable both self-cleaning and antibacterial properties, there are some disadvantages related to TiO_2. The main disadvantage is that TiO_2 adsorbs mainly the UV light due to its larger band gap (3.25 eV).[124] Some of approaches to increase its efficiency and to shift its absorbance to the visible region include metal (Au, Ag, Pt, Pd, Cu and *etc.*)[77,125–132] and non-metal doping (C, N).[133] Dopants can narrow the band gap of TiO_2 that causes its absorption peak to appear in the visible spectrum, therefore increasing the efficiency of the doped TiO_2. Another common disadvantage of TiO_2 and other light-induced materials is that their incorporation in organic materials causes the degradation of the matrix due to ROS production. It was reported that a white powdery material was formed on the surface of TiO_2-based paints when exposed to sunlight and this phenomenon is known as the chalking effect.[134]

1.5.1.4.1: Photocatalytic mechanism of TiO_2

TiO_2 is a well-known semiconductor that is composed of two energy bands; the valance and conduction bands. When TiO_2 absorbs a photon of UV light, an electron is promoted from the valance band to the conduction band resulting in the formation of an electron-hole pair (**Fig. 1.4**). Afterwards, these reactive species participate in oxidation or reduction

processes within the TiO_2 itself or with adsorbents at the surface. The main reactive species, the hydroxyl radical, is generated through the following series reactions:

$$TiO_2 + hv \rightarrow e^- + h^+$$

$$h^+ + H_2O_{(ads)} \rightarrow HO^\bullet + H^+$$

$$h^+ + OH^-_{(surface)} \rightarrow HO^\bullet$$

$$e^- + O_2 \rightarrow O_2^{\bullet-}$$

$$2O_2\bullet^- + 2H_2O \rightarrow 2HO^\bullet + 2OH^- + O_2\ [135]$$
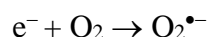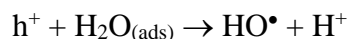
The hydroxyl radicals generated by redox processes on the TiO_2 surface are extremely reactive and completely non-selective. Therefore, they are potent biocides and capable of oxidizing most organic compounds at the catalyst surface.[135]
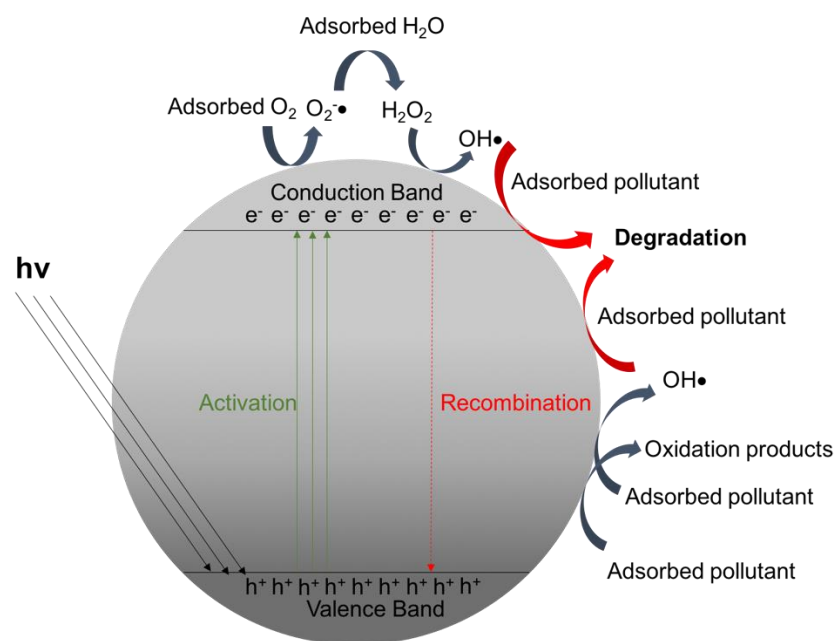
Fig. 1.4 General mechanism of the photocatalysis on the surface of titanium dioxide.

31

1.5.2: Photodynamic therapy

Light has been utilized to treat skin disorders, tracing back thousands of years to the ancient civilisations of Egypt, Indian and China. They used combinations of plant extracts (e.g. Ammi majus) and sunlight to treat skin diseases such as vitiligo. Nowadays, the active ingredient of this plant (psoralen) is employed globally in the treatment of psoriasis.

Phototherapy was first utilized by the Nobel Prize winner Niels Finsen in the treatment of lupus vulgaris, a tuberculosis skin condition, in the 1890's by applying light directly onto the lesions.[136,137] Photodynamic therapy (PDT) evolved from this initial work and involves the use of combination of a photosensitizing agent and a light source to produce toxic reactive oxygen species.[138]

PDT has successfully been utilized to treat bladder cancer with the photosensitizer Photofrin®. Additionally, PDT was approved to treat other cancers including bronchial[139] and skin cancers.[140] Over the past decade PDT has been developed and approved to treat age-related macular degeneration that is the major cause of vision lose among the elderly in the Western world. Treatment involves intravenous injection of the photosensitizing agent Visudyne® and has been employed over two million cases to date.[141] When PDT is utilized to destroy bacteria, it is termed "photodynamic inactivation".[142]

The concept of bacterial cell destruction by using the combination of light and dye was firstly introduced by a medical student named Oscar Raab in 1900.[143] He reported the deactivation of *Paramecium caudatum* stained with acridine orange upon exposure to high intensity light. Following this finding, his supervisor, Hermann von Tappeiner, indicated oxygen was essential for the phototoxic effect of the dye and they coined the term "photodynamic action" in 1907 to describe this reaction and hence the field of Antimicrobial Photodynamic Therapy (aPDT) was born.[144,145]

PDT is particularly advantageous for antimicrobial application. In this therapy, radical species can be regarded as non-selective microbicides[135,146] because they show a non-site specific and multi-site attack mechanism against microorganisms. Therefore, it reduces the

chance of the development of bacterial resistance since resistance only develops when a microbicide targets to a specific site.[146]

Photodynamic therapy (PDT) requires three components for treatments: light, a photosensitizer, and molecular oxygen.[147] The process begins when a ground state photosensitizer (PS) absorbs light of an appropriate wavelength and gets transformed into an excited singlet state. This single state of the PS readily decays back to the ground state with the emission of light (fluorescence) or heat or are converted into an excited triplet state.[148] The excited state PS can either transfer the energy to a substrate (e.g. water) to generate radical ions that react with oxygen to generate cytotoxic reactive oxygen species such as superoxide (O_2^-), hydrogen peroxide (H_2O_2), and hydroxyl radicals (OH^-) which is known as a type I reaction or it can react with molecular oxygen producing singlet oxygen ($^1O_2$) which is known as a type II reaction. These reactive oxygen species may result in significant damage to bacterial cells *via* several different mechanisms including oxidation of membrane lipids and amino acids in proteins, cross-linking of proteins and oxidative and nucleic acids (**Fig. 1.5**).[149,150]
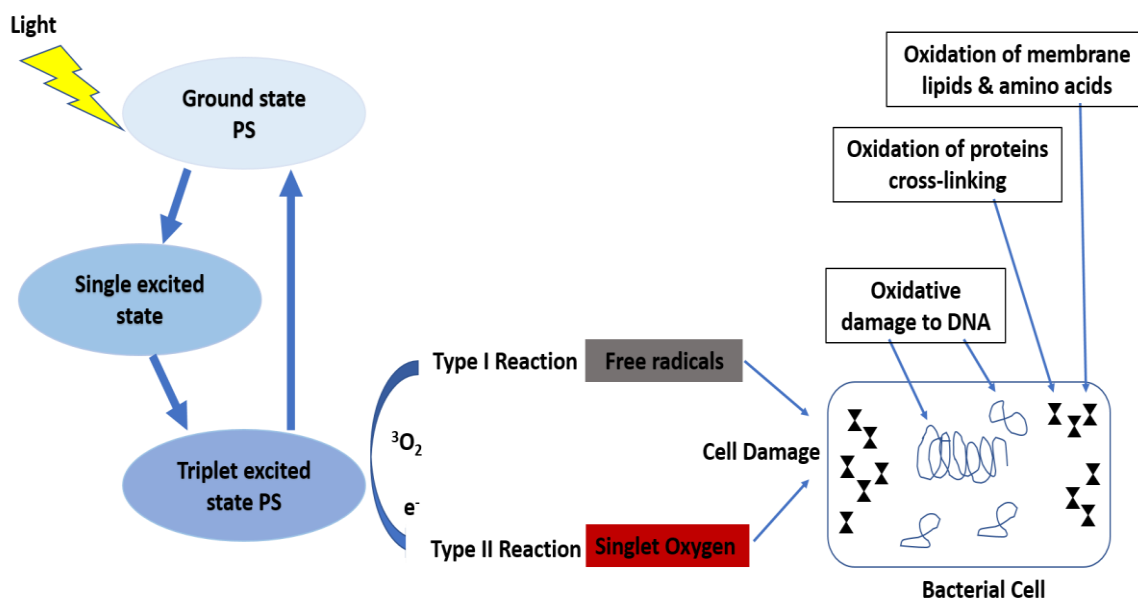
Fig. 1.5 Schematic diagram explains the mechanism of action of PDT.

Importantly, the $^1O_2$ species are generated without transformation of the photosensitizer dye, hence allowing each single dye molecule to generate many times its own concentration of $^1O_2$.[151] Over time, however, the dye will be degraded during light irradiation via a process known as "photobleaching" which can caused by both type I and type II reactions. Also, it should be noted that dye molecules do not have to be taken up bacterial cells or even adsorbed to the bacterial surfaces to exert a bactericidal effect. Since a $^1O^2$ molecule can travel a distance of between 100-300 nm, it has the ability to diffuse from its site of production.[152,153]

1.5.2.1: The mode of action of photosensitizers

Larson et al. have suggested three modes of action by which photosensitizer agents can interact with the cell:

1. The agent accumulates outside the cell, producing reactive oxygen species (ROS) in solution, which can enter the cells of the target pathogen and react to cause cellular damage.

2. The PS attaches to or localize in the cell membrane via hydrophobic or coulombic interactions and upon illumination the PS transfers energy to target biomolecules within the cell, leading to ROS generation that result in cell damage.

3. The PS diffuses into the interior of the cell and react with an intracellular target such as a protein (including enzymatic damage) or the nucleus (including genetic damage).

1.5.2.2: Photosensitizer properties

Photosensitizers (PSs) are planar unsaturated organic molecules with extensive electron delocalization.[154] Hence, they have a tendency to be deeply coloured since the energy required to excite the electron in the highest occupied molecular orbital (HOMO) to the lowest unoccupied molecular orbital is low in comparison to less delocalized molecules and hence, the visible absorption bands tend to be in the longer wavelength (red) spectral region and reflect the high probability of electronic excitation. The first photosensitizer dye

used for bacterial photo-deactivation was acridine orange (Fig. 1.6).[155] Most of the dyes that have been used over the last 100 years to treat cancer and other tissue diseases are primarily porphyrin-based compounds.[156] In addition, different non-porphyrin based dyes have been employed including xanthenes (e.g. rose Bengal)[157] and phenothiazinium salts (e.g. toluidine blue (TBO) and methylene blue (MB)).[158]

In respect of their use for antimicrobial applications, they should possess the ideal characteristics which are:

i. High $^1O_2$ quantum yield

ii. Broad spectrum of action against a wide range of microorganisms including bacteria, fungi, yeasts, viruses and parasitic protozoa.

iii. Efficacy independent of the antibiotic-susceptibility of the target pathogens.

iv. Ability to result in significant reduction in pathogen populations while causing no damage to the host tissues

v. Low probability of promoting the onset of mutagenicity

vi. Inhibition of regrowth of the microorganisms after multiple treatments.

vii. Availability of formulations allowing specific delivery of the PS to the infected area.

Currently available PSs do not meet all of these criteria; some are close and with some chemical manipulation could be promising candidates as antimicrobial PSs. There are several groups of PSs that are being currently utilized for lethal photosensitization of pathogens and for treating infectious diseases, including phenothiaziniums, acridines, cyanines, porphyrins, phthalocyanines, chlorins, and psoralens (**Table 1.3**). An overview of phenothiaziniums is discussed in this section.

Table 1.3 Absorption maxima of photosensitizers.

Photosensitizer	λmax range in buffer (nm)
Acridine	400-450
Cyanine	350-800
Phenothiazinium	620-660
Phthalocyanine	670-780
Porphyrin	600-650
Psoralen	300-380

1.5.2.2.1: Photosensitizer-based antibacterial surfaces

Light-activated antimicrobial agents (LAAAs) can be utilized in PDT. It involves using combination of light sensitive agents and light in an oxygen-rich environment. These adsorb photons of energy from light and transfer this energy to surrounding oxygen molecule so that toxic oxygen species such as singlet oxygen and free radicals are formed. These species are very reactive and can cause lethal damage to bacteria proteins, lipids, nucleic acids and other cellular components.[159]

Photosensitizers utilized in PDT are generally heterocyclic ring type, as demonstrated in **Fig. 1.6**, show low toxicity in the dark, but which produce cytotoxic species upon photo-activation in the presence of oxygen.[160,161] These photosensitizers can be classified as (a) porphyrin-based and (b) chlorophyll-based structures and (c) dye molecules.[161]

Phenothiazine dyes such as methylene blue, toluidine blue and crystal violet are compounds which possess a core structure comprising a planar tricyclic heteroaromatic ring with the formula $S(C_6H_4)_2NH$, with an absorption range of λmax = 620-660 nm. Since

these dyes show minimal toxicity to human cells and are capable of producing high quantum yields of singlet oxygen, in recent years they have attracted attention to be used as photo-activated antimicrobial agents.
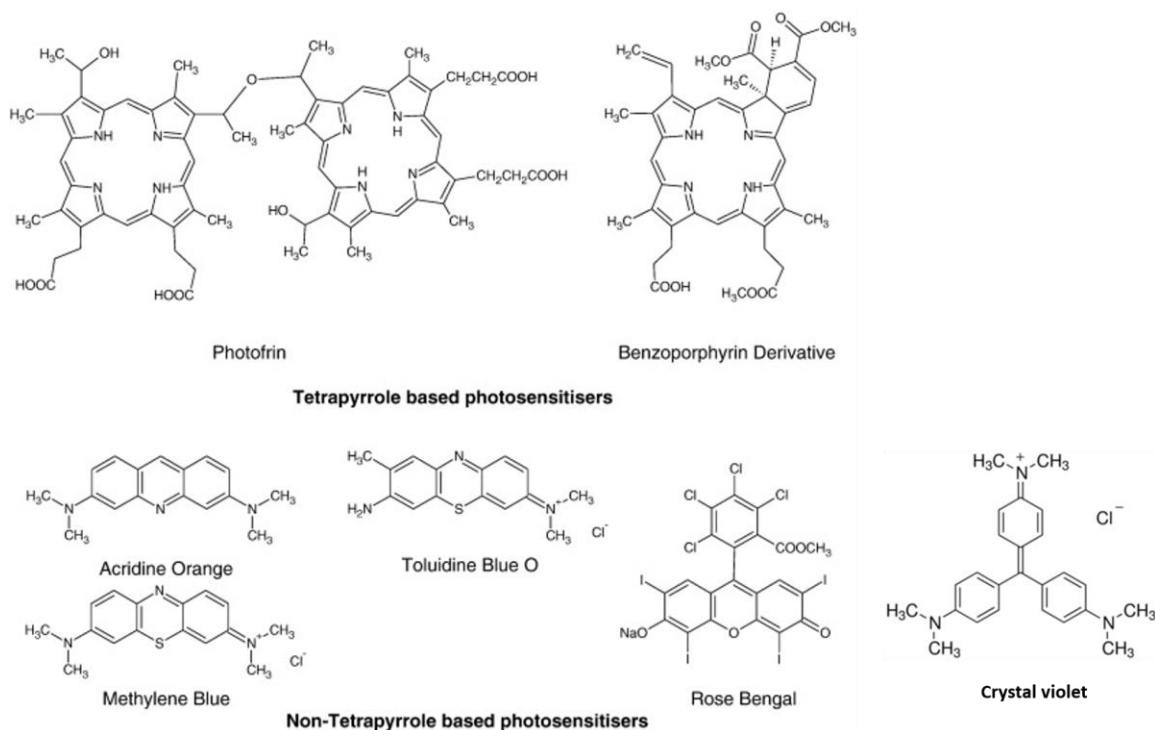
Fig. 1.6 Some chemical structures of tetrapyrrole-based and non-tetrapyrrole based photosensitiser compounds.[160]

Photosensitizers such as methylene blue can be efficaciously incorporated into medical grade polymers by the exposure of the polymers to specific solvents that induces the polymer swelling.[162–166] After the swelling process, the photosensitizer dye molecules can diffuse throughout the polymeric matrix.[167] When removing the swelling solution, the evaporation of any trapped solvent molecule in the swollen polymer occurs and the polymer shrinks to its original size, finally ending up with strongly coloured dye-encapsulated polymer sections.[162–166]

The dye incorporated polymers using this simple ''swell-encapsulation-shrink'' technique showed the potent photo-inactivation against both Gram-positive and Gram-negative

37

bacteria, when irradiated with either a laser light source[163–166] or a white light source of an appropriate wavelength.[162]

1.5.2.3: Antimicrobial Photodynamic Therapy (aPDT): Is resistance possible?

The main mechanism of ROS is thought to mainly cause damage to the cytoplasmic membrane and DNA.[168] The membrane can be destroyed through multiple pathways including leakage of cellular contents or inactivation of membrane transport systems and enzymes.[169] On the other hand, DNA repairing systems can repair DNA chain.[170] Hence, it was demonstrated that even though DNA damage takes place, it cannot be the main cause of bacterial cell photo-killing process,[168] because *Deinococcus radiodurans*, a very efficient DNA repair mechanism, can be destroyed by aPDT.[171]

There are not many investigations to determine if bacteria can develop resistance after a number of consecutive aPDT treatments. One study reported that the photo-inactivation of two bacterial species (*Peptostreptococcus micros* and *Actinobacillus actinomycetemcomitans*) by two PS did not induce significant resistance development even after ten subsequent irradiation treatments.[172] Moreover, *Pedigo et al*. used antibiotic resistant strains of *S. aureus* and *E. coli* in order to study the development of resistant bacteria after repetitive photosensitization sessions using methylene blue. While there was no significant decrease in bactericidal activity towards *E. coli* after eleven consecutive exposures, for MRSA negligible resistance was observed through twenty five repeated aPDT treatments.[173]

1.5.3: Nature Inspired Antifouling coatings

Fouling organisms have been present on Earth for billions of years and they have developed a multitude of survival mechanisms against physical and chemical attack.[174,175] One of the main mechanisms facilitating survival is the phenomenon of biofilm formation. A pathogenic biofilm can show remarkable resistance to the natural immune systems and antibiotics[175–177]. Specifically, Gram-negative *Pseudomonas aeruginosa* are responsible for 10-15% of HAIs worldwide and possess high intrinsic antibiotic resistance.[178] Also, biofilms can show remarkable resistance against a broad range of treatments such as

chlorine bleaching for 60 min[176] and continuous flushing with multiple biocides over 7 days.[179]

Bacteria are capable of forming biofilms in a wide range of natural and anthropogenic environments on all type of surfaces[180,181], posing serious effects on the function of a wide range of systems including plumbing, oil wells, medical implants and catheters, air conditioning and other systems[182], causing environmental, social and economic implications. Biofilm formation on medical devices causes half of all hospital-acquired infections (HIAs) associated with substantial morbidity, mortality[183–185] and hospitalization cost between $28 and $45 billion to the U.S. economy per year.[186]

Many strategies have been employed to reduce the detrimental effects of biofouling, which can be broadly categorized into two main categories; (i) chemical approaches that inactivate bacteria that do attach to the surface i.e. bactericidal activity or (ii) physical approaches that inhibit initial bacterial attachment to the surface i.e. anti-biofouling activity.[187,188] Chemical approaches include the use of biocide/release coatings such as antibiotics,[189–191] metal/metal oxide nanoparticles.[192–194] However, chemical coatings are usually susceptible to degradation, depletion and desorption[195]. Furthermore, the use of biocidal agents can accelerate the emergence of multi and pan-drug resistant strains.[196] Therefore, a "physical", non-cytotoxic strategy to inhibit biofilm formation rather than treating it is of great interest without contributing selective pressure and accelerating antibacterial resistance of pathogenic organisms.

To solve this problem, fouling-release coatings have emerged as a promising approach, which have great potential to be utilized for longer periods of time. In nature, many creatures have developed different adaptions that allow them to show excellent anti-fouling properties over extended periods of time. Some of them include nanoscale surface characteristics on shark skin, mucus-based layer coatings on fish scales and the generation of natural biocidal agents on the fronds of macroalgal species (e.g. *Delisea pulchra*).[197]

It should be noted that bacteria are complex microorganisms that possess different surface chemistry, hydrophobicity, cell membranes, surface charges, shapes and hardness as well

as having pili and flagella to modify their attachment. [198–202] Therefore, the elaboration of surfaces that repel all types of bacteria is to date not possible.

In this section, three different surfaces will be explained in detail, which are hydrophilic surfaces, superhydrophobic surfaces and slippery surfaces.

1.5.3.1: Hydrophilic Polyethylene glycol (PEG)-based Coatings

Attachment of pathogenic bacteria to biomedical devices and the subsequent biofilm formation is a major problem.[203] The type of interaction varies from one species of bacterium to another and perhaps also between strains within a species because of mutations or differential adaptive responses, therefore adding to the complexity of the problem. Researchers have found that bacteria can attach to surfaces through the deposition of a layer of proteins, and hence protein-resistant surfaces should also resist the bacterial attachment.[204] Thus, there have many investigations into rendering surfaces protein-resistant using PEG that is flexible and show large steric repulsion forces.[203–206]

The correlation between the chain length of PEG brushes and the attachment of various bacteria was investigated with a conclusion that the higher molecular weight PEG exhibited more effective protein-resistant properties. Moreover, the relatively hydrophobic bacteria (*P. aeruginosa*) attached more strongly compared to the hydrophilic one (*S. epidermis*) due to hydrophobic interactions that promoted the adhesion of the bacteria on the surface. [203]

Even though PEG-modified surface is one of the most effective approaches to design protein-resistant surfaces, it is not effective in preventing bacterial attachment, maybe because of the complex mechanisms that bacteria use to attach to a surface.[204] Furthermore, PEG undergoes oxidative degradation in complex media, making it unsuitable for use for long periods of time.[207,208]

1.5.3.2: Superhydrophobic surfaces

A water droplet can interact with a surface in different ways. When a droplet hits a surface, the interaction with the surface ranges from superhydrophilicity,[209] in which the shape of

water droplet becomes a flat puddle because of the strong water-surface interaction and can fully wet the surface, to superhydrophobicity, in which the water droplet becomes a near-spherical droplet and is repelled by the surface because of weak water-surface interaction.

In nature, different plants, insects and animals possess superhydrophobic properties in order to survive in extremely aggressive environments. The most famous example is the Lotus leaf. Even though in Asia the Lotus has been symbol of cleanliness for centuries, its self-cleaning mechanism was explained in 1997 after the introduction of the scanning electronic microscope.[210] Because of the low surface energy of waxes and the surface topography consisting of a hierarchical micro/nano structures as demonstrated in **Fig. 1.7**, the Lotus leaves have superhydrophobic surfaces with a water contact angle of over 170° and very low water roll-off angles.
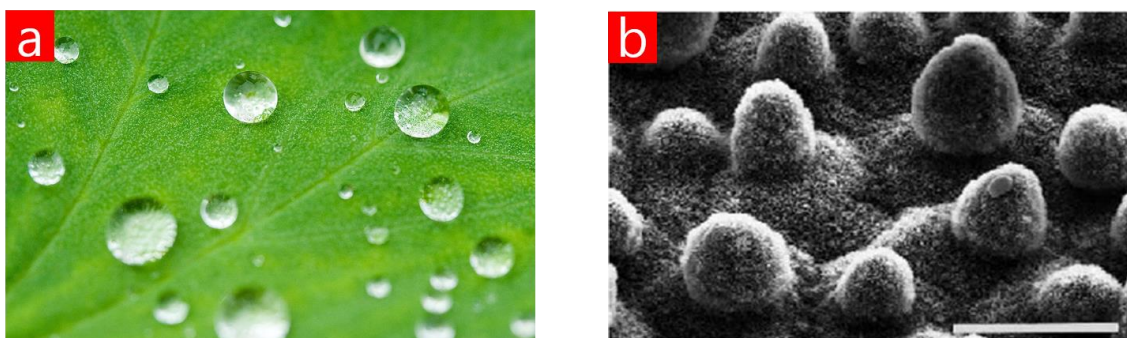
Fig. 1.7. (a) Water droplets on the Lotus leaf. (b) A scanning electron microscopy (SEM) image of a Lotus leaf exhibiting a highly rough surface microstructure. Scale bar = 20 µm.[211]

Such surfaces minimize the contact area between water or the dirty particles and the leaf surface owing to the entrapped air between the surface structures. This significantly reduces the adhesion of water and the dirty particles to the surface. When water forms near-spherical droplets, they roll across the surface facilitating the dirty particles to be picked up, as shown in **Fig. 1.8**. This phenomenon is known as the "Lotus effect". Contrarily, on a tilted smooth surface the water droplet will slide off the surface without taking away the dirty particles from the surface. More precisely, superhydrophobic surfaces are regarded as easy-to-clean surfaces rather than self-clean surfaces. For example, a superhydrophobic surface in a paper machine was examined and it was concluded that the surface was not

self-cleaning (i.e. not being clean by itself) but contaminated due to the paper machine environment. However, the surface could be easily cleaned by a gentle water rinse because of the low adhesion force of the contaminants to the surface.[212]
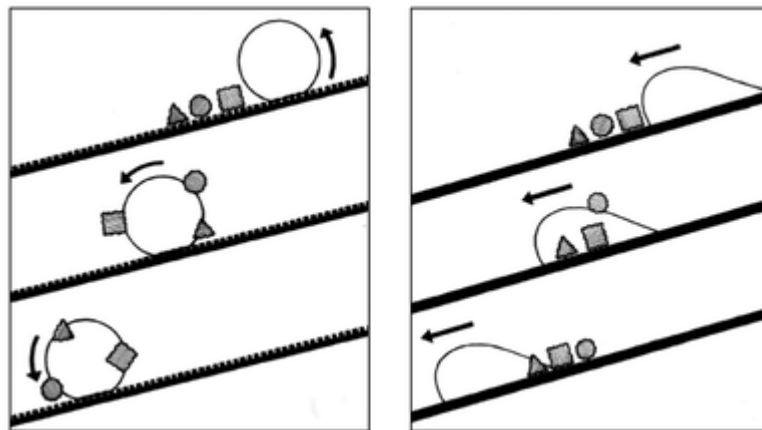
Fig. 1.8. Schemes show the relationship between surface wettability and self-cleaning properties. The dirt particles are redistributed by water on a smoot hydrophobic surface (on the left) while they are removed by water from rough a superhydrophobic (water-repellent) surface (on the right).[211]

The influence of superhydrophobic surfaces made of using different materials and synthesis methods on bacterial adhesion has been widely investigated.[213–218] Overall, such surfaces can prevent bacterial attachment rather than destroying them directly[219,220] by reducing the adhesion force between bacteria and a solid surface that enable the easy removal of bacteria before a thick biofilm is established on the surface.[215]

There are different investigations on the interaction of bacterial cells with superhydrophobic surfaces and it has been shown that reducing protein adsorption and the entrapped air layer between the bacteria cells and the surface has been identified as crucial factors to reduced bacterial adhesion. In general, hydrophobic surfaces and surfaces with contact angles of 60-90° attract proteins.[221] Contrarily, superhydrophobic surfaces have been shown to lead to a low protein adsorption,[222,223] hence resulting in a low bacterial adhesion.[221,224,225]

Some researchers have investigated the bacterial adhesion patterns and its possible mechanism on superhydrophobic surfaces. For example, laser ablated superhydrophobic

titanium surfaces were investigated for their ability to retain four coccoid bacteria including *Staphylococcus aureus* CIP 65.8[T], *Staphylococcus aureus* ATCC 25923, *Staphylococcus epidermis* ATCC 14990[T] and Planococcus *maritumus* KMM 3738. It was found that each species tended to preferentially adhere to the crevices between the microscale features of the surface, while the upper regions of the microscale features were essentially cell-free. An explanation for this has been proposed. Since surfaces with hierarchical topographical structures are usually highly hydrophobic because of their exceptional ability to trap air, a large proportion of the surface is occupied by air. Therefore, small particles with low mass (i.e. bacteria) usually cannot cross an air-water interface because of the effects of surface tension. Based on this phenomenon, the bacterial cells were unable to contact with the superhydrophobic underlying substrate owing to occupation of the surface with nano-sized bubbles. As a result, they began to accumulate in the tri-phase interface that provides the best shelter from water turbulence. Afterwards, the cells slide across the nanobubbles within the nanotopographical features (**Fig. 1.9**). This theory can explain an increased bacterial adhesion with time because of the replacement of trapped air.[226]
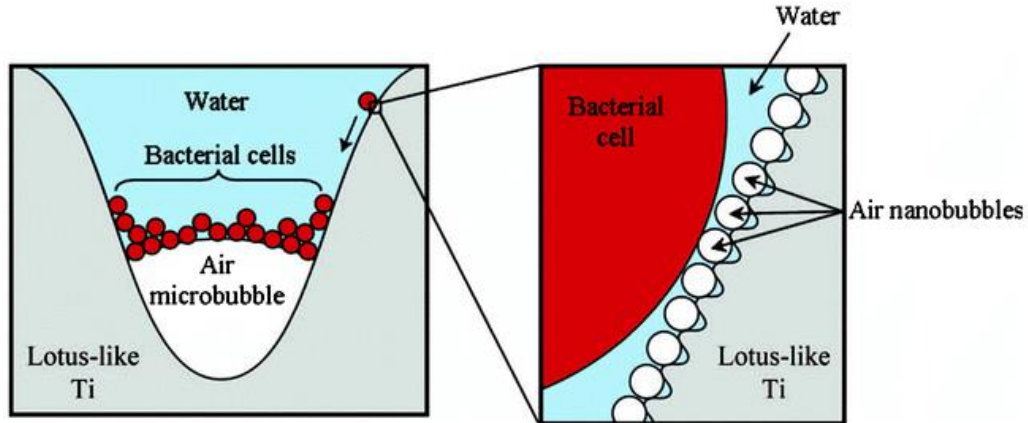
Fig. 1.9 Proposed mechanism by which bacterial cells accumulate at the tri-phase interface on immersed superhydrophobic Ti surfaces.[226]

1.5.3.3: Slippery surfaces

Superhydrophobic surfaces based on trapped air may easily fail since the stability of air pockets can be destroyed by different factors including various liquid environments, pressure and hydrodynamic shear.[227,228] Also, superhydrophobic surfaces would usually

suffer from weak wear resistance because of the surface micro/nano structures and fast degradation of surface chemical composition. As a result, any defects in the surface chemistry could provide favorable sites for bacterial attachment. Additionally, superhydrophobic surfaces in the Cassie state tend to irreversible wetting (the Wenzel state), especially with the generation of a bacterial surfactant, reducing their efficiency in submerged environments.[229] Recently, a different concept based on the peristome of pitcher leaves has been developed to inhibit the bacterial adhesion on surfaces even under wet conditions.

Pitcher plants have pitcher-shaped leaves in order to capture prey (i.e. insects), as demonstrated in **Fig. 1.10**.[230–232] The pitchers present visual and olfactory signals to attract insects. Since the pitcher rim (peristome) is slippery because of the microscale surface topographical features and secretion of hygroscopic nectar, the insects fall into the bottom part of the pitcher that is filled with a digestive fluid, making them drown and subsequently decompose.[232]
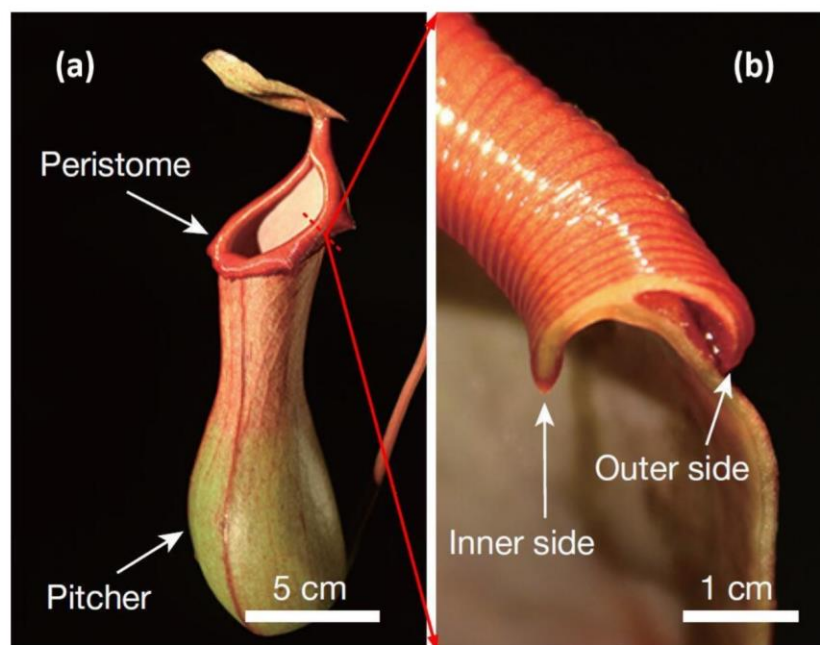
Figure 1.10 (a) Optical images of a Nepenthes pitcher plant. (b) The cross section of the peristome of the Nepenthes pitcher plant.[233]

Based on the mechanism inspired by the slippery surface of the pitcher plant, novel liquid-repellent surfaces, named "slippery liquid-infused porous surface(s) (SLIPS), has been developed by infusing perfluorinated liquids onto nanofibrous Teflon membranes. SLIPS are based not upon an unstable and transient solid-air Cassie-type interface, but rather on a stable, immobilized and smooth liquid surface locked in place by a micro/nano-porous solid, offering great potential to be used in a range of areas such as fluid transportation, airplane and watercraft coatings, and medical applications since they show low contact angle hysteresis, self-healing, anti-icing and anti-biofouling properties.[234–240]

Attempts at fabricating slippery surfaces with combinations of roughness, porosity surface chemistry and various infused liquids have been carried out.[241–243] In general, stable SLIPS can be designed based on three important criteria: (i) the surface energies of the solid and the lubricating fluid need to be well-matched; (ii) a microporous structure on the substrate is required to improve the surface area for the adhesion of the lubricating fluid and its immobilization; and (iii) the lubricating fluid and the ambient fluid must be largely immiscible.[244]

SLIPS surfaces exhibited exceptional ability to inhibit biofilm formation of diverse types of bacteria including *Pseudomonas aeruginosa, Staphylococcus aureus, and Escherichia coli*. The antifouling ability of SLIPS is attributed to a very weak adhesion of bacteria to the fluid interface of the SLIPS, allowing easy removal of adhered bacteria from the surface even under weak shear forces. [245]

1.6: Research aims

This thesis details novel routes toward antibacterial surfaces for potential use in hospital touch surface applications. These surfaces will be examined and their antibacterial efficacy will be evaluated. The thesis describes the following studies:

a) The antibacterial activity of photo-active dye, crystal violet (CV)-incorporated polymers

b) An investigation of the effects of different ZnO concentration on the antibacterial activity of crystal violet when incorporated into polymers.

c) A two-step chemical vapour deposition (CVD) method for fabricating novel antibacterial and water-repellent surfaces.

d) An investigation of the bacterial adhesion to superhydrophobic and slippery surfaces.

It is hopeful that these surfaces can be utilized in healthcare applications, to reduce microbial surface contamination and subsequently, reduce the risk of HAIs.

Chapter 2: THE ANTIBACTERIAL PROPERTIES OF LIGHT-ACTIVATED POLYDIMETHYSILOXANE CONTANING CRYSTAL VIOLET

2.1: Introduction

The current rapid emergence of resistant bacteria and the simultaneous downward trend in the fabrication of novel antimicrobial agents to combat resistant strains is a global threat to the treatment of life-threating infections. For instance, antibiotic-resistance bacteria significantly reduces the likelihood of treating infected wounds effectively and causes delayed wound healing and complications such as septicaemia that can result in death.[246] Hence, there is a great of interest in the development of non-invasive and non-toxic novel antimicrobial strategies that work more efficiently and faster compared to the current antibiotics, to which pathogens will not be able to quickly develop resistance.[247] In this context, lethal photosensitization (LP) is an alternative approach to current antimicrobial agents and the application of LP to treat an infection is known as photodynamic therapy (PDT).

Light-activated antimicrobial agents (LAAAs), known as photosensitizer dyes (e.g. crystal violet), can be incorporated into surface coatings to reduce the prevalence of microbial surface contamination. These modified coatings destroy bacteria by generating reactive oxygen species upon illumination with a light source. These species use a "multi-site attack" mechanism against pathogenic microorganisms unlike most antibiotics, which use a single pathway of attack, and therefore the occurrence of the development of bacterial resistance is improbable, indeed none have been reported to date.[248,249]

This chapter reports the light-activated antibacterial activity of polydimethylsiloxane (PDMS) coated with crystal violet (**Fig. 2.1**). PDMS is chosen to be a supporting base due to its unique features including high flexibility, chemical inertness and low cost.[250,251] Also, it is capable of absorbing a broad range of aromatic materials.[252] The crystal violet coated polymer samples were prepared by using a ''swell-encapsulation-shrink'' method. The objective of this work was to study the effectiveness of CV-incorporated PDMS in killing

the Gram-negative bacterium, *Escherichia coli,* and the Gram-positive bacterium, *Staphylococcus aureus,* using white light.
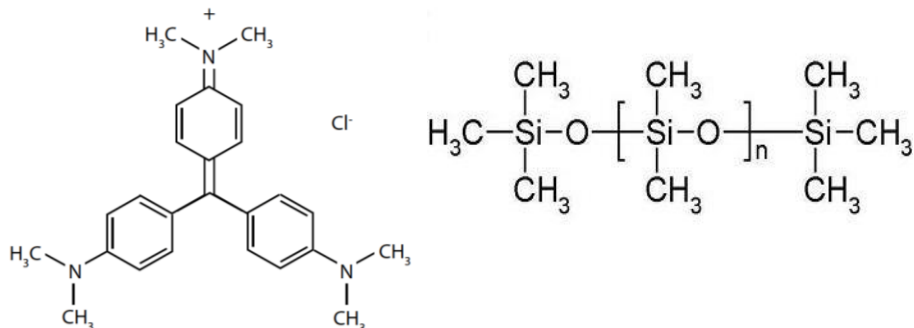
Fig. 2.1 Chemical structures of (on the left) the photosensitizer dye, crystal violet, and the silicone elastomer polydimethylsiloxane (on the right).[253,254]

2.2: EXPERIMENTAL

2.2.1: Chemicals and Substrates

The reagents and substrates used in materials synthesis were as follows: Crystal violet (Sigma, U.K), acetone (VWR), and the substrate was SYLGARD® 184 Silicone Elastomer (Dow Corning Corporation Ltd.). The silicone elastomer consists of a two-part curable silicone elastomer. The precursor, Slygard 184, can be cross-linked using its curing agent and the final material is polydimethylsiloxane (PDMS).

2.2.2: Material Preparation

2.2.2.1: Elastomer preparation

Silicone elastomers were prepared using viscous liquid polydimethylsiloxane as a starting material; this was mixed with the crosslinking agent in a 10:1 ratio, and spread uniformly on to glass squares. The polymer was then cured at 100 °C for 45 min. After cooling, the sheet was cut into smaller pieces (squares 2.0 x 2.0 cm).

2.2.2.2: *Polymer System Optimization – Organic solvent*

Silicone polymer squares (1 cm^2) were immersed in crystal violet - organic solvent solutions (750 ppm crystal violet, 100 % organic solvent) prepared using the following organic solvents: water, ethanol, methanol, acetone, toluene, hexane, chloroform and tetrahydrofuran (THF). The silicone sections were allowed to swell under dark conditions for 24 h. The samples were subsequently removed and allowed to air-dry overnight, after which they were washed (distilled water) and towel-dried.

2.2.2.3: Polymer Samples Prepared for Antibacterial Testing

The following modified silicone samples (2 cm^2) were prepared for antibacterial testing:

(i) **Control samples:** Silicone polymer squares (2 cm^2) were used as negative controls.

(ii) **Crystal violet-coated silicone:** Silicone polymer squares (2 cm^2) were immersed in a acetone swelling solution saturated with crystal violet (750 mg/L) for 24 h in the dark. Afterwards, the samples were washed and air-dried in the dark at room temperature for 24 h.

2.2.3: Materials Characterization

A Perkin-Elmer Lambda 950 UV-vis Spectrometer was used to measure the UV-vis absorption spectra analyses of the polymers within the range 400-800 nm. IR analysis of the polymers was performed within the range of 400-4000 cm^{-1} with an accumulation of 16 scans per sample using a Bruker Platinum ATR.

2.2.4: Functional Testing

2.2.4.1: Water Contact Angle Measurement

Equilibrium water contact angle measurements (~3 μL) on: untreated silicone and crystal violet-coated silicone were obtained using an FTA 1000 Drop Shape Instrument. The contact angle measurement for each sample type was taken to be the average value of 5

measurements, using a droplet of deionized water dispensed by gravity from a gauge 27 needle and the samples were photographed side on. The data was analyzed using FTA32 software.

2.2.4.2: Leaching test

The stability of the CV coated elastomer in solution was determined: CV coated sections (2 cm^2) were immersed in phosphate buffered saline (PBS) (10 ml, 37 °C) for 335 hours. The UV-Vis absorbance of the PBS (596 nm, Pharmacia Biotech Ultrospec 2000) was measured periodically to monitor leaching of the CV from the polymer into the surrounding solution. The concentration of the CV in solution was determined on the basis of its absorbance at 596 nm, compared to a calibration curve.

2.2.4.3: Bactericidal assay

Pure PDMS polymer (control) and CV-coated polymer were used to determine the bactericidal activity of the materials against *E. coli* ATCC 25922 and *S. aureus* 8325-4. The bacteria were stored at -70 °C in Brain Heart Infusion broth (BHI, Oxoid) containing 20% (v/v) glycerol and propagated on either MacConkey agar (MAC, Oxoid Ltd.) in the case of *E. coli* or Mannitol Salt agar (MSA, Oxoid Ltd.) in the case of *S. aureus*, for a maximum of 2 subcultures at intervals of 2 weeks.

BHI broth (10 ml) was inoculated with 1 bacterial colony and cultured in air at 37 °C for 17 h with shaking at 200 rpm. The bacterial pellet was recovered by centrifugation (20 °C, 4000 x g, 5 min), washed in (10 ml) and centrifuged again (20 °C, 4000 x g, 5 min) to recover the bacteria, which were finally resuspended in PBS (10 ml). The washed bacterial suspension was diluted 1 in 1000 in PBS to give an inoculum of approximately 10^6 cfu/ml.

Duplicates of each polymer sample (2 cm^2) were inoculated with 25 µl of the inoculum and covered with a sterile cover slip (18 mm x 18 mm). The samples were then irradiated for 4 hours in the case of *E. coli* and for 2 hours in the case of *S. aureus* utilizing a white light source (General Electric 28 W Watt MiserTM T5 2D compact fluorescent lamp). The light intensity was arranged to emit an average light intensity of 6500 ± 300 lux at a distance of

16 cm from the samples. A further set of samples (in duplicate) was maintained in the dark for the duration of the irradiation time. Post irradiation, the inoculated samples and cover slips were placed into PBS (5 ml) in 50 ml plastic tubes and vortexed for 60 seconds. The neat suspension and ten-fold serial dilutions (100 µl) were plated on the appropriate agar, incubated aerobically overnight at 37 °C and the colonies enumerated to determine the number of surviving bacteria. The bacterial numbers in the inocula were also determined in each experiment by viable colony counting. Each experiment included two technical replicates and the experiment was reproduced three times.

2.2.4.4: Statistical Significance

The Mann-Whitney U test was used to determine the statistical significance of the following comparisons: (i) the activity of the CV-treated polymer compared to the pure polymer when both were incubated in the dark and (ii) the activity of the irradiated CV-treated polymer compared to the same material incubated in the dark.

2.3: Results and Discussion

2.3.1: Materials Synthesis

A facile "swell-encapsulation-shrink" method was used to incorporate the triarylmethane dye, crystal violet, into non-toxic PDMS. Previous studies have shown that the swelling amount of PDMS is dependent upon the type of solvent. To induce polymer swelling and subsequent incorporation of the dye, PDMS sections (1 cm x 1 cm) were exposed to crystal violet swelling solutions prepared using a range of solvents for 24 h. **Fig. 2.2** shows the resulting modified polymer sections after swell-encapsulation of CV in the presence of various organic solvents either immediately post-immersion. It is obvious that solvents such as THF, toluene, hexane, chloroform result in extreme polymer swelling. Even though the polymer swells to a large extent in hexane, no visible encapsulation of the dye is observed because of the insolubility of the dye in hexane. However, despite the insolubility of the dye in both THF and toluene, an efficacious uptake of the dye is achieved. Moreover, the study showed that water, ethanol, methanol caused poor uptake of the dye, whereas acetone and chloroform resulted in the most efficacious uptake of the dye. Since the use

of acetone as a swelling solution to incorporate photosensitizer dyes into different polymers without material deformation has been well established,[166,255,256] it was used to swell-encapsulate the dye into the polymer.
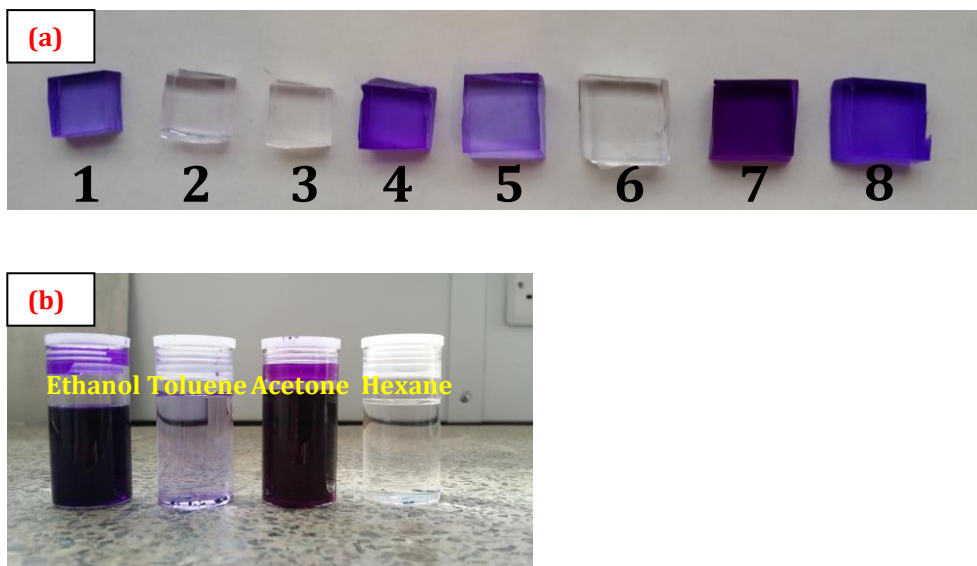
Fig. 2.2 (a) Crystal violet-incorporated polymer sections prepared by immersion in crystal violet/ organic solvent swelling solutions for 24 h (immediately post-removal from swelling solution. Organic solvents used are as follows: 1. water, 2. ethanol, 3. methanol, 4. acetone, 5. toluene, 6. hexane, 7. chloroform, 8. THF. (b) Polymer sections immersed in different crystal violet/ organic solvent swelling solutions (100 % solvent).

Dye-impregnated polymer was prepared using a swell-encapsulation-shrink method. (**Fig 2.3**). In this method, polydimethylsiloxane squares (2 cm x 2 cm) were placed in an acetone solution saturated with CV for 72 h in the dark. They were subsequently removed from the solution, washed and air-dried (24 h) so that the solvent evaporated. This method generated a purple-colored silicone that had shrunk to its original size and contained physically encapsulated CV.
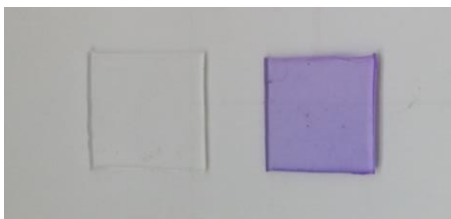
Fig. 2.3 Images of PDMS samples before -on the left- and after the swell-encapsulation-shrink process in acetone with 750 ppm of crystal violet –on the right.

2.3.2: Materials Characterization

The IR spectrum of the samples was obtained by ATR (**Fig. 2.4**). The spectra detected no significant change across the sample range after embedding CV in the polymer matrix. The results demonstrated that the swell-encapsulation-shrink technique had no influence on the physical and chemical structure of the silicones. IR spectra only gave peaks related to the host polymer matrix.
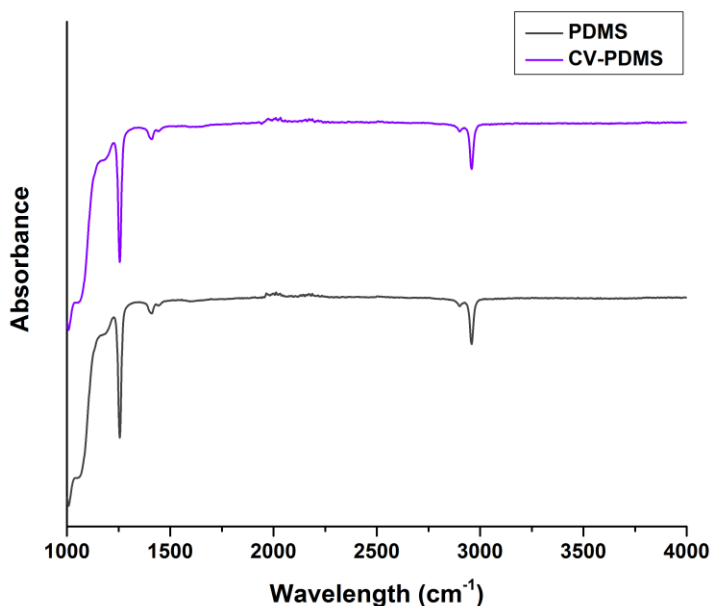
Fig 2.4 FTIR spectra of plain PDMS and CV-coated PDMS.

The UV-vis absorbance spectra of silicone samples were measured within the range 400-800 nm (**Fig. 2.5**). While pure PDMS does not show any absorbance in the visible region, when immobilized in 750 ppm CV solution, the main absorption peak of CV-encapsulated silicone is at $\lambda \approx 590$ nm, with a shoulder peak of weaker intensity at $\lambda \approx 533$ nm.
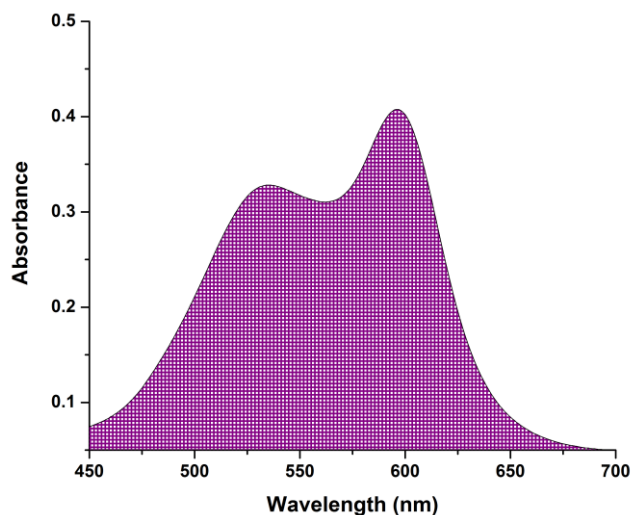
Fig. 2.5 UV-vis absorbance spectra of CV-coated silicon polymer at a concentration of 100 ppm.

The light source used in this work was a General Electric 28 W Watt MiserTM T5 2D compact fluorescent lamp with a color temperature of 3500 K, which emits light across the visible spectrum. This light source was employed since it has the same characteristics as fluorescent lights utilized in hospitals in the United Kingdom. The spectral profile of the lamp is composed of approximately 405, 435, 495, 545, 588 and 610 nm (**Fig. 2.6**). It can be seen that the absorbance of the crystal violet silicone includes four of the main emission peaks of the light source.

Spectral power distribution 3500K
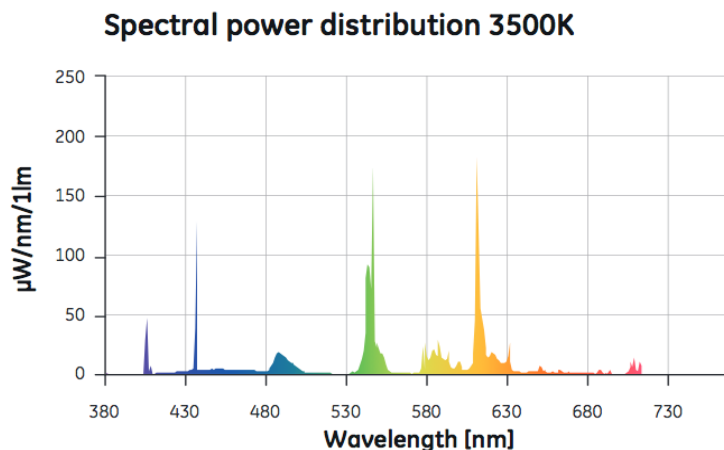
Fig. 2.6 Spectral Power Distribution of General Electric 28W MIser™ 2D lamp.

2.3.3: Functional Testing

2.3.3.1: Water Contact Angle Measurements

The contact angles of water on both the untreated elastomer and the treated elastomer were measured (**Table 2.1**). The table shows that the surface of untreated PDMS was hydrophobic with a water contact angle of 99.1°. In addition, a slight increase in the wetting properties of the untreated elastomer was seen when contrasted with the treated elastomer after the swell-encapsulation-shrink process. However, this was within the error of the experiment.

Table 2.1 Average contact angle measurements (°) ± standard deviation of PDMS samples.

Samples	Water contact angle (^{0})
Untreated PDMS (Control)	99.1 ± 1.7
CV-treated PDMS	101.1 ± 2.2

2.3.3.2: Leaching Study

In order to examine whether there had been any leaching of the CV-incorporated polymer, the polymer was placed in PBS and leaching measured spectroscopically as a function of time (**Fig. 2.7**). The data demonstrates that the sample released some CV into solution upon immersion (the first measurement of the solution was taken after 20 min from the sample immersion), although the leaching of dye from the polymer plateaued quickly with time. Over a period of more than 300 h, the leaching of CV into the solution was $\approx 3 \times 10^{-7}$ M (within experimental error) at 37 ˚C.
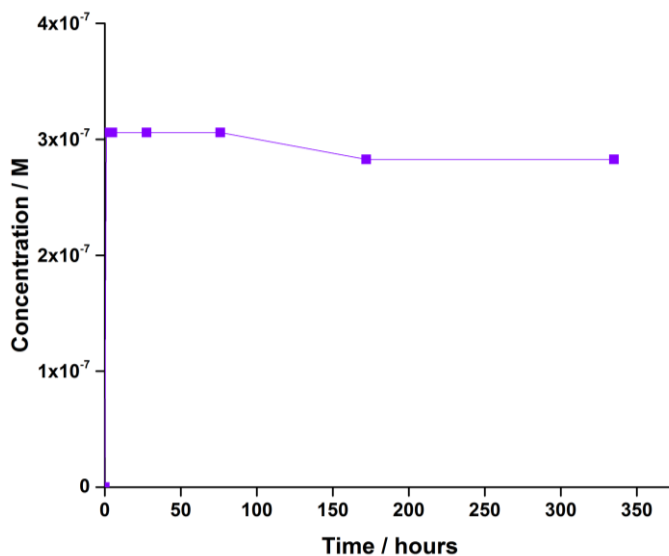
Fig. 2.7 Leaching of crystal violet (mol dm^{-3}) from a CV-coated silicon polymer into PBS solution at   37 ^{o}C, was measured as function of time (hours).

A major problem of PDT is that the photosensitizer can localize at high concentrations within the body or onto the skin.[257] For instance, the unwanted accumulation of a photosensitizer to the skin can cause swelling, sunburn and blistering.[258] Therefore, this would not be an issue for CV-incorporated PDMS as a potential material for invasive devices since the amount of dye that leached from the polymers was minimal.

2.3.4: Bactericidal activity

The antibacterial activities of both untreated and CV-embedded silicon polymers were assessed against two common hospital-associated pathogens; the Gram-negative bacterium, *E. coli* and the Gram-positive bacterium, *S. aureus.* A white light source similar to those commonly found in UK hospitals was used to activate the antimicrobial activity of the dye-coated polymer.

Fig. 2.8 demonstrates that neither the control silicone sample, nor silicone containing CV showed significant bactericidal activity in the dark for 2 h. On the other hand, exposing the CV-containing polymer to light resulted in the most potent lethal photosensitization with bacterial numbers reduced below the detection limit (P = 0.002) compared to the control elastomer sample after 2 h of exposure to a white light source emitting an average light intensity of 6500 ± 300 lux at a distance of 16 cm from the samples.

When tested against E. coli in the dark over a period of 4 h (**Fig. 2.8**), no reduction in the numbers of *E. coli* was observed for the untreated polymer. Similarly, there was no detectable kill on the surface of the CV-encapsulated silicone samples stored in the dark for the same period of time. However, the samples containing CV showed a significant lethal photosensitization resulting in a statistically significant reduction in the number of *E. coli* following exposure to white light for 4 h. (> 4 log reduction; P = 0.002)

Overall, these results indicate that the polymer with encapsulated dye is not toxic to bacterial cells without a light source but exhibits highly significant bactericidal activity in the presence of light. Also, the difference in susceptibility between Gram-positive and Gram-negative bacteria has been observed in other studies with the latter generally more resistant presumably as a result of their more complex cell wall structure.[259]
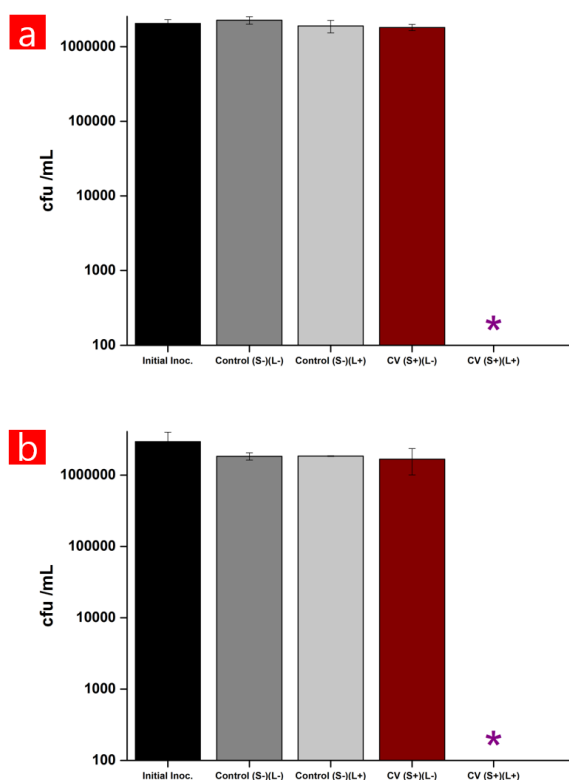
Fig. 2.8 Numbers of (a) *S. aureus* and (b) *E. coli* on the surfaces of the polymers after 2 h and 4 h exposure, respectively. Bars on the graph represent the: initial inoculum, control elastomer (control) and CV-encapsulated elastomer (CV). (L+ = white light exposure, L- = no white light exposure, S+ = CV dye present, S- = CV dye not present). The asterisk indicates where the bacterial numbers are below the detection limit of 100 cfu/mL.

In order to validate the antibacterial performance of the polymers fabricated in this chapter, their photobactericidal activity was compared to other antibacterial CV-containing surfaces published in the literature. Over the last decade, The Materials Research Centre at University College London (UCL) has used a facile, well-established "swell-encapsulation-shrink" technique to incorporate different photosensitizer dyes into medical grade polymers that has led to the development of potent light-activated antimicrobial materials that induce the lethal photosensitization of both Gram-positive and Gram-negative bacteria.[260–262] This can either be achieved upon short-term illumination using a laser source,[260–262] or over a longer duration using standard hospital lighting to activate the photobactericidal activity of the polymer .[261] Overall, these studies have concluded that the

antibacterial activity of a LAAA depends on the concentration of the agent, the exposure time, and they are usually more effective against Gram-positive bacteria compared to Gram-negative bacteria.[263,264] Moreover, the production of ROS is correlated with the light intensity, and a ~600 nm laser was demonstrated to be more effective compared to white light from a hospital lamp because of higher flux. However, laser technology is not practical to be used in the sterilization of commonly touch surfaces in healthcare facilities. On the other hand, while white light, from a common hospital light source, can be easily applied. Hence, white light-activated antibacterial surfaces are of great interest. For instance, the data presented here shows that a relatively short white light illumination time of CV-PDMS is more effective at killing the Gram-positive bacterium, *S. aureus*, than either methylene blue-polyurethane or toluidine blue-polyurethane (2 h vs. 24 h).[265] The difference in efficacy may be correlated with the diffusion distance of ROS. The diffusion distance of singlet oxygen has been previously estimated as around 0.2 microns within the polymer.[266] Since MB and TBO are distributed evenly throughout the polymer, the dyes incorporated within the polymer will not contribute to antibacterial activity and only dye near the polymer surface will play a role. Therefore, we speculated that high concentrations of CV on the surface of the polymer would lead to increased production of ROS thereby increasing the kill of surface-loaded bacteria.[261]

In addition, Sandeep *et al.*[267] incorporated crystal violet into polyurethane. When irradiated with white light for 2 h, CV-coated polymers demonstrated a 1 log and 1.4 log reduction in *S. aureus* and *E. coli*, respectively. In another study,[268] CV embedded polyurethane showed some photodynamic antibacterial activity against *E. coli* and *S. aureus,* causing 0.5 and 2 log orders of both bacteria, respectively, with illumination of white light (28-W domestic lamb bulb) for 2 h. These results highlight the effective photobactericidal activity caused by the CV-embedded PDMS surfaces reported here, resulting in the lethal photosensitization of both *S. aureus* and *E. coli* in 1.5 and 3 hours, respectively.

In this chapter, it was shown that CV could make PDMS antimicrobial towards representative Gram-positive and Gram-negative bacteria that are significant causes of nosocomial infection under ambient light conditions. Thus, this self-disinfecting surface can be employed in a wide range of application areas from healthcare environments to

electronic devices including tablet and mobile phone covers and computer keyboards. The intensity of the white light source utilized to activate the photo-antimicrobial properties of the polymer was 10500 ± 250. The lighting conditions in this study can be compared to the brightness of different locations in UK hospitals, as recommended by the Department of Health (Table 2.2).[259,269,270] Therefore, it is anticipated that it would be more efficacious to employ light-activated antimicrobial coating in examination rooms and operating theaters, where light intensities are highest.

Table 2.2 Recommended light intensities for various areas in the UK healthcare environments.[259,269,270]

Environment	Light intensity /lx
Operating theatre	10 000-100 000
Pathology lab	8000
Ward corridors	≥ 200
A & E examination room	1000

However, it is also possible to achieve significant kills in areas of lower light intensity if the illumination time is prolonged. In addition, it should be noted that in these experiments, very high bacterial loads (~ 6.3 x 10^4 cfu cm^{-2} for *E.coli*, ~ 5.1 x 10^4 cfu cm^{-2} for *S.aureus*) were used to examine the antibacterial effect of the polymer, much higher than the levels reports on contaminated hospital surfaces (up to an equivalent of 3060 cfu cm^{-2} with average values of <100 cfu cm^{-2}).[261]

2.4: Conclusion

In this work light-activated antimicrobial PDMS polymer was prepared successfully using a facile swell-encapsulation-shrink method utilizing CV. When photo-activated by a standard hospital light source, the CV embedded polymer was potent at killing suspensions

of *S. aureus* in just 2 hours and *E*. coli in just 4 hours, with a minimum of a 4-log reduction in the numbers of both bacteria. Consequently, the presence of CV in PDMS can extend its use in antimicrobial applications.

Chapter 3: SYNERGETIC COMBINATION OF ZINC OXIDE NANOPARTICLE WITH CRYSTAL VIOLET AS A WHITE-LIGHT ACTIVATED ANTIBACTERIAL PAINT

3.1: Introduction

Metallic nanoparticles (NPs) are promising antibacterial agents owing to their large surface area to volume ratio, suggesting an alternative pathway to combat the ever-increasing bacterial resistance problem.[271] Of them, ZnO is a striking one because of its excellent stability, robustness, biocompatibility and long shelf life.[272,273] The antibacterial activity of ZnO has been well exploited under irradiation with light (UV or white light) and in the absence of light.[274–278] Similar to LAAAs, the proposed mechanism of their antibacterial activity is thought to be *via* oxidative stress as a result of ROS production[279] though additional mechanisms have also been proposed.[109,112,113,194,280]

Further enhancement of antibacterial activity of photosensitive dyes has been observed upon incorporation of various NPs (e.g silver, gold and zinc oxide).[262,267,268] Even though these materials show potent photobactericidal activity, they include complex, labor-intensive, time consuming synthesis of NPs. Also, these NPs can be implemented only to soft materials such as polymers and silicones by the ''swell-encapsulation-shrink'' process.

In this chapter, a simple, scalable and versatile approach is reported for fabricating highly efficacious white-light activated self-sterilizing surfaces applicable for a broad range of substrates, by mixing commercial ZnO NPs and PDMS followed by CV incorporation. This type of material outperforms its counterparts in many aspects such as its ease of fabrication, the inexpensive materials utilized, in addition to the material's high versatility for being coated on a wide range of substrates (e.g metal, glass, wood and soft polymer plates) (**Fig. 3.2**). The objective of this work was to examine the effectiveness of CV-incorporated nanoparticle doped polymer matrix in killing two common pathogens: the Gram-negative bacterium, *E. coli* and the Gram-positive bacterium, *S. aureus*, commonly correlated with nosocomial infection. The results showed that the synergistic combination of CV and ZnO NPs led to superior antibacterial activity of the polymers.

3.2: EXPERIMENTAL

3.2.1: Chemicals and Substrates

The reagents and substrates used in materials synthesis were as follows: Crystal violet (Sigma, U.K), acetone (VWR), ~ 60 nm Zinc oxide nanoparticles (Sigma, U.K) and the substrate was SYLGARD® 184 Silicone Elastomer (Dow Corning Corporation Ltd.)

3.2.2: Materials Synthesis

3.2.2.1: Elastomer preparation

Blank silicone elastomers were prepared using viscous liquid polydimethylsiloxane (Dow Corning Corporation Ltd.) as a starting material; this was mixed with the crosslinking agent in a 10: 1 ratio, and spread uniformly on to glass substrates followed by curing at 100 °C for 45 min. After the cooling, the polymer sheets were peeled off from the substrates and were cut into smaller pieces (squares 2.0 x 2.0 cm).

3.2.2.2: Preparation of ZnO-NPs/PDMS composites

Polymer/nanoparticle composites with varying contents of ZnO fillers (0 wt%, 0.5 wt%, 1 wt%, and 5 wt%) ZnO NPs (Sigma Aldrich, UK) with different concentrations (1,2,3, wt% ZnO NPs) were dispersed in PDMS (10: 1 ratio). This mixture was homogenized by hand-stirring. Afterwards, the slurry was degassed in a desiccator for 15 min followed by casting on glass substrates. Finally, they were cured in a pre-heated oven (100 °C) for 45 min.

3.2.2.3: Preparation of polymers with embedded crystal violet

Crystal violet solutions (CV) were prepared at a concentration of 750 ppm in acetone (Sigma Aldrich). 2.0 cm^2 samples of both the un-doped PDMS and the ZnO-containing polymers were placed into the CV solutions and left to swell for 24 h. The samples were removed, washed and left to dry in the dark at room temperature for 24 h.

Table 3.1 The polymer matrices embedded with photosensitizer dye and different ZnO NP contents represented by various sample IDs and average contact angle measurements (°) ± standard deviation of the samples.

Sample ID	ZnO (g)	PDMS (g)	Photosensitizer (CV)	Water Contact angle (°)
PDMS(Control)	-	10.0	-	97.0 ± 1.80
CV	-	10.0	+	100.8 ± 0.82
0.5Zn	0.5 g	10.0	-	96.1 ± 3.51
0.5Zn-CV	0.5 g	10.0	+	102.9 ± 3.30
1.0Zn	1.0 g	10.0	-	98.3 ± 1.57
1.0Zn-CV	1.0 g	10.0	+	99.5 ± 1.37
5.0Zn	5.0 g	10.0	-	100.0 ± 4.62
5.0Zn-CV	5.0 g	10.0	+	102.4 ± 0.98

3.2.3: Materials characterization

A PerkinElmer Lambda 950 UV-vis spectrometer was used to measure the UV-vis absorption spectra of the polymers within the range 400–700 nm. IR analysis of the polymers was performed within the range of 400–4000 cm^{-1} with an accumulation of 16 scans per sample using a Bruker Platinum ATR. X-ray diffraction pattern was carried out using a Stoe diffractometer with monochromated Mo Kα1 radiation (λ = 0.7093 Å) in transmission mode over the angle range 2–40°/2θ°.

3.2.4: Functional Testing

3.2.4.1: Water contact angle measurements

Equilibrium water contact angle measurements (~ 3.0 μL) were measured for each type of sample using a FTA 1000 Drop Shape Instrument. The average contact angle measurement over ≥ 5 measurements was calculated, using a droplet of deionized water dispensed by gravity from a gauge 30 needle, with a camera that photographed the samples side on. The data was analyzed using FTA32 software.

3.2.4.2: Leaching test

The stability of the CV coated elastomers in solution was determined: the CV coated sections (2.0 x 2.0 cm^2) were immersed in phosphate buffered saline (PBS) (2.5 ml, 37 °C) for an extended period of time. The UV-vis absorbance of the PBS (596 nm, Pharmacia Biotech Ultrospec 2000) was measured periodically to monitor leaching of the CV from the polymer into the surrounding solution. The concentration of the CV in solution was determined on the basis of its absorbance at 596 nm, comparing it with a calibration curve.

3.2.4.3: Dye Adherence Testing

All samples containing crystal violet were wiped rigorously with a 70% isopropyl alcohol wipe (AZOwipeTM, Synergy Health) to determine whether the dye adhered to the sample surface.

3.2.5: Bactericidal assay

A range of elastomer samples (2 cm x 2 cm^2) was used in the antibacterial experiments: pure PDMS polymer (control), zinc oxide-incorporated (ZnO), crystal violet coated PDMS (CV), 0.5 % ZnO-doped PDMS (0.5Zn), 0.5 % ZnO-doped PDMS with CV (0.5Zn-CV), 1 % ZnO-doped PDMS (1.0Zn), 1 % ZnO-doped PDMS with CV (1.0Zn-CV), 5 % ZnO-doped PDMS (5.0Zn) and 5 % ZnO-doped PDMS with CV (5.0Zn-CV). These samples were evaluated against *E. coli* ATCC 25922 and *S. aureus* 8325-4 . The bacteria were stored at -70 °C in Brain-Heart-Infusion broth (BHI, Oxoid) containing 20% (v/v) glycerol

and propagated on either MacConkey agar (MAC, Oxoid Ltd.) in the case of *E. coli* or mannitol salt agar (MSA, Oxoid Ltd.) in the case of *S. aureus*, for a maximum of 2 subcultures at intervals of 2 weeks.

BHI broth (10 ml) was inoculated with 1 bacterial colony and cultured in air at 37 °C for 17 h with shaking, at 200 rpm. The bacterial pellet was recovered by centrifugation (20 °C, 4000 x g, 5 min), washed in PBS (10 ml) and centrifuged again (20 °C, 4000 x g, 5 min) to recover the bacteria, which were finally re-suspended in PBS (10 ml). The washed bacterial suspension was then diluted 1 in 1000 in PBS to give an inoculum of approximately 10^6 cfu ml^{-1}.

Duplicates of each polymer sample were inoculated with 25 μl of the inoculum and covered with a sterile cover slip (18 mm x 18 mm). The samples were then irradiated for up to 90 min in the case of *E. coli* and 45 min in the case of *S. aureus* utilizing a white light source (General Electric 28 W Watt MiserTM T5 2D compact fluorescent lamp). The light intensity was arranged to emit an average light intensity of 6500 ± 300 lux at a distance of 25 cm from the samples. A further set of samples (in duplicate) was maintained in the dark for the duration of the irradiation time. Post irradiation, the inoculated samples and cover slips were placed into PBS in a 50 ml plastic tube and vortexed for 60 seconds. The neat suspension and tenfold serial dilutions were plated on the appropriate agar incubated aerobically overnight at 37 °C and the colonies enumerated to determine the number of surviving bacteria. The bacterial numbers in the inoculum were also determined in each experiment by viable colony counting. Each experiment included two technical replicates and the experiment was reproduced three times. The data was analyzed using the Mann–Whitney U test.

3.3: Results and Discussion

3.3.1: Materials Synthesis

CV and ZnO NPs were incorporated into PDMS by a facile two-step procedure to fabricate a potent bactericidal polymer-nanocomposite. The first step involved mixing ZnO NPs

with an average diameter of 60 nm with PDMS (monomer: crosslink = 10:1 in mass) by mechanical rabbling on the basis of a series of PDMS/ZnO NPs with varying nanoparticle content as shown in **Table 3.1**. Then, the resultant milky polymer was degassed under vacuum to remove entrapped air bubbles. Finally, the polymer was cast on glass substrates and cured in a pre-heated oven at 100 °C. While PDMS is transparent, the ZnO-embedded polymers are white.

In the second step, these modified polymers were coated with CV by using a ''swell-encapsulation-shrink'' method. In this process, the polymer squares (2 x 2 cm) were immersed in 750 ppm CV solutions in acetone for 24 h under dark conditions. They were subsequently removed from the solution, washed and towel dried, resulting in a dark purple-coloured polymer square indicating an efficacious uptake of the dye onto the polymer surfaces (**Fig. 3.1**).
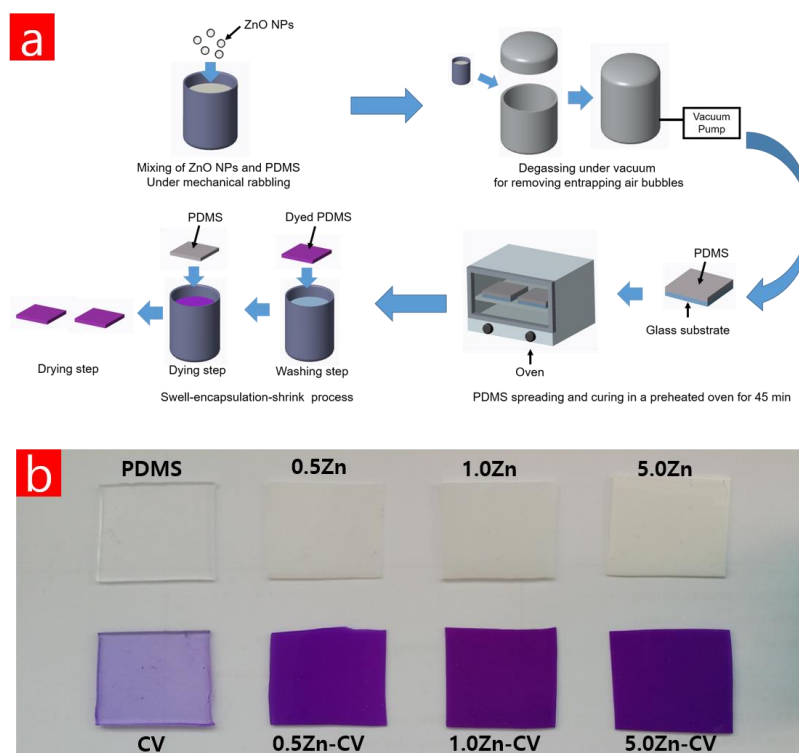
Fig. 3.1 (a) Schematic view and process flow of the polymer paint containing ZnO and CV. (b) Photograph of the PDMS/ZnO samples with different nanoparticle content (0.50 to 5.0 wt%) samples before -on the top- and after the swell-encapsulation-shrink   process in acetone with 750 ppm of crystal violet –on the bottom.
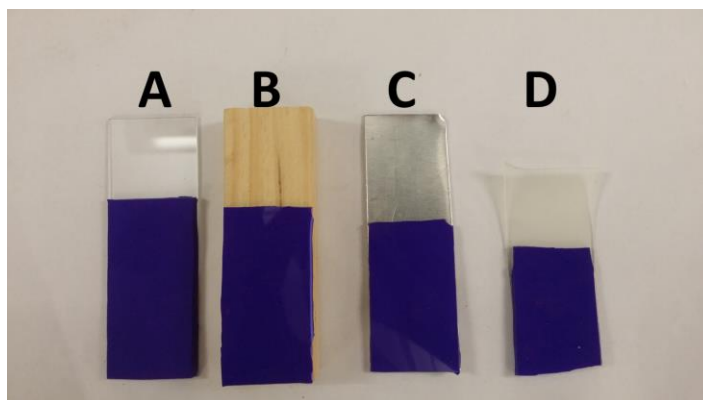
Fig. 3.2. White light activated antibacterial paint coated (a) glass, (b) wood, (c) metal (aluminum), and (d) soft polymer (polyurethane) plates.

3.3.2: Materials Characterization

Fig. 3.3 shows FT-IR spectroscopy of the polymer films, from which no significant change was confirmed across the ZnO/PDMs composite films from 0 to 5 wt% of ZnO nanoparticle concentration before and after the "swell-encapsulation-shrink" process. The similarity between the untreated and treated samples can be attributed to the strong absorbance bands of the polymer and because of the low concentrations of dye present in the samples. Consequently, the results indicate that the incorporation of ZnO NPs and CV in the silicones had no significant influence on the internal structures of the films within the detection limit of FT-IR. IR spectra only gave peaks related to the host polymer matrix.
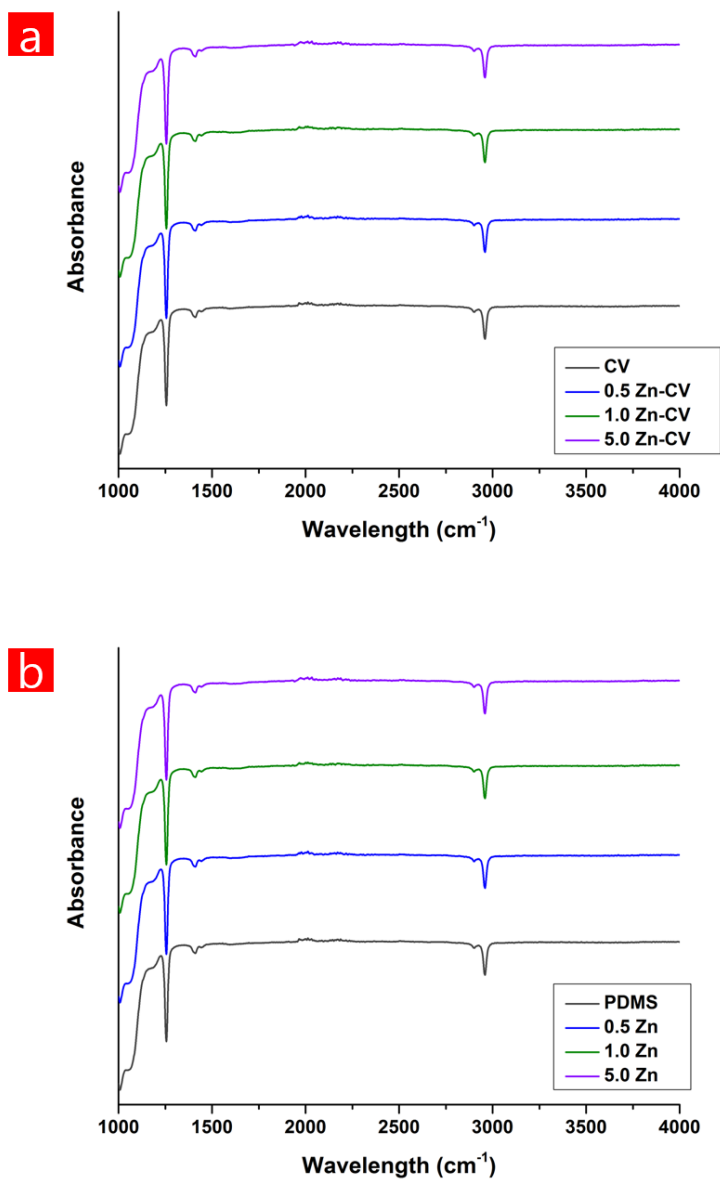
Fig. 3.3 FT-IR spectra of ZnO/PDMS composite films (a) before and (b) after the swell-encapsulation shrink process in acetone with 750 ppm of crystal violet.

The presence of the ZnO NPs was confirmed by X-ray diffraction (XRD) and functional testing of the polymer films. The X-ray diffraction of neither the 0.5Zn nor the 1.0Zn samples displayed no discernible reflection because of the low density of the ZnO NPs embedded within the polymers, while the peaks of crystalline plane of ZnO appeared when ZnO concentration increased to 5.0 wt% (**Fig. 3.4**). (Peaks at $2\theta = 31.7°$, $34.4°$, $36.2°$,

47.6°, 56.5° assigned to (100), (002), (101), (102) and (110) planes, respectively). Also, it can be seen that the incorporation of CV into the polymer does not impact on the internal structure of the polymer film, in good agreement with the experimental results of Fig. 3.2.
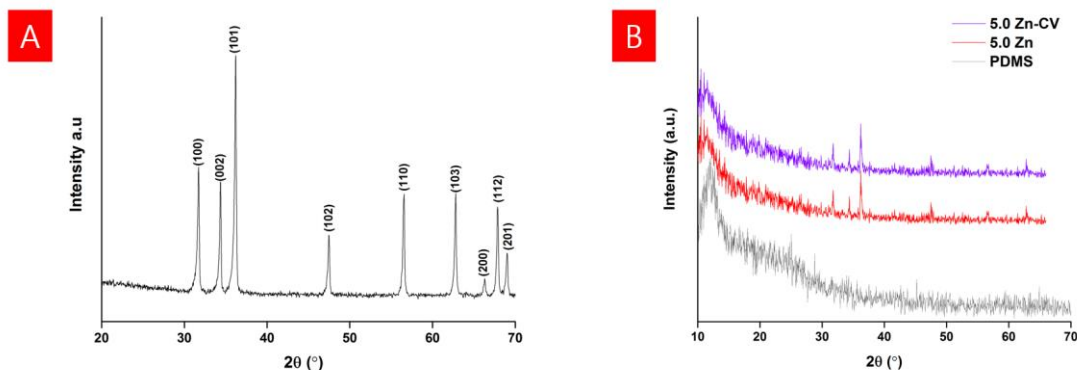
Fig. 3.4. XRD pattern of (a) ZnO nanopowder and (b) PDMS, 5.0Zn and 5.0Zn-C. The peaks were indexed to polycrystalline wurtzite structure.

The UV-vis absorbance spectra of uncoated and CV-coated silicone samples were measured between 450-700 nm (**Fig. 3.5**). While bare PDMS does not give any absorbance peak in the visible region, when coated with CV, the main absorption peak of PDMS containing CV alone is at $\lambda \approx 590$ nm, with a shoulder peak of weaker intensity at $\lambda \approx 533$ nm. Regarding the ZnO-CV samples the peak maxima and intensity is very different, which demonstrates that dye uptake increases with the increase in ZnO concentration. This phenomenon has been demonstrated in another study in which gold nanoparticles enhanced the UV-visible absorption of toluidine blue.[281]
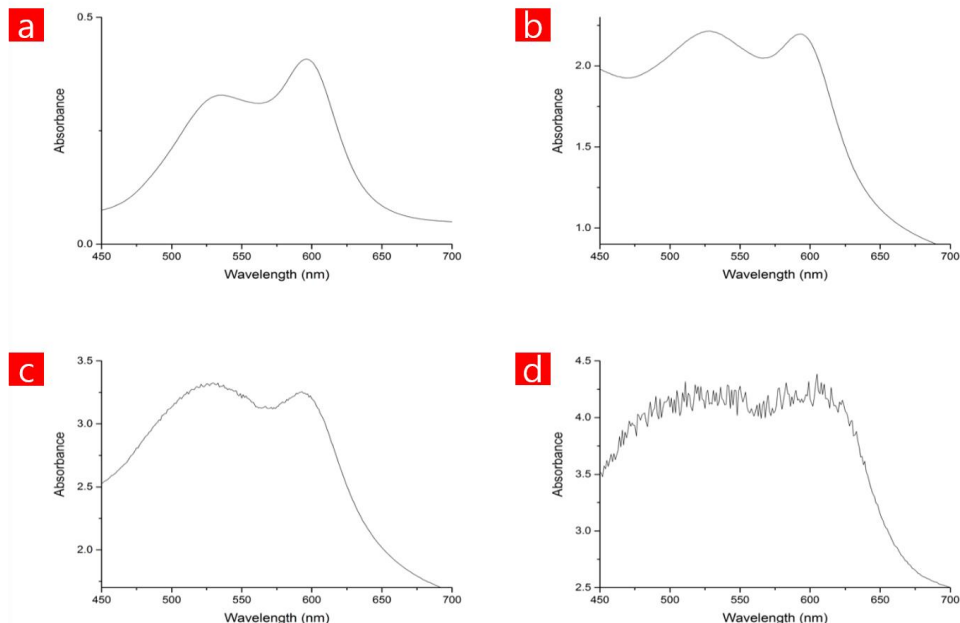
Fig. 3.5 UV-vis absorbance spectra of (a) CV, (b) 0.5Zn-CV, (c) 1.0Zn-CV and (d) 5.0Zn-CV.

The contact angles of water on the silicone samples are measured (**Table 3.1**). It is obvious that the surface of pure silicone was hydrophobic with a water contact angle of 97.0° ± 1.8 while no significant difference in the wetting properties of the treated samples was observed, varying in contact angle ± 6 degree.

In order to examine whether there was leaching of the dye-incorporated polymers, they were placed in 10 ml of PBS solution at 37 °C and the CV leachates were measured spectroscopically as a function of time (**Fig. 3.6**). It can be seen that all of the CV-coated samples leached dye into PBS after 24 h and that the amount of CV leaching was correlated with increasing the nanoparticle weight. Over a period of more than 300 hours, the CV concentration of all of the samples plateaus at below 8.5×10^{-7} M and overall, no further leaching was observed, indicating stability of the dye in the polymers. In addition, a similar set up was used to detect whether the ZnO-incorporated samples release nanoparticle into PBS solution. There was no observable change in the amount of leaching, the colour or conductivity of the solution (data not shown), showing that, in contrast to CV, the ZnO in the polymer matrix is more stable to leaching in contrast to CV.
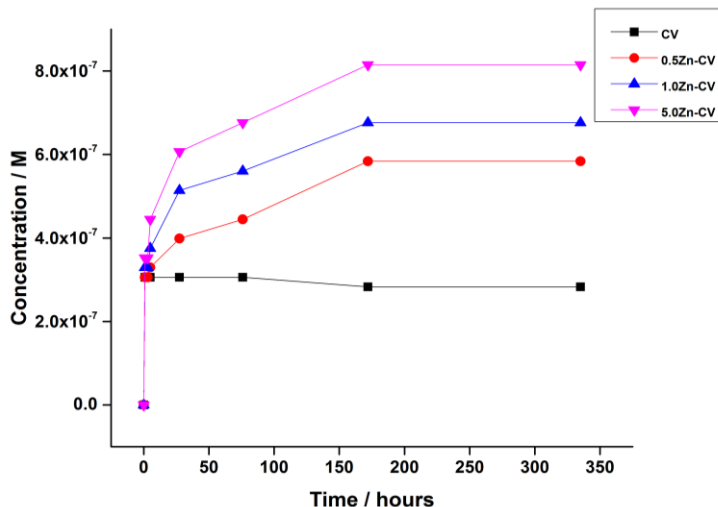
Fig. 3.6 Leaching of crystal violet (mol dm^{-3}) from the polymer into PBS solution at 37 °C was measured as a function of time (hours).

3.3.3: Antibacterial activity

The antibacterial activity of a series of modified silicone samples was testing using representative Gram-positive and Gram-negative bacteria, *S. aureus* and *E. coli*, respectively, both of which are key causative agents of HAIs. A General Electric 28 W Watt MiserTM T5 2D compact fluorescent lamp, similar to those commonly found in UK hospitals, was used to activate the antibacterial activity of the dye-coated polymers while a control set of polymers was stored under dark conditions for the duration of white light illumination.

The photo-activated and intrinsic bactericidal activities of the following samples were tested: undoped PDMS polymer (control), zinc oxide-incorporated (ZnO), crystal violet coated PDMS (CV), 0.5 % ZnO-doped PDMS (0.5Zn), 0.5 % ZnO-doped PDMS with CV (0.5Zn-CV), 1 % ZnO-doped PDMS (1.0Zn), 1 % ZnO-doped PDMS with CV (1.0Zn-CV), 5 % ZnO-doped PDMS (5.0Zn) and 5 % ZnO-doped PDMS with CV (5.0Zn-CV).

Fig. 3.7(a) demonstrates the lethal photosensitization of *S. aureus* when exposed to the different polymers in the dark or following 45 min of exposure to a white light source emitting an average light of 6500 ± 300 lux at a distance of 25 cm from the samples. Under

dark conditions (45 min), none of the samples showed significant kill of *S. aureus*. Similarly, exposure to white light over a period of 45 min caused no significant decrease in the number of viable *S. aureus* on the 0.5 Zn sample surface compared to the control sample. However, a greater reduction in bacterial numbers was apparent on the surfaces of both the 1.0Zn and the 5.0Zn samples (*P*-value < 0.01 for both). Furthermore, the 0.5Zn-CV combination caused an approximately 1 log reduction in bacterial numbers, with enhanced kill compared to the sample containing CV alone (0.35 log reduction). The effect of both the 1.0Zn-CV and the 5.0Zn-CV was even more remarkable, reducing bacterial numbers to below the detection limit (≥4 log) following exposure to white light for 45 min.
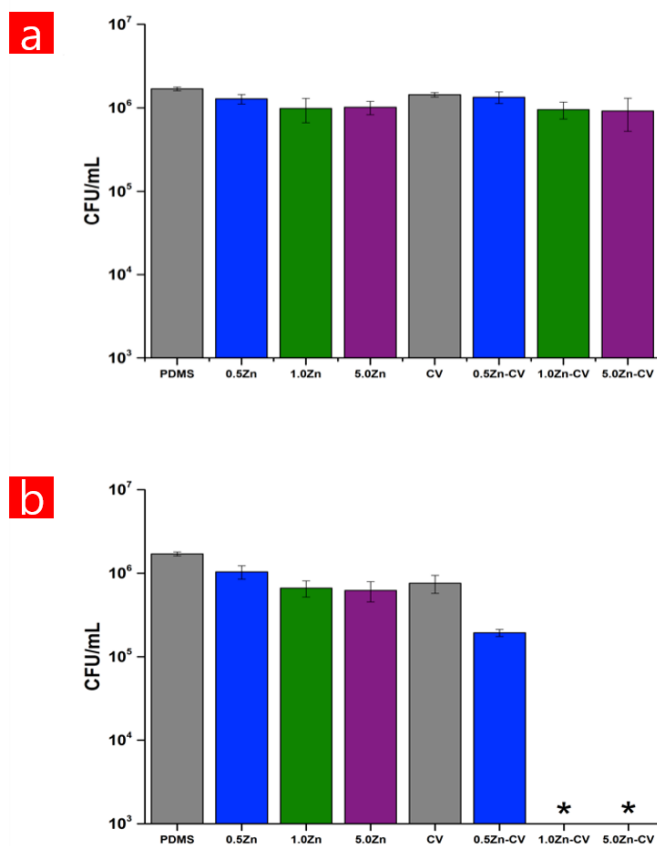
Fig. 3.7 Viable counts of *S. aureus* 8325-4 after incubation on modified PDMS polymers incubated at 20 °C under (A) dark conditions and (B) exposed to white light illumination for 45 min. * Indicates where the bacterial numbers are below the detection limit of 1000 cfu mL^{-1}.

The photo-activated and intrinsic bactericidal activities of the same polymers were investigated against the Gram-negative bacterium, *E. coli*, under the same conditions but with a longer exposure time. **Fig. 3.8** demonstrates the activity of the samples against *E. coli* in the dark over a 90 min period, where no significant reduction in the numbers of viable bacteria was observed on the surfaces of 0.5Z, 1.0Z and 5.0Z samples compared to the control polymer. On the other hand, except the polymer containing CV alone all the samples containing ZnO and coated with CV displayed statistically significant (*P*-value < 0.01) activity relative to the control sample.
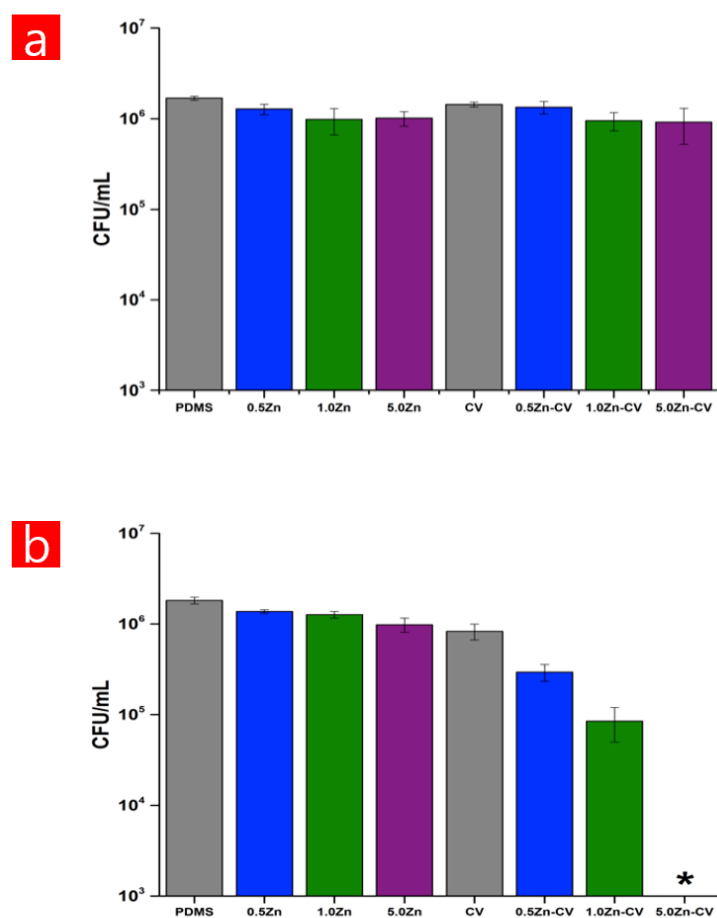
Fig. 3.8 Viable counts of *E. coli* after incubation on modified PDMS polymers incubated at 20 °C under (A) dark conditions and (B) exposed to white light illumination for 90 min. * Indicates where the bacterial numbers are below the detection limit of 1000 cfu mL^{-1}.

Exposure to white light for a period of 90 min induced significant decreases in the number of viable bacteria was observed on the 0.5Z-CV sample (0.70 log reduction) and the 1.0Z-CV sample (1.33 log reduction). Moreover, the 5.0Z-CV displayed a highly significant reduction in bacterial numbers after 90 min of irradiation, with bacterial numbers reduced to below the detection limit ($\geq$4 log, *P*-value = 0.002).

As expected from previous studies, there was a difference between the bactericidal activity of the polymers against the Gram-positive and the Gram-negative bacteria, which is most probably due to the differences in cell wall structures.[266] Gram-positive bacteria possess a single thick peptidoglycan layer while Gram-negative bacteria contain a thinner peptidoglycan layer but possess a second (outer) membrane,[249] making them less susceptible against photodynamic inactivation compared to Gram-positive bacteria.[261,282] Overall, the results show that the polymer containing ZnO or CV alone does not possess potent antibacterial properties. Hence, it is required to combine both agents into the polymer to fabricate a superior self-sterilizing material that shows efficacious photobactericidal activity against both *E. coli* and *S. aureus*.

The mechanism of antibacterial activity of ZnO is still unclear but there are various mechanisms proposed in the literature, including the production of ROS,[274,275,283–287] the release of zinc ions[192,276,283,288] and the accumulation of NPs in the bacterial cytoplasm and on the outer membrane of Gram-negative bacteria.[274] Some studies showing significant antibacterial activity of ZnO in the dark attributed this to the release of zinc ions from a ZnO suspension that penetrate into the bacteria damaging DNA and resulting in cell death.[193,278,289] However, there are many studies indicating that the concentrations of released Zn^{2+} ions were not high enough to cause the nanotoxicity.[274,275,290,291] Lakshmi et al. proved that its antibacterial activity is mainly attributed to ROS in the dark[292] rather than release of zinc ions (zinc ion dissolution) and ZnO internalization.[13,194,277,278] They proposed the following mechanism for the generation of ROS under dark conditions originated from the interaction between water and superoxide radicals that are mediated through singly ionized oxygen vacancy (i.e. surface defects).

$$O_2 + e^- \rightarrow \bullet O_2^-$$

$$\bullet O_2^- + H_2O \rightarrow \bullet HO_2 + OH^-$$

$$\bullet HO_2 + \bullet HO_2 \rightarrow H_2O_2$$

$$H_2O_2 + \bullet O_2^- \rightarrow O_2 + \bullet OH + OH^-$$
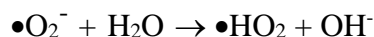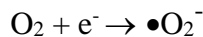
In contrast to ZnO, the antibacterial behavior of CV is well established. Upon illumination of the dye, two different photochemical pathways; one is to generate hydroxyl radicals ($\bullet OH$) and superoxide ions ($O_2 \bullet^-$) through electron transfer process (Type I) or singlet oxygen ($^1O_2$) through energy transfer (Type II).[293] Photo-generated ROS can attack bacteria *via* a non-site specific multiple attack mechanism (unlike antibiotics which usually have a singlet target) including the disruption of cellular membranes and DNA by means of oxidative damage, making bacteria unlikely to develop resistance since resistance normally develops when a bactericide has a singletarget.[165,256,294]

To validate the antibacterial effectiveness of these surfaces, their photobactericidal activity was compared to other antimicrobial systems published in the literature. For example, Sehmi *et al*. reported CV-coated ZnO NPs (18.3 ± 4.9 average diameter size) incorporated polyurethane squares via a two-step dipping procedure. Upon illumination with a white light source (6600 ± 990 lux), these materials induced lethal photosensitization of both *E.coli* and *S.aureus* in 1 and 4 hours, respectively, with bacterial levels reduced below the detection limit of 10^2 CFU mL^{-1}.[295] Another similar work was carried out by incorporating smaller ZnO NPs (3.3 ± 1.1 average diameter size) with CV into polyurethane squares. Illumination of these samples using a white light source (3750 ± 250 lux) caused 3.36 log kill of *S. aureus* after 1 h. Under the same conditions, lethal photosensitization of *E. coli* was observed after 6 h with ≥ 4 log reduction in bacterial numbers.[249] Improved bactericidal efficacy was observed with the the 5.0Zn-CV surfaces reported here, achieving decreases in bacterial numbers of greater than 4 logs for both *S. aureus* and *E. coli* in only 45 and 90 min, respectively.

Crystal violet, a topical antiseptic, possesses antibacterial, anti-fungal properties.[253] It is still listed by the World Health Organization even though new drugs have superseded its use in the medical field and clinical trials showed its efficiency to treat infected wounds, superficial skin and MRSA infections.[296,297] Regarding real-world applications, it is imperative that the dye incorporated in the polymer does not leach significantly or rub off upon contact with hands or disinfectant wipes that are often used to reduce the risk of the spread of infection. To determine the stability of the modified polymers, they were vigorously wiped with AZO wipes that are utilized to clean hard surfaces on the wards in University College London Hospital NHS Trust hospitals. There was no visual evidence of dye removal from the modified polymer after rigorous wiping with 70% alcohol, and hence, transmission of dye upon touching is unlikely. Furthermore, the CV-coated samples have showed excellent stability under aqueous solutions at 37 ˚C. The amount of CV leached from the samples was relatively small relative to the concentration (20 000 ppm) resulting in dermal irradiation or sensitization over an extended period of clinical assessment.[297] Also, adverse effects of the NP on human health should be considered. Since ZnO NPs have been widely utilized in the cosmetics and food industry, their toxicity on humans has been extensively investigated, with a conclusion that it depends on many factors such as their size, shape, route of administration and dosage. Studies have showed that their penetration through skin is improbable although other routes of administration of these nanoparticles can demonstrate harmful effects at high doses (>100 μg mL^{-1}).[298,299]

3.4: Conclusion

In this study, ZnO NPs have been successfully embedded with different nanoparticle concentration in PDMS followed by incorporating CV using a simple ''swell-encapsulation-shrink'' process to fabricate a light-activated antibacterial paint. The ZnO/CV composites possess superior antibacterial activities that are dependent upon the concentration of zinc in the polymer films. Among them, the 5.0Zn-CV is proved to be very efficacious antibacterial polymer surface, which are active in light conditions relevant to UK hospitals and exhibiting lethal photosensitization of *S. aureus* in just 45 min and of *E. coli* in just 90 min, with a minimum of a 4-log reduction in the numbers of both bacteria. Therefore, it has potential applications from healthcare settings to electronic devices (e.g.

tablet covers) to help reduce bacterial surface contamination and thus reduce the risk of the spread of infection.

Chapter 4: COPPER-BASED SUPERHYDROPHOBIC AND ANTIBACTERIAL COATINGS BY AEROSOL ASSISTED CHEMICAL VAPOUR DEPOSITION

4.1: Introduction

Pathogens such as MRSA, *E. coli* and *C. difficile*, can survive for long periods of time on inanimate surfaces, making a continuous source of transmission of infectious agents. Biofilms can form in 24 hours when microbial cells stick to each other and attach to a surface,[300] causing approximately 80 % of all medical infections. Also, cells protected by an extracellular matrix within biofilms can be up to 100-1,000 times more resistant to antibiotics and disinfecting agents compared to planktonic cells.[301] Bacterial colonization of surfaces is known to have an adverse effect on the function of a diversity of materials such as textiles, medical catheters, dental implants and resistant contact lenses.[302–304]

Antibacterial surfaces may either (i) inhibit the attachment of bacteria i.e. anti-biofouling activity or (ii) destroy bacteria that do attach to the surface i.e. bactericidal activity.[187,188] In this context, the liquid-repellent feature of natural or artificial surfaces plays a crucial role in preventing biofouling by reducing the contact area between bacterial cells and the surface and adhesion strength[305–307]. Studies about the correlation between liquid-repellency and antibiofouling properties can be traced back to the discovery of the "Lotus effect".[211] Lotus leaves possess excellent self-cleaning properties due to the presence of the complex micro/nanoscopic architectures on their leaves that impart superhydrophobicity. Such surfaces show excellent non-wetting properties because of a water angle greater than 150° and water droplets easily roll-off carrying away dirt particles and bacteria.[308] Several studies have demonstrated that bacterial adhesion is significantly influenced by surface wettability. For instance, *Arima et al.* reported that bacteria could effectively adhere onto surfaces with contact angles of 40-70°.[309] Contrarily, Freschauf *et al.* found that various shrink-induced superhydrophobic polymers greatly prevented the attachment of *E. coli*.[216] Even though anti-biofouling surfaces can reduce bacterial adhesion, they are not able to inactivate adherent bacteria. Hence, the combination of antibacterial agents (i.e. copper)

and superhydrophobicity would be most effective at reducing the load of colonizing bacteria relative to materials showing either property alone.

Various nanomaterials such as TiO_2, ZnO and SiO_2 have been demonstrated to exhibit remarkable antibacterial properties. Among these metal-based NPs, copper-based nanomaterials have attracted considerable attention due to their unique chemical, physical and biological properties.[144,310] At low concentrations copper is a cofactor for metalloproteins and enzymes, thus, proving to be a low toxicity material compared to other metals.[311] Copper (Cu) has been known for some time to be an excellent biocide, and both copper ions and NPs have shown antibacterial activity against a broad range of bacterial species.[312–314] Recently, Hassan *et al*. demonstrated both copper and copper-based films showed excellent antibacterial activity against both Gram-positive and Gram-negative bacteria.[315] There are very few reports on synthesis of Cu NPs using a "green method" that does not exert adverse effects to human health and the environment. For medical applications, it is imperative that the synthesis of these NPs should rely on non-toxic chemicals, environmentally benign solvents and renewable materials.

In previous chapters, highly photo-bactericidal polymer surfaces have been fabricated. However, they largely require light to be activated. It has been reported that the average light intensity in hospitals ranges between 1,000 lux in an accident and emergency (A & E) examination room to 10,000-100,000 lux in an operating theatre. Moreover, actual light intensity measurements in some hospital wards were as low as ~200 lux.[316,317] To overcome this problem, this chapter reports the efficacious bactericidal activity of Cu NP-coated PDMS films without the need for light. A simple, eco-friendly and effective technique was proposed for coating small-sized copper nanoparticles (Cu NPs) (~3.5 nm in size) onto a curable silicone polymer, polydimethylsiloxane (PDMS), facilitated by a simple two-step deposition process using aerosol assisted chemical vapour deposition (AACVD). The presence of the Cu-NPs on the superhydrophobic polymer film was confirmed by UV-vis spectroscopy, scanning electron microscopy (SEM), transmission electron microscopy (TEM), energy dispersive X-ray spectroscopy (EDX) and functional testing. The material was characterized using a range of techniques including electron microscopy, water contact angle measurement and elemental mapping. The antibacterial activity of the modified film

was tested against the Gram-negative bacterium, *E. coli* ATCC 25922, and the Gram-positive bacterium, *S. aureus* 8325-4 and the film shows highly significant antibacterial activity against both bacteria (>4 log reduction in bacterial numbers) in 15 min and 60 min, respectively. In addition, all the CVD modified samples results in a significant reduction in bacterial cell adhesion compared to the control materials. Therefore, the combination of antibacterial agents and superhydrophobicity can lead to a new concept in developing novel antifouling materials that has dual mode of action-the superhydrophobicity helps limit bacterial adhesion combined with a copper-induced bacterial kill under any lighting conditions.

4.2: EXPERIMENTAL

4.2.1: Chemicals and Reagents

$CuCl_2.2H_2O$ (Sigma, UK) and L-ascorbic acid (Sigma, UK) were utilized in nanoparticle synthesis. Laboratory solvents were purchased from Fisher Scientific Limited and of the highest possible grade. Sylgard® 184 Silicone Elastomer was purchased from Dow Corning Corporation Ltd, which consists of two-part silicone elastomers (base and curing agent). The precursor, Sylgard 184, can be cross-linked with the curing agent and the final polymer is polydimethylsiloxane (PDMS).

4.2.2: Materials Synthesis

4.2.2.1: Aerosol Assisted Chemical Vapour Deposition

Chemical vapour deposition (CVD) is a versatile technique to deposit gas phase reactants (precursors) onto a solid substrate creating thin films. The process involves first the transportation of precursor molecules into a reaction chamber and to the substrate by an inert carrier gas such as nitrogen and argon. This results in the formation of a solid material on the substrate as a result of a sequence of reactions of gaseous precursor molecules under an activated environment (e.g. heat, light, plasma). The deposition takes place near or on the surface of the substrate, starting with the decomposition of precursor solution followed by physisorption or chemisoption of atoms and nucleation on the surface. Depending upon

the different requirements for particular type of materials, a broad-range of variations of CVD are commonly utilized, including metal-organic CVD (MOCVD),[318] low pressure CVD (LPCVD),[319] plasma enhanced CVD (PECVD),[320] laser assisted CVD (LACVD)[320] and aerosol assisted CVD (AACVD).[321]

In this chapter, aerosol assisted CVD (AACVD) was utilized to create novel polymer-nanocomposite films, which is a liquid-phase CVD process. Primarily precursors are dissolved in a solvent that are vaporized by an ultrasonic humidifier (nebulizer), producing a 'precursor milt'. Afterwards, the generated aerosol is transported into a cold-walled CVD reactor by an inert carrier gas (e.g. N_2). Evaporation of the solvent occurs when the aerosol reaches the pre-heated substrate, after which deposition is made onto the substrate. Molecules that are not deposited can be lost from the activated complex and extracted as waste gas. There are several possible mechanisms for the reactions resulting in film deposition. They include the decomposition of the precursor, heterogeneous nucleation, homogeneous nucleation, adsorption and chemical reactions. The general process during deposition is shown in **Fig. 4.1**.
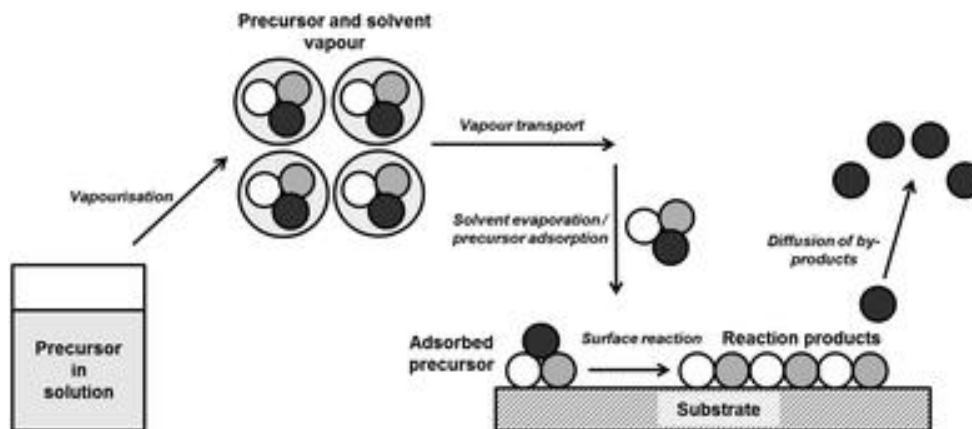
Fig. 4.1 Schematic illustration of the deposition process in AACVD reaction.[321]

4.2.2.2: Aerosol Assisted Chemical Vapour Deposition of Polymer Solutions

The two components of Sylgard® 184 Silicone Elastomer (0.70 g) were dissolved in (70 ml) with rapid stirring. To prevent premature curing the mixture was used immediately after stirring for deposition studies.

The depositions were carried out in a cold-walled horizontal-bed CVD reactor. The reactor contained top and bottom plates, both composed of SiO_2 coated barrier glass (dimensions: 140 x 45 x 5 mm; barrier thickness 50 nm) supplied by Pilkington NSG. A carbon block on which the bottom plate was placed heated the CVD reactor. The top plate was positioned 8 mm above and parallel to the bottom plate, the complete assembly was enclosed within a quartz tube. The aerosol of the precursor solution was generated using a PIFCOHEALTH ultrasonic humidifier with an operating frequency of 40 kHz and 25 W of power. The aerosol generated was moved to the reactor using a nitrogen gas flow via PTFE (polytetrafuoroethylene) and glass tubing, where it entered between the top and bottom plates. The reactor waste gas left *via* an exhaust.

Nitrogen flow carried the vapour from the flask until all liquid was gone, which took typically 50-60 min per deposition. The depositions were carried out at 390 °C and 350 °C respectively with an air-flow of 0.8 L min^{-1}. The thin films of superhydrophobic PDMS and Cu NPs on PDMS were deposited. Then, the heated carbon block was then turned off and allowed to cool to room temperature; the nitrogen flow was left on for a further 15 min. The cooled plates were removed and handled in air. The deposition of the films occurred to the top plate.

4.2.2.3: Deposition of Copper Nanoparticles

Precursors solutions of copper nanoparticles were prepared according to Xiong et al.[322] *In a typical preparation process, $CuCl_2.2H_2O$ aqueous solution was prepared by dissolving $CuCl_2.2H_2O$ (10 mmol) in 50 ml deionized water. A flask containing $CuCl_2.2H_2O$ aqueous solution was heated to 80 °C in an oil bath with magnetic stirring. A 50 ml L-ascorbic acid aqueous solution (0.6 M) was added dropwise into the flask while stirring. The mixture was kept at 80 °C until a dark solution was obtained for 16-18 h.

The copper nanoparticles were deposited using the same AACVD method as described in this section immediately after the deposition of Sylgard without cooling the reactor to room temperature. 5 ml of the solution was diluted to 50 ml with methanol and was used as a precursor solution. The flow rate of 0.8 L/min was used. The deposition of nanoparticles

always occurred on the top plate; the substrate temperature was kept constant at 350 °C.

4.2.3: Materials Characterization

A Perkin-Elmer Lambda 950 UV-vis Spectrometer was used to measure the UV-vis absorption spectra analyses of the copper nanoparticle solution within the range 250-400 nm. Scanning electron microscopy was performed using secondary electron imaging on a JEOL 6301 field emission instrument with Oxford instruments EDX spectrometer attached. Transmission electron microscopy (TEM) images were recorded using a JEOL JEM 1200EX with a 4 megapixel Gatan Orius SC200 charge-coupled device (CCD) camera at an acceleration voltage of 120 kV. Powder X-Ray Diffraction (XRD) pattern was measured on a Bruker-Axs D8 (GADDS) diffractometer using monochromated Cu Kα radiation. Atomic force microscopy (AFM) measurements were performed in air on a Veeco Dimension 3100 using a Nanosurf Easyscan 2 system fitted with a NCLR cantilever. Non-contact tapping mode was used to build a topological map of each sample over a 5 x 5 μm area and roughness statistics extracted using post-process software (Gwyddion). Adherence tests were carried out by applying Scotch Home and Office masking tape to the deposited films with even pressure applied by hand, followed by removal in one swift motion. Any difference in the film appearance was noted.

4.2.4: Functional Testing

4.2.4.1: Surface Hydrophobicity Measurements

Water contact angle measurements were carried out using an FTA-1000 drop shape instrument; $\approx$3 μL water droplets were used to minimize any gravitational effects. The water droplet images were analyzed using a digital protractor to obtain the water contact angles on the surface. A range of points across the substrates was tested, with 5 measurements made on each film. Water slip angles were also measured, noting the angle to the horizontal at which 10 μL water droplets moved on the surface. Many positions across the substrates were tested.

4.2.5: Bactericidal Assay

A range of different samples (1 cm x 1 cm) were used in the antibacterial experiments: uncoated microscope glass (control), uncoated PDMS (PDMS), CVD treated PDMS (S-PDMS) and copper nanoparticle-encapsulated silicone (Cu-PDMS). These samples were evaluated against *E. coli* ATCC 25922 and *S. aureus* 8325-4. The bacteria were stored at -70 °C in Brain-Heart-Infusion broth (BHI, Oxoid) containing 20% (v/v) glycerol and propagated on either MacConkey agar (MAC, Oxoid Ltd.) in the case of *E. coli* or Mannitol Salt agar (MSA, Oxoid Ltd.) in the case of *S. aureus*, for a maximum of 2 subcultures at intervals of 2 weeks.

BHI broth (10 ml) was inoculated with 1 bacterial colony and cultured in air at 37 °C for 17 h with shaking, at 200 rpm. The bacterial pellet was recovered by centrifugation (20 °C, 4000 x g, 5 min), washed in phosphate buffered saline (PBS, 10 ml) and centrifuged again (20 °C, 4000 x g, 5 min) to recover the bacteria, which were finally re-suspended in PBS (10 ml). The washed bacterial suspension was then diluted 1 in 1000 in PBS to give an inoculum of approximately 10^6 cfu/ml.

To ensure that the bacterial suspension did not bounce off the surface of the material, 10 μl of the inoculum was placed gently on to the material from a pipette tip held close to the surface and covered with a sterile cover slip (22 mm x 22 mm) to provide good contact between the bacteria and the surface of the sample. The samples were then incubated at room temperature for the allocated exposure time. Post incubation, the inoculated samples and cover slips were placed into PBS in sterile plastic tubes and mixed on a vortex mixer for 20 seconds. The neat suspension and ten-fold serial dilutions were plated on the appropriate agar, incubated aerobically overnight at 37 °C and the colonies enumerated to determine the number of surviving bacteria. The bacterial numbers in the inoculum were also determined in each experiment by viable colony counting. Each experiment included two technical replicates and the experiment was reproduced three times. The data was analysed using the Mann-Whitney *U* test.

4.2.6: Bacterial Attachment Assay

Bacteria were grown in an overnight culture to 10^7 cfu/ml. Then, 10 μL of the bacterial suspension was placed on the specimen, which was placed at room temperature for 60 minutes. The specimens were then rinsed twice by gently dipping in PBS to remove any unattached cells. Afterwards, the samples were transferred into sterile conical tubes containing 3 mL of fresh PBS. The tubes were mixed using a vortex mixer for 5 minutes and then placed in an ultrasonic bath and sonicated for 15 minutes to release the attached cells from the biomaterial. After an additional vortex mix for 1 min, the suspensions were serially diluted with PBS and enumerated on the appropriate agar plates. The experiment was reproduced five times.

4.3: RESULTS AND DISCUSSION

4.3.1: Material Characterization

4.3.1.1: Characterization of Copper Nanoparticles

A simple green route was utilized to produce the Cu NPs by drop-wise addition of L-ascorbic acid to copper (II) chloride solution at 70 °C. The dispersion became colourless when L-ascorbic acid was added, and gradually turned to yellow, orange, brown and further heating resulted in a dark brown solution indicating that reaction was completed. Non-toxic antioxidant, L-ascorbic acid, was used as both reducing Cu^{+2} to Cu^0 and capping the NPs to prevent aggregation and oxidation.[322]

Transmission electron microscopy (TEM) was utilized to study the morphology and the size distribution of the Cu NPs. The typical TEM images of the particles reveal that the Cu NPs are well-separated, spherical without any agglomeration (**Fig. 4.2(a)**). The average particle size was determined to be 3.56 ± 0.8 nm (**Fig. 4.2(b)**). EDX elemental composition showed minimal oxidation of the NPs and a strong presence of Cu (**Fig. 4.2(c)**).
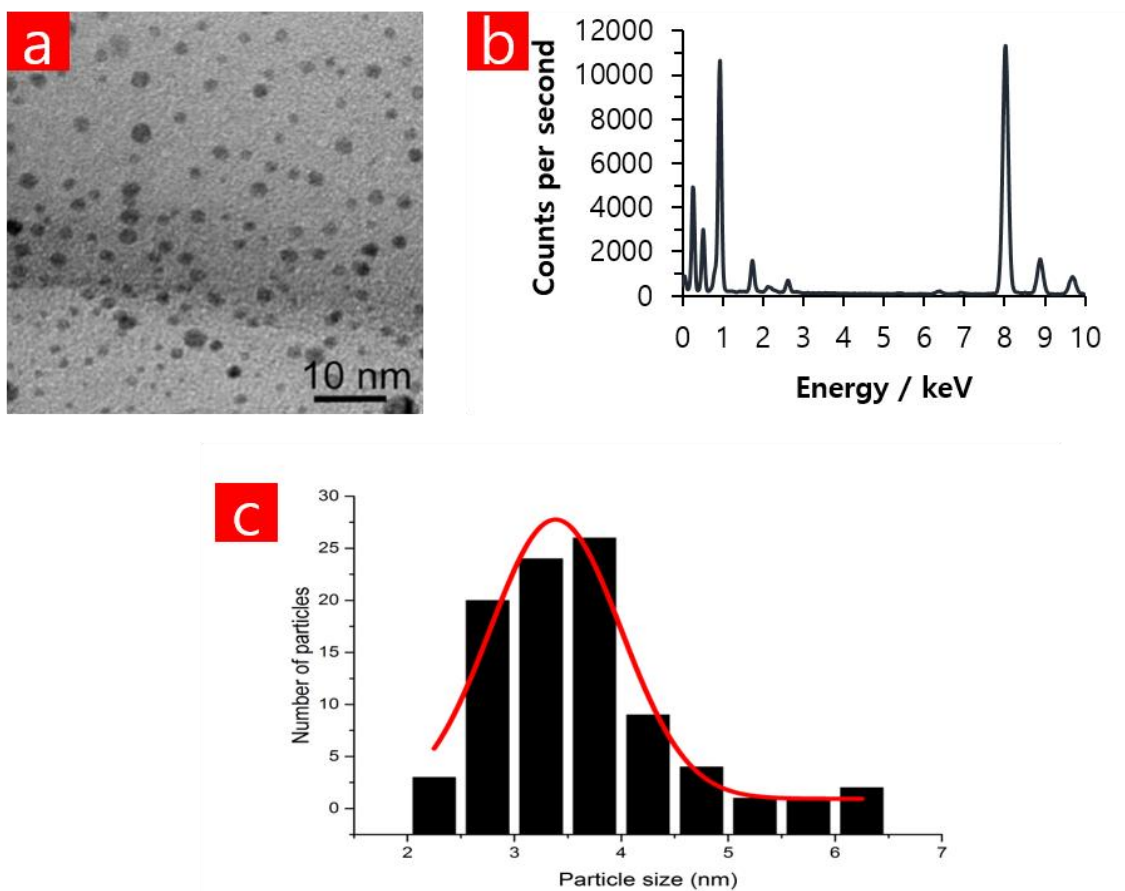
Fig. 4.2 (a) HR-TEM image, (b) EDX spectrum and (c) size distribution of the prepared Cu NPs.

4.3.2: Materials Synthesis

4.3.2.1: Deposition and Characterization of Modified Polymer samples

A facile two-step AACVD process was carried out to create novel composite thin film on glass which is expected to simultaneously show superhydrophobic and antibacterial properties. Firstly, AACVD was carried out using a chloroform solution of the thermosetting Slygard-184 (base and curing agent) at 390 °C, where the chloroform solvent evaporates and the thermoset polymer is cured. This followed by a methanol solution of Cu NPs, which was deposited onto the as-prepared polymer thin film at 350 °C by a second CVD step (**Fig. 4.3(a)**). While PDMS films are white-opaque, copper-containing films are

metallic brown in colour (**Fig. 4.3(b)**). The films were uniform and showed good coverage across the glass surface.
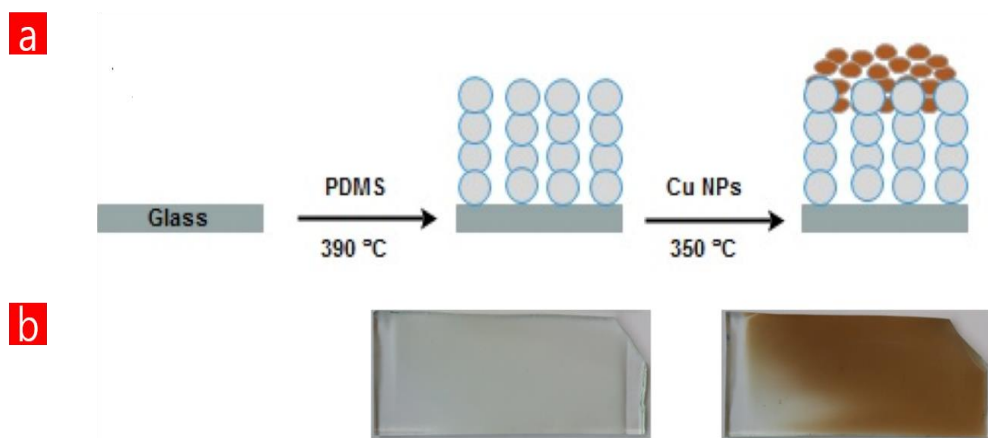
Fig. 4.3 (a) Schematic to show fabrication of Cu NPs coated PDMS. (b) Images of Sylgard 184 polymer deposited via AACVD at 390 °C – on the left- and after the NP deposition at 350 °C- on the right-. The sample dimensions are 14 cm x 4.5 cm x 0.5 cm.

The morphology of the films was investigated using scanning electron microscopy (SEM), atomic force spectroscopy (AFM) and transmission electron microscopy (TEM). Cu NPs were deposited onto PDMS matrix through the AACVD deposition process. Therefore, they were expected to be anchored on the PDMS surface and this was confirmed by both SEM and TEM images. SEM images revealed that PDMS films by AACVD had a very rough surface consisting of interlocking particles with surface protrusions around 3-5 μm in length (**Fig. 4.4(a-b)**)and spherical Cu NPs were uniformly attached to the surface protrusions (**Fig. 4.4(c)**).
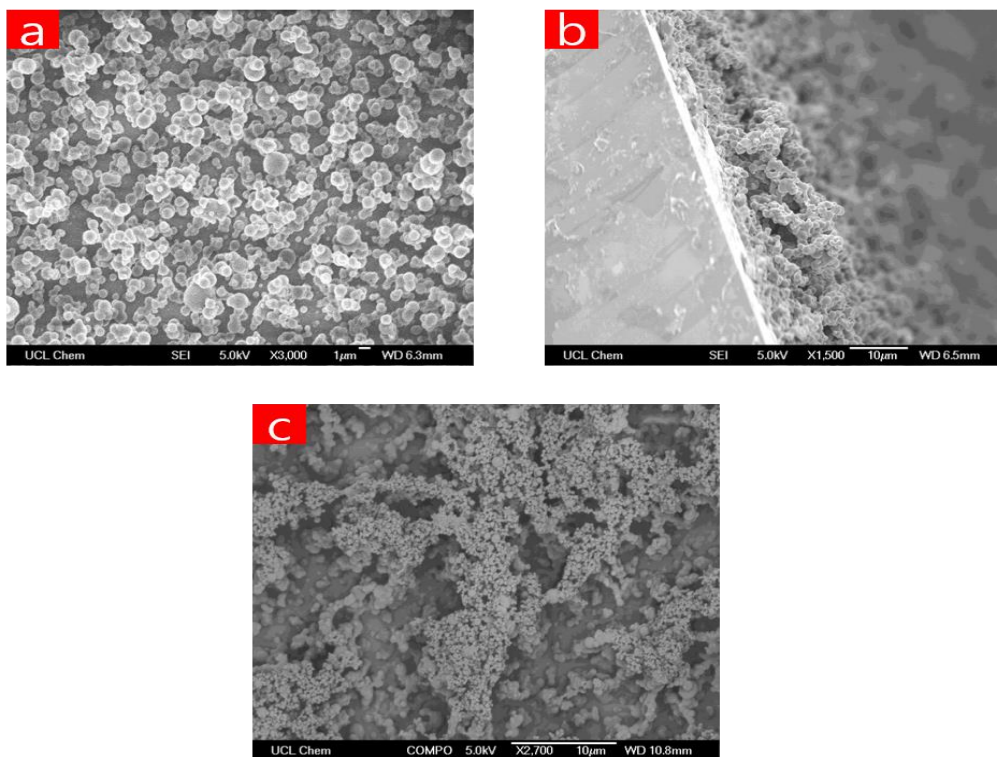
Fig. 4.4 SEM images of (a) and (b-side view) PDMS film grown by AACVD of Sylgard 184 in chloroform at 390 °C in 3000x and 1500x magnifications, respectively; (c) after coating with Cu NPs at 350 °C in 1500x magnification.

The surface morphology and roughness of the samples was further examined by atomic force microscopy (AFM). The two-dimensional and three-dimensional AFM images of the samples are shown in **Fig. 4.5**. Both the glass and the PDMS sample had rather smooth surface with R_{rms} (root-mean-square-roughness) of 0.132 nm and 2.175 nm, respectively. After CVD treatment with PDMS, the glass surface dramatically roughened with R_{rms} of 0.278 μm. However, with Cu-incorporation, the roughness of the hybrid film slightly reduced to R_{rms} of 0.230 μm.
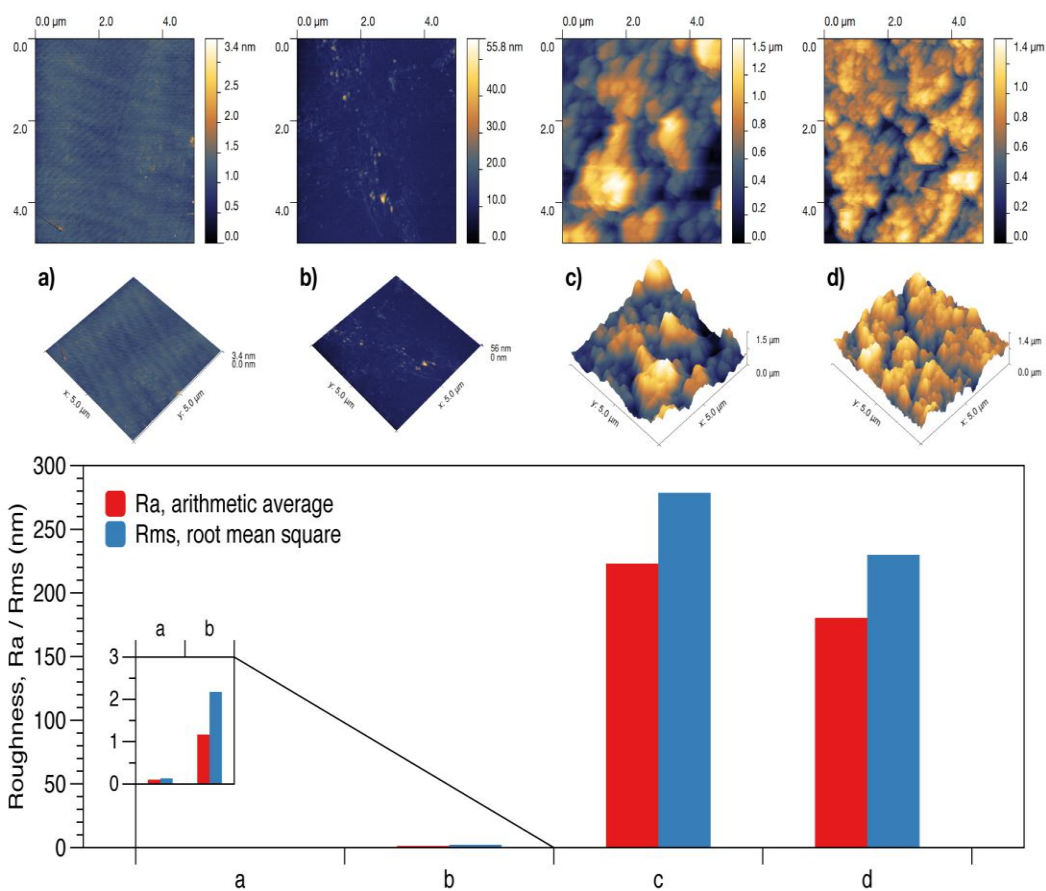
Fig. 4.5 Two-dimensional (top) and three-dimensional AFM images of (a) plain glass, (b) plain PDMS, (c) CVD-treated PDMS and (d) Cu-coated CVD-treated PDMS.

The surface of bare glass was hydrophilic with a water contact angle of $48 \pm 3°$ while bare PDMS film was hydrophobic with a water contact angle of $111 \pm 5°$ due to the presence of water-repelling C-H groups on the surface. During the AACVD process, PDMS with low-surface energy was cured resulting in a highly rough surface converting the glass substrate to superhydrophobic with water contact angle up to $155 \pm 2°$ (**Fig. 4.6 (a)**). The protrusions act to trap air under a water droplet as surface roughness is increased, leading to a Cassie-Baxter wetting mechanism. No significant change in the wetting properties was observed upon coating of the Cu-NPs into the polymer matrix with a contact angle of $151 \pm 2°$ (**Fig. 4.6(b)**).

While the water droplets (10 μl) adhered to the S-PDMS surface slide away at a tilting angle of less than 10°, the Cu-PDMS surface is extremely slippery compared to the S-PDMS, enabling the water droplets to readily roll off, even at 1° tilt angle. Low tilt angles confirmed a Cassie-Baxter wetting mechanism on these surfaces with the successful trapping of air underneath water droplets within the film porosity.
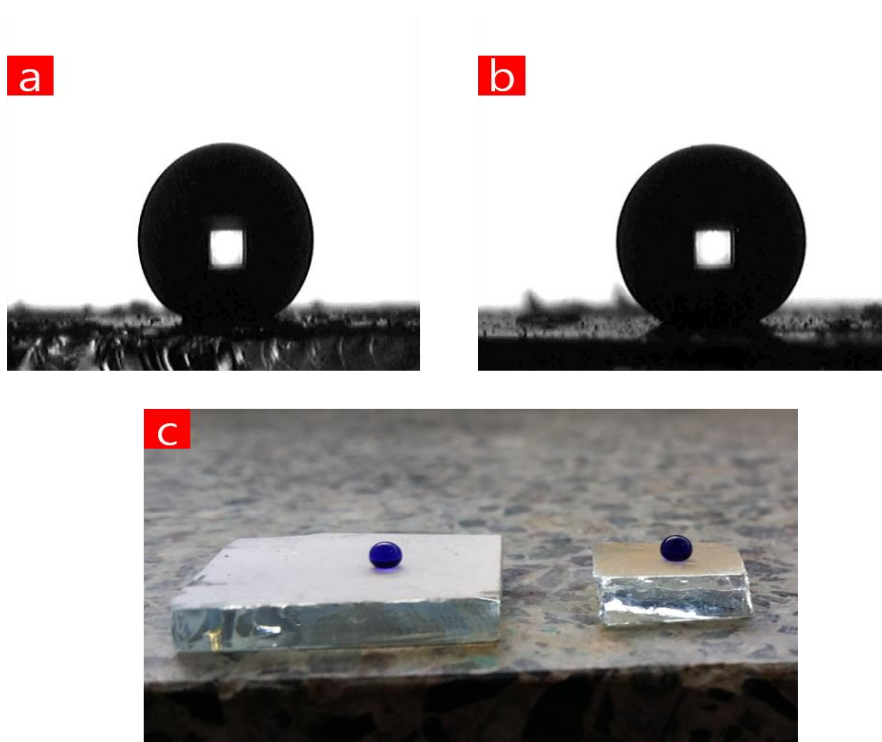
Fig. 4.6 Water droplets (3 μL) on the surface of (a) S-PDMS and (b) Cu-PDMS; (c) Photograph showing a 5 μL droplet of water on the surfaces of S-PDMS (on the left) and Cu-PDMS (on the right).

Fig. 4.7(a-b) shows the TEM image of the Cu-PDMS composite and its corresponding elemental mapping. It can be clearly seen that Cu NPs were distributed throughout the polymer matrix. Also, elemental distributions from the EDS spectrum indicate that the elements Cu, Si and Cl are the main constituents (**Fig. 4.7(c-e)**). While the elements Cl and Cu are associated with the synthesis of the NPs, the Si comes from the polymer itself consisting of a flexible (Si-O) backbone and a repeating (Si(CH$_3$)$_2$) unit.[323]
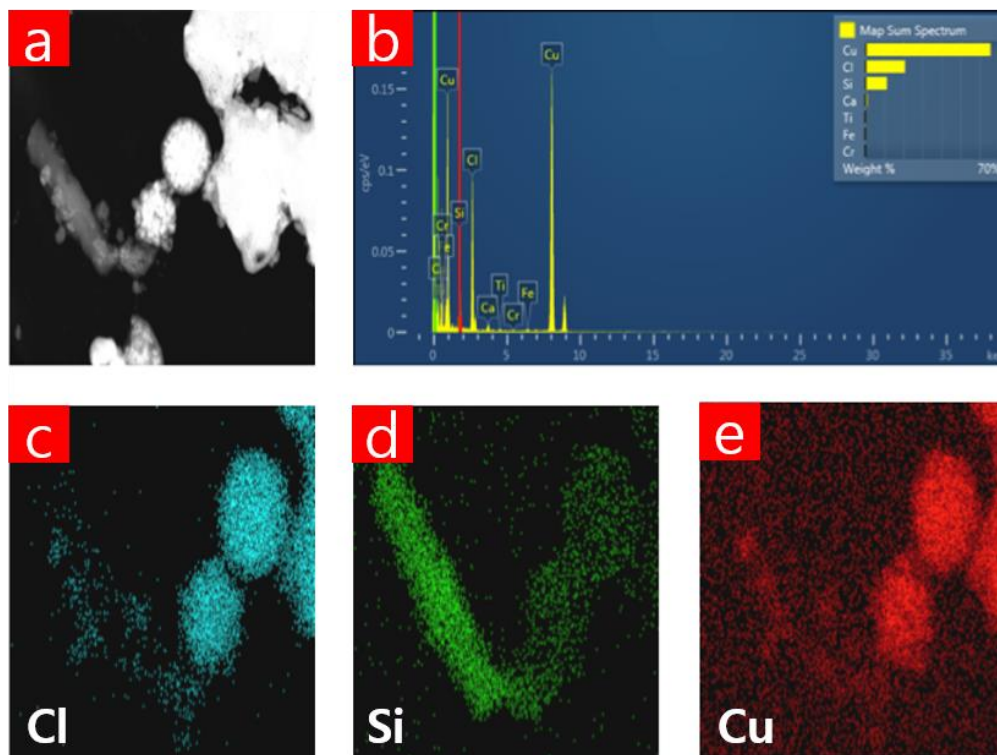
Fig. 4.7 TEM images (a) colloidal Cu NPs and (b) Cu-PDMS composite and (c-e) energy dispersive X ray spectrum and mapping of the Cu-PDMS composite for the elements Cl, Si and Cu.

4.3.3: Microbiological testing

The antibacterial activities of the following samples under dark conditions were evaluated against two model hospital-associated pathogens; the Gram-negative bacterium, *E. coli*, and the Gram-positive bacterium, *S. aureus*; a glass sample (control), a bare polymer sample (PDMS), a CVD treated polymer (S-PDMS) and a Cu-coated CVD-treated polymer sample (Cu-PDMS).

Fig. 4.8(a) shows that no reduction in the number of *E.coli* was observed on the samples after 15 min compared to the control sample when Cu NPs were absent. However, all Cu-coated samples achieved significant bacterial kill for all exposure times ($P < 0.01$). A 2.3-log reduction in *E. coli* numbers was achieved after 10 min of exposure to the sample

coated with Cu NPs and > 4 log reduction was achieved after 15 min with the materials containing Cu NP.
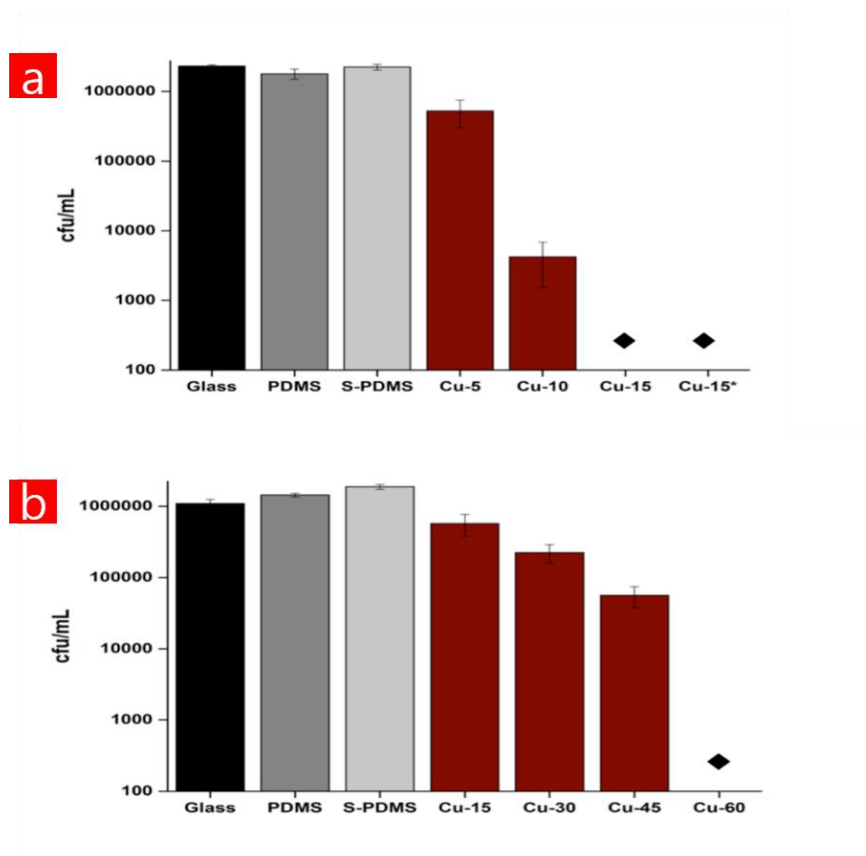
Fig. 4.8 Numbers of (a) *E. coli* after incubation on the surfaces of the samples in the dark and (b) numbers of *S. aureus* after incubation on the surfaces of the samples in the dark. The black lozenges indicate where the bacterial numbers are below the detection limit of 100 cfu/ml. Black bars refer to uncoated glass. Gray bars refer to bare PDMS (no nanoparticle). White-gray bars refer to CVD treated PDMS (S-PDMS). Red bars refer to Cu NPs coated CVD-PDMS (Cu) with different time intervals. Bare glass, PDMS and S-PDMS samples were exposed to *E. coli* and *S. aureus* for 15 min and 60 min, respectively while dip-coated Cu-PDMS (Cu*) was exposed to *E. coli* for 15 min.

In the case of *S. aureus*, there was no detectable kill of *S. aureus* on the surface of either bare PDMS or CVD treated PDMS after 1 h in the dark compared to the glass sample (**Fig. 4.8(b)**). However, the samples coated by Cu NPs demonstrated a 0.69 log reduction in viable bacteria after 15 min (P < 0.01). Moreover, a 1.4-log reduction in viable bacteria

was observed after 45 min on the surface of the Cu coated PDMS samples whereas after 1 h the number of *S. aureus* was reduced to below the detection limit (>4 log reduction; P = 0.02).

The antibacterial mechanism of Cu NPs is still under debate,[324] however several mechanisms have been proposed. Some studies suggest that copper increases intracellular ROS production causing oxidative stress and DNA damage.[325,326] Furthermore, copper may damage the cell membrane.[327] Moreover, their antibacterial activity may be attributed to the continuous release of copper ions under wet conditions[328] that attach to the bacterial cell wall. This interaction may lead to cell death by disrupting the cell membrane.

4.3.4: Anti-adhesion properties

A bacterial adhesion test was carried out with app. 10^7 cfu/ml of the two bacterial species after 1 h period of incubation. It was observed that bacterial adhesion rates on the samples were greatly affected by surface wettabilities as shown in **Fig. 4.9**. The glass sample had the greatest attachment of *S. aureus*. With high contact angles the number of adherent bacteria was significantly reduced compared to glass alone with 38% and 80% of the bacteria adhering to the bare PDMS and Cu-PDMS, respectively. CVD treated PDMS was superior to Cu-PDMS inhibiting 87% of bacterial attachment compared to glass alone (**Fig. 4.9(b)**).

With *E. coli*, the highest level of adherence was observed on bare PDMS while the S-PDMS showed the least attachment (**Fig. 4.9(b)**). The number of bacteria adhered to the Cu-PDMS surface was 50% of that on the glass surface. These results demonstrated that CVD modification improves the non-fouling nature of the bare PDMS surfaces against *E. coli* and *S. aureus*.
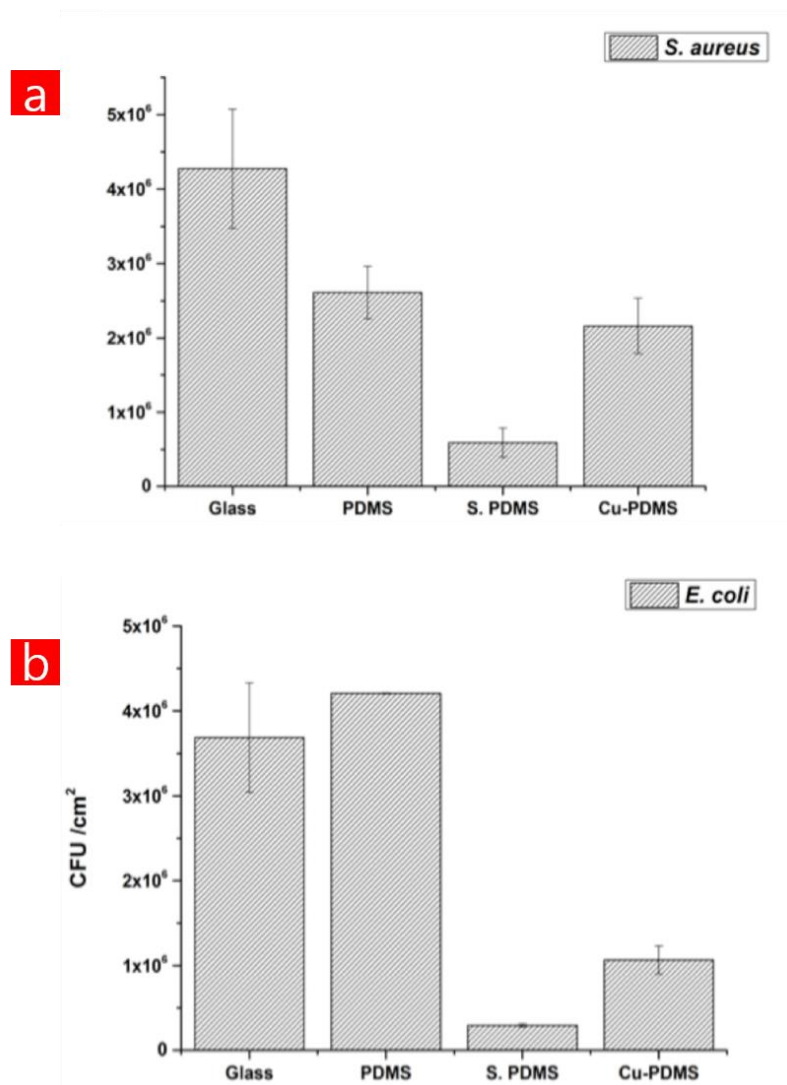
Fig. 4.9 Adherence of (a) *S. aureus* and (b) *E. coli* to the sample surfaces including uncoated glass (glass), bare PDMS (PDMS), CVD treated PDMS (S-PDMS) and Cu NPs coated CVD-PDMS (Cu-PDMS).

The different levels of bacteria attachment of the samples can be explained by two models; *Wenzel*[329] and *Cassie-Baxter*.[50] The *Wenzel* model states that no air is under the droplet so that the water penetrates the surface porosity leading to full contact with the surface and hence is relatively sticky. On the other hand, *Cassie-Baxter* states that air is trapped between the water droplet and the surface protrusions, therefore demonstrating the lotus effect..[214,330–332] Thus, the surfaces with Cassie-Baxter wetting properties significantly prevented bacterial attachment, suggesting an alternative application as an antibacterial surface.

95

The small surface features that make up most superhydrophobic materials means that most have a poor mechanical durability; this is the main problem limiting the worldwide application of these coatings. Therefore, robustness of the superhydrophobic samples was tested using a standardized scotch tape test (ASTM).[333] While CVD treated PDMS passed the test, the Cu NPs coating were removed from the substrate that was used in the antibacterial test because it had weak adhesion strength with the polymer. To overcome this problem, the Cu coated polymer sample was dip-coated into a %1 PDMS-CHCl$_3$ solution (withdrawal rate of 120 cm min^{-1}) followed by curing so that a thin layer of PDMS was deposited into the micropillars. Then, the dip-coated Cu-PDMS before and after the test was examined with SEM images, contact angle measurements and antibacterial test. The dip-coated Cu-PDMS was again tested against *E. coli* and it decreased the bacterial counts to below the detection limit (>4 log reduction) in 15 min (**Fig. 4.8(a)**). Also, the images confirmed that the coating remained stable and retained superhydrophobicity (**Fig. 4.10**).
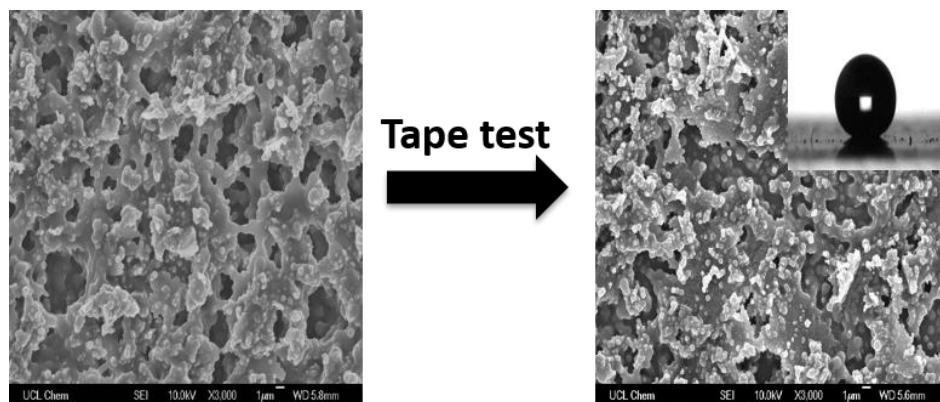
Fig. 4.10 SEM images of the Cu coated PDMS surface that was exposed to the tape test.

PDMS has been used in a wide range of applications including sensors and microfluidic channels because of its properties including high flexibility, low cost, non-toxic nature, chemical inertness and easy preparation.[8,252,334] Therefore we anticipate that the loading of Cu NPs onto PDMS may extend its use in antibacterial applications from air filters to touch surfaces such as door handles and bed rails in clinical environments. Consequently, this

may help disrupt the cycle of transmission of microorganisms between patients, healthcare staff and the environment.

4.4: Conclusions

In this work, we have successfully fabricated a novel superhydrophobic antibacterial thin films by creating a second layer of Cu NPs upon the first layer of superhydrophobic thin film *via* AACVD. The modified sample showed superhydrophobicity with a water contact angle of 151° as well as remarkable water bouncing properties. It was potent at killing suspensions of *S. aureus* in just 1 hour and *E. coli* in just 15 min, with a minimum of a 4-log reduction (99.99 % kill) in the numbers of both bacteria. Moreover, the CVD treated samples greatly prevented the adhesion of both types of bacteria compared to glass and PDMS samples. This novel hybrid surface may help decrease the incidence of infection in healthcare environments as it works in a novel two-fold manner- preventing bacteria sticking and inactivating those that do.

Chapter 5: EXTREMELY DURABLE BIOFOULING-RESISTANT COPPER BASED SELF-STERILIZING SURFACES

5.1: Introduction

Superhydrophobic surfaces that show extreme water-repellent properties have attracted enormous scientific and industrial interest because of their use in a broad range of applications including self-cleaning,[335,336] antifouling,[337,338] anti-icing[339] and water/oil separation.[340] However, such surfaces usually suffer from low mechanical robustness hindering their real-world applications. Hence, nowadays, the mechanical durability of superhydrophobic surfaces are of great interest[341] to employ such surfaces in practical applications.

In Chapter 4, superhydrophobic antibacterial copper coated polymer films were fabricated *via* AACVD. The films showed significant bactericidal activity as well as a significant reduction in bacterial cell adhesion compared to the control materials. However, normal contacts (e.g. finger touch, abrasion and scratching) could destroy the micro/nano-roughness features or remove most of the hydrophobic layer on the surface, causing loss of the surface superhydrophobicity. Also, such surfaces depending upon trapped air may have limited use under different conditions such as liquid environments, pressure and hydrodynamic shear that may easily fail the stability of air pockets.[227] Hence, it is unlikely that self-sterilizing coatings based on one property (e.g. surface energy) are able to reduce biofouling and hence new strategies need to be developed to generate mechanically durable materials with multifunctional properties (e.g. bactericidal, surface topography and lubricity).[342,343]

Recently, a different concept has been introduced to make self-cleaning surfaces inspired by Nepenthes pitcher plants with an immobilized lubricant liquid in hierarchical texture to form slippery liquid-infused porous surfaces (SLIPS). Due to their unique slippery characteristics (e.g. liquid repellency, smoothness, self-healing and robustness), they find great applications including fluid transportation, airplane and watercraft coatings. It has been shown slippery surfaces exhibited excellent repellency against blood cell, protein and bacteria over longer periods of time.[236,344]

In this Chapter, a facile, low-cost, scalable strategy was developed to design robust superhydrophobic (SH) and slippery surfaces (SLIP) based upon particle-filled polymer composites. Commercial copper particles were spread on the un-cured PDMS-hexane solution surface with the use of a sieve. Then, the PDMS matrix was completely cured after removing the excessive particles by washing. The accumulation of particles results in surface roughness and the required low surface energy is provided by both the particles and the PDMS matrix. Consequently, the resultant material showed superhydrophobicity with high water contact angle (CA, > 155˚) and very low sliding angle (SA, < 10˚). The particles are commercial and utilized as received without any modification. In addition, the mechanical durability of the modified samples is systemically examined against different mechanical actions. The results show that the SH samples were mechanically robust against sandpaper abrasion (100 g, 50 cycles), finger-wiping and scratching. These surfaces with extreme mechanical durability and anti-biofouling properties can be prepared in large scale without the need for any expensive materials and special equipment, which can offer numerous applications that require prolonged biofilm resistance even under harsh environmental and fouling conditions. Chemical composition, structure, wetting and mechanical properties of the as-prepared samples were characterized in detail Moreover, the antifouling properties of the samples were investigated against two key bacterial species associated with HAIs.

5.2: EXPERIMENTAL

5.2.1: Chemicals and Reagents

Copper powders (Cu) were purchased from Sigma-Aldrich. Laboratory solvents were purchased from Fisher Scientific Limited and of the highest possible grade. Sylgard® 184 Silicone Elastomer was purchased from Dow Corning Corporation Ltd, which consists of two-part silicone elastomers (base and curing agent). The precursor, Sylgard 184, can be cross-linked with the curing agent and the final polymer is polydimethylsiloxane (PDMS).

5.2.2: Materials Synthesis

5.2.2.1: Preparation of Superhydrophobic and Lubricant-Infused Surfaces

Different materials including glass, silicone, paper and steel were used as substrates in this work. Firstly, the PDMS pre-polymer (20 g), its curing (2.0 g) agent and hexane (30 ml) were mixed in a beaker and stirred for 10 min at room temperature to obtain a transparent solution. Then, the substrates were dip-coated into the solution (withdrawal rate of 120 cm min^{-1}) so that a thin sticky layer of PDMS was deposited on the substrates. Copper powders were carefully spread on the sticky surface by using a sieve until the surface was completely covered by the copper powders. After overnight, the Cu coated PDMS surfaces were fully cross-linked at 100 ˚C for 1h in order to immobilize the copper particles. After the cross-linking of PDMS, redundant copper particles were removed by water. Also, the slippery surface was prepared through absorption of silicone oil.

5.2.3: Materials Characterization

Scanning electron microscopy was performed using secondary electron imaging on a JEOL 6301 field emission instrument with Oxford instruments EDX spectrometer attached. Atomic force microscopy (AFM) measurements were performed in air on a Veeco Dimension 3100 using a Nanosurf Easyscan 2 system fitted with a NCLR cantilever. Non-contact tapping mode was used to build a topological map of each samples over a 5 x 5 μm area and roughness statistics extracted using post-process software (Gwyddion).

5.2.4: Functional Testing

5.2.4.1: Surface Hydrophobicity Measurements

Water contact angle measurements were carried out using an FTA-1000 drop shape instrument; ≈3 μL water droplets were used to minimize any gravitational effects. The water droplet images were analyzed using a digital protractor to obtain the water contact angles on the surface. A range of points across the substrates was tested, with 5

measurements made on each film. Water slip angles were also measured, noting the angle to the horizontal at which 20 µL water droplets moved on the surface. Many positions across the substrates were tested.

5.2.4.2: Bacterial Biofouling Tests.

Suspensions *of E. coli* ATCC 25922 and *S. aureus* 8325-4 with densities of approximately 1×10^8 cells/mL were prepared overnight in BHI broth and the treated glass samples (3.0 x 2.5 cm^2) were immersed in the suspensions at 37˚ for 48 h.

Following incubation, the samples were gently removed from the bacterial suspensions. Samples for analysis of the stained and dried biofilms were immediately stained by incubating in a 0.1% (w/v) solution of crystal violet in water for 20 min, gently rinsed in deionized water to remove excess stain, then dried. The dried samples were placed in sterile plastic tubes filled with ethanol. After a 60-min incubation, a plate reader was used to measure the absorbance of the solubilized CV at 590 nm.

5.2.4.3: Robustness tests

Both hard (glass slide, and steel) and soft (silicone and paper) substrates were involved in the robustness tests, such as knife scratch and finger-wipe. For knife-scratch tests, water was first dropped on the surfaces to test the wettability, and then a scalpel was used to scratch the superhydrophobic surfaces along a meshy path, followed by the water dropping test to confirm the robustness of the superhydrophobic surfaces. For a finger-wipe test, water was firstly dropped on the surfaces to test the wettability, and then a finger tried to remove the coating from the superhydrophobic surfaces, followed by the water dropping test to compare the robustness of the superhydrophobic surfaces with or without PDMS overlayer coating.

To further demonstrate the robustness, a glass slide sample was tested via sandpaper-abrasion method. The superhydrophobic surfaces were placed facedown onto the sandpaper (standard glasspaper, grit no. 240). These surfaces were longitudinally and transversely (10 cm for each direction) abraded by the sandpaper under a weight at 100 g,

respectively; this process is defined as one cycle. Fifty cycles of mechanical abrasion tests were carried out on the glass slide sample, and water contact angles were measured at the end of every five cycles.

Also, adherence tests were carried out by applying Scotch Home and Office masking tape (3M™) to the deposited films with even pressure applied by hand, followed by removal in one swift motion. Any difference in the film appearance was noted.

5.3: RESULTS AND DISCUSSION

5.3.1: Material preparation and characterization

A facile, inexpensive, scalable, substrate-independent method was reported to create slippery antibiofouling coatings. In a typical preparation process, the first stage involved preparing a transparent solution of PDMS, curing agent and hexane in a mass ratio of 1/10/10, respectively. Then, various substrates (e.g. glass, silicone, steel and paper) were dipped into the transparent solution to prepare a sticky PDMS interlayer on the substrates. Afterwards, copper particles were carefully spread on the un-cured PDMS coated substrates with the use of a sieve until they were completely covered by the particles. The particles sunk slowly from the surface to the bottom in the un-cured polymer matrix overnight followed by full cross-linking of PDMS at 100˚ for 1 h (denoted as uncoated SH-Cu). The next step was to again dip-coat the Cu-coated substrates with PDMS-hexane solution to enhance the mechanical robustness of the surfaces followed by curing so that a thin layer of PDMS was penetrated into the particles to act as an interconnection between them. The resulting material was denoted as SH-Cu. In the last step, the silicone lubricant liquid was spread on the SH-Cu *via* capillary effect and was denoted as SLIP-Cu. (**Fig. 5.1**)
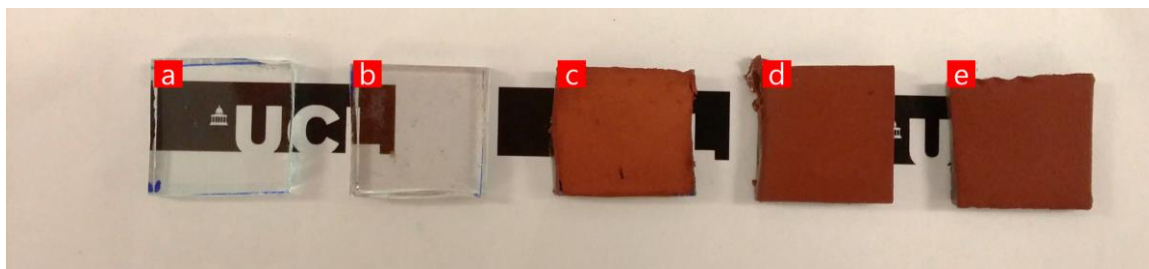
Fig. 5.1 Images of (a) plain glass, (b) PDMS-coated glass, (c) uncoated SH-Cu glass, (d) coated SH-Cu glass and (e) SLIP-Cu glass.

SEM was used to characterize the surface morphology of the as-prepared samples. It was revealed that the plain glass possessed a very smooth surface. Similarly, after coating with PDMS, the topography of the glass almost remained unchanged. However, when coating with Cu particles, a rough surface was formed with hierarchical micro- and nanoscale sheet structures by assembly of Cu particles that look like flower clusters with average diameter of about 2-3 µm (**Fig. 5.2 (a)**). Post PDMS coating resulted in a thin layer of PDMS into the micropillars. (Fig. **5.2 (b)**). On the other hand, after the lubricant infusion, the hierarchical microscale structures were occupied by silicone oil, leading to a flat liquid film on the surface (**Fig. 5.2 (c)**).
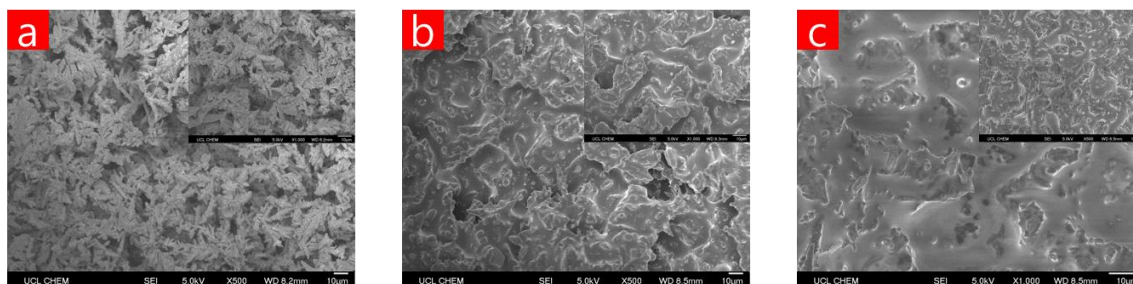
Fig. 5.2 SEM images of the surface morphologies of (a) uncoated SH-Cu (b) SH-Cu (c) SLIP-Cu. The magnifications are x500 and x1000 for the inset images.

The commercial Cu particles with a surface energy of 26.7 mN/m[345] exhibit hydrophobicity and can be used to render surfaces superhydrophobic, originating from its hydrophobic nature and intrinsic microstructure (**Fig. 5.3**). Hence, Cu based PDMS coated different substrates have large roughness because of presence of flower-like Cu particles and low

surface energy owing to both the particles and PDMS, which are two crucial factors in yielding superhydrophobic surfaces.
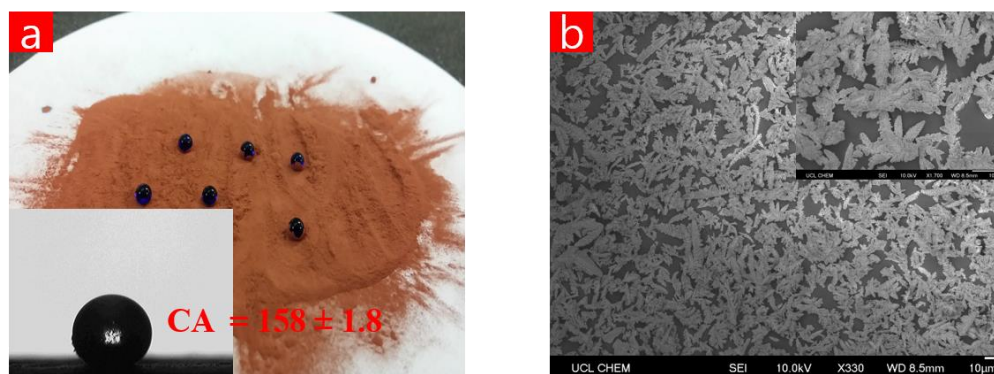
Fig. 5.3 (a) Optical photograph of methylene blue-dyed water droplets on one layer of the copper powder and (b) SEM photograph of Cu particles. The inset is a high magnification photograph of a water droplet.

Wetting properties of the samples were characterized by contact angle (CA) and sliding angle (SA) measurements using water as a test liquid. As demonstrated in Fig. **5.4**, while water droplets would either completely spread or show semi-spherical shapes on the plain substrates depending on the type of the material, they resemble typical spherical balls on all the Cu-coated substrates, showing CAs of > 155˚ of and SAs of < 5˚, enabling them to readily slide off. The Cu particles not only enhanced the surface roughness but also changed the surface energy that led to the superhydrophobic behavior. However, when the superhydrophobic surfaces were wetted by silicone oil, the contact angles dramatically decreased to about 100˚, indicating that the lotus-inspired superhydrophobic coating was converted to the pitcher-inspired slippery coating.
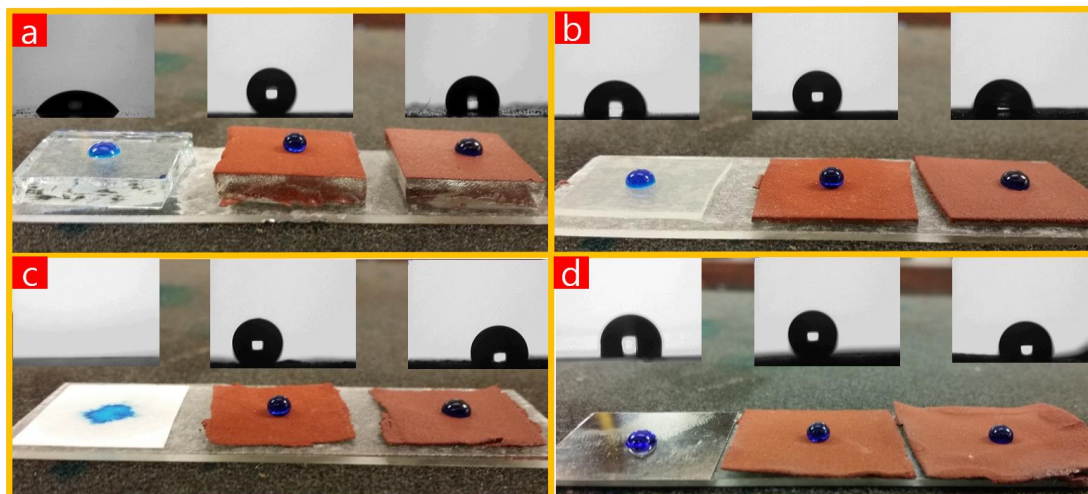
Fig. 5.4 Optical images of the untreated and treated surfaces (superhydrophobic and slippery), respectively, on different substrates: (a) glass, (b) silicone, (c) paper and (d) steel. The inset images show water contact angles of the substrates.

To further examine the remarkable water repellency, the SH-Cu glass sample was completely submerged in water. Unlike the bare glass and SLIP-Cu-glass (**Fig. 5.5 (b and c)**), SH-Cu sample demonstrates an obvious bright plastron layer (i.e. a layer of air) because of the total reflectance of light at the air layer trapped on the surface, preventing the glass from wetting, characteristic of a SH surface (**Fig. 5.5 (a)**).[346] This phenomenon demonstrated that the coating possessed typical Cassie mode superhydrophobicity[347] and therefore, a jet of water can also bounce off the coating without leaving any trace, showing excellent water repellent property (**Fig. 5.6 (a)**). Unlike the SH-Cu surface, the SLIP-Cu surface showed an inelastic collision of impacted water flow (**Fig. 5.6 (b)**).

Figure 5.5 (a) The SH glass surfaces is capable of trapping air in aqueous environment, leading to an underwater air-film. (b) and (c) In comparison, the air-film cannot be stabilized by the SLIP and plain glass samples.
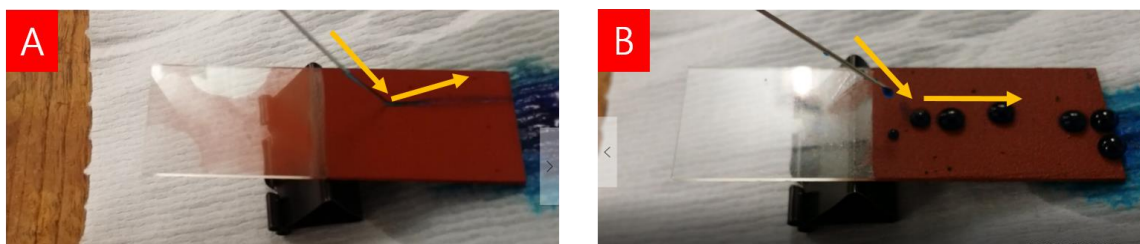
Fig. 5.6 Continuous water flow on (a) the S.H-Cu and (b) the SLIP-Cu surface.

Slippery Cu (SLIP-Cu) samples were fabricated following three criteria: (1) affinity of lubricating liquid with solid surface, (2) the testing liquid must show immiscibility with the lubricant and (3) requirement of hydrophobic solid substrate. The first criterion was fulfilled by taking silicone oil as a lubricant liquid that completely spreads on SH-Cu films. Since silicone oil can swell crosslinked PDMS, the swelling increases its affinity with PDMS coated films. Second requirement was satisfied by using water as a test liquid that is immiscible with the silicone oil. Finally, third criterion was satisfied automatically because both PDMS and Cu particle coated films are inherently hydrophobic. Satisfying these criteria, silicone oil infused slippery surfaces were fabricated on various substrates to slide off water droplets upon tilting. Each of these substrates shows very low contact angle hysteresis and low sliding angle for 15 µl droplet volume inclined at 15˚.

Converting a surface from superhydrophobic to slippery bring many advantages.[234,348] For instance, although superhydrophobic surfaces demonstrate outstanding water repellency, they usually fail to repel low-surface tension liquids[349] and become significantly contaminated in biological media.[350] In order to test the resistance of the coatings to different liquids, water (72 mN/m), glycerol (63.4 mN/m) and horse blood (E & O Lab. Ltd.) were placed on the surfaces at a titling angle (TA) of 10˚. Methylene blue-dyed water droplets, glycerol and blood completely spread on the pristine glass, while they slid on the surface leaving behind a trace a long its traveled path. In contrast, water droplets readily slid down at the titled SH-Cu surface without wetting while the surface was contaminated by low-surface-tension liquids (i.e. glycerol and blood). On the other hand, all tested liquids can easily slide down SLIP-Cu surface with a TA of 10˚ without leaving any traces, indicating its outstanding liquid-repellent properties (**Fig. 5.7**). This is because when the lubricant silicone oil was infused with the SH surfaces, its porous microtexture was able to

lock in and sustain a layer of lubricant liquid because of high chemical affinity of the lubricant to the underlying porous solid. Therefore, the resultant slippery samples showed excellent anti-wetting behavior against even low-surface-tension liquids. Since liquids cannot penetrate through this constant lubricant overlayer, and experience liquid-liquid interaction at the interface with lubricant, hence avoiding pinning on the solid and leading to extremely low values of CAs and SAs and thus high droplet mobility.
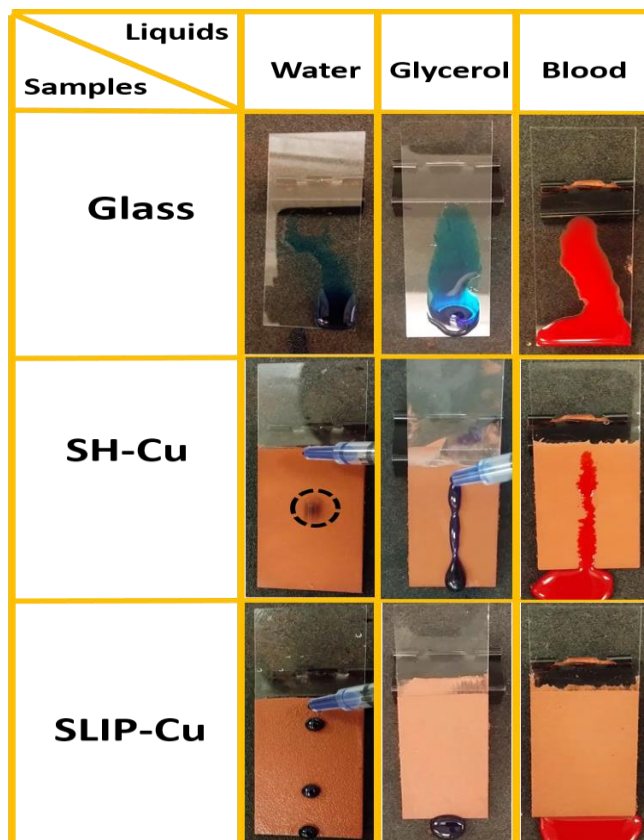
Fig. 5.7 Snapshots taken in the course of flowing water, glycerol and blood on the pristine glass, S.H-Cu glass and SLIP-Cu glass at a TA of 10˚. The water was labeled by methylene blue.

In many industrial applications, the anti-fouling properties of solid surfaces are vital. To examine the anti-fouling abilities of the untreated and treated filter papers were inserted into methylene blue dyed water. As demonstrated in **Fig. 5.8**, the pristine filter paper got dyed while SH-Cu and the SLIP-Cu filter papers could sustain their original clean surface after being immersed into the dyed-water for twenty consecutive test cycles. The prepared micro/nano-structures on the SH-Cu sample can store a certain amount of air in the coating

surface. Moreover, the surface energy of the superhydrophobic coating was lower than that of the methylene blue dyed water. Based on the above two points, an air layer formed on the coating surface to inhibit penetration of the dyed water into the coating. These phenomena showed that the prepared coatings possess outstanding anti-fouling abilities, offering many industrial potential applications. As for the slippery filter paper, a combination of slipperiness and the presence of the liquid layer prevented it from wetting.
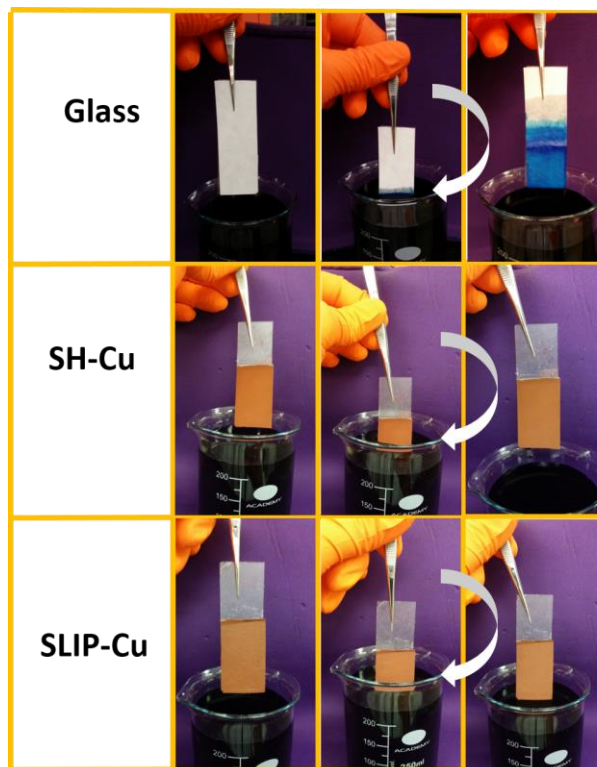
Fig. 5.8 Self-cleaning test was performed on pristine filter paper, S.H-Cu filter paper and SLIP-Cu filter paper.

In real-world applications, superhydrophobic coatings usually depend on a fragile micro/nano structure for their excellent water-repellency that are hence prone to wear by abrasion resulting in the loss of surface superhydrophobicity. Therefore, it is essential to examine the mechanical stability of the fabricated superhydrophobic coatings.

Different methods have been carried out to examine mechanical properties of the coatings. (i) Scotch tape, finger-wipe and bending tests were applied to characterize adhesion of the Cu particles to the underlying substrate, (ii) the surfaces were scratched (horizontal and

vertical cuts) by a scalpel and (iii) sand paper test was applied to show the resistance of the coatings to massive mechanical damage.

The adhesion strength of the coating was characterized by tape peel test and by bending of the sample. Dense coverage of copper particles was found on the pealed tape from the SH-Cu surface without PDMS coating, while the coated surface did not reveal much, suggesting improved stability of the particles post PDMS coating (**Fig. 5.9**).

Fig. 5.9 Tape adhesive test of the uncoated and coated S.H-Cu samples (from left to right).

Moreover, the SH-Cu silicone sample were repeatedly bent forwards and backwards, from -90 to 90 (defined as 1 cycle) over 100 folding cycles (**Fig. 5.10**). Any delamination, fracturing, cracking or peeling of the coating was not observed even after 100 repeated bending cycles and the coating showed extreme water repellency and water droplets rolled away easily.
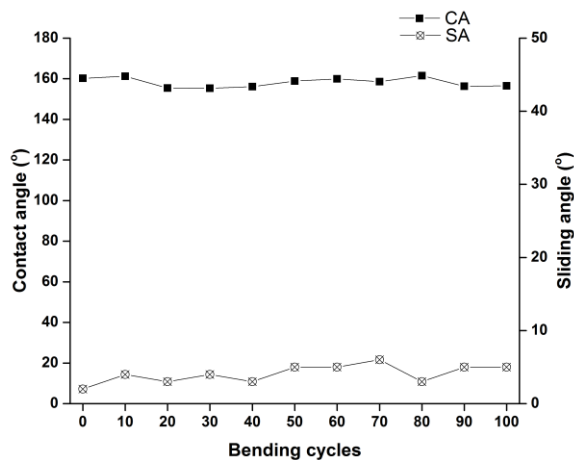
Fig. 5.10 Plot of water contact/sliding angles as a function of bending times.

The strong adhesion of the coating could also be reflected through the sandpaper abrasion test that was performed using 240 grit SiC sandpaper as an abrasion surface. The SEM image in **Fig. 5. 11 (c)** demonstrates that the sand paper consisted of irregular structures with diameters in 20-50 µm, which would easily damage the coatings. SH-Cu sample with a weight of 200 g above it was put face-down to sandpaper and moved 10 cm along the ruler (**Fig. 5.12 (a)**); the sample was then contra-rotated by 90 and moved 10 cm along the ruler (**Fig. 5.12 (b)**). This process is defined as one abrasion cycle, which provides that the surface is rubbed longitudinally and transversely in each cycle and totally 50 cycles (1000 cm) were carried out. The CAs of the coatings was measured as a function of abrasion cycles and for the sake of comparison, the prepared glass surfaces with and without PDMS overlayer coating were tested.

As shown in **Fig. 5.11**, a huge amount of coating material was worn off from the superhydrophobic surface without PDMS coating after each abrasion cycle, hence exposing the underlying hydrophobic silicone substrate and causing loss of superhydrophobicity, upon being abraded for 10 cycles. Although repeated abrasion process resulted in removal a few outmost layers of the material without PDMS coating, it still sustained its superhydrophobic behavior. Therefore, these materials show mechanical abrasion tolerance until they are worn out.
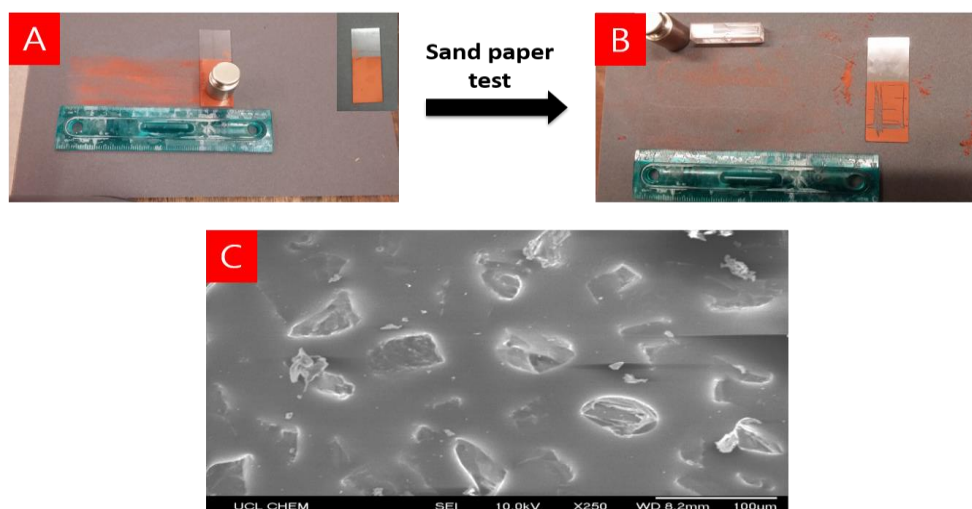
Fig. 5.11 One cycle (A) and ten cycles (B) of the sandpaper-abrasion test of the uncoated SH-Cu glass sample after 10 cycle. (C) SEM image of the sandpaper surface.

Contrarily, **Fig. 5.12 (c)** shows that the CAs of the PDMS-coated superhydrophobic coating maintained its superhydrophobicity with CAs larger than 150° and SAs lower than 10° even after 50 cycles of sand abrasion, indicating its high tolerance upon mechanical damage. The results suggest that the PDMS overlayer would provide physical support to the partially embedded particles, protecting them from being worn out. It is well known that PDMS is an elastic polymer. The elastic micro-structures on the superhydrophobic surface can be compressed to avoid being broken.[351] The deformation will recover to its original structures when the external force is removed and help to stabilize the air cushions trapped in the microstructures that are essential to sustain the durable superhydrophobic surfaces. Therefore, the superhydrophobic surface shows outstanding mechanical durability.
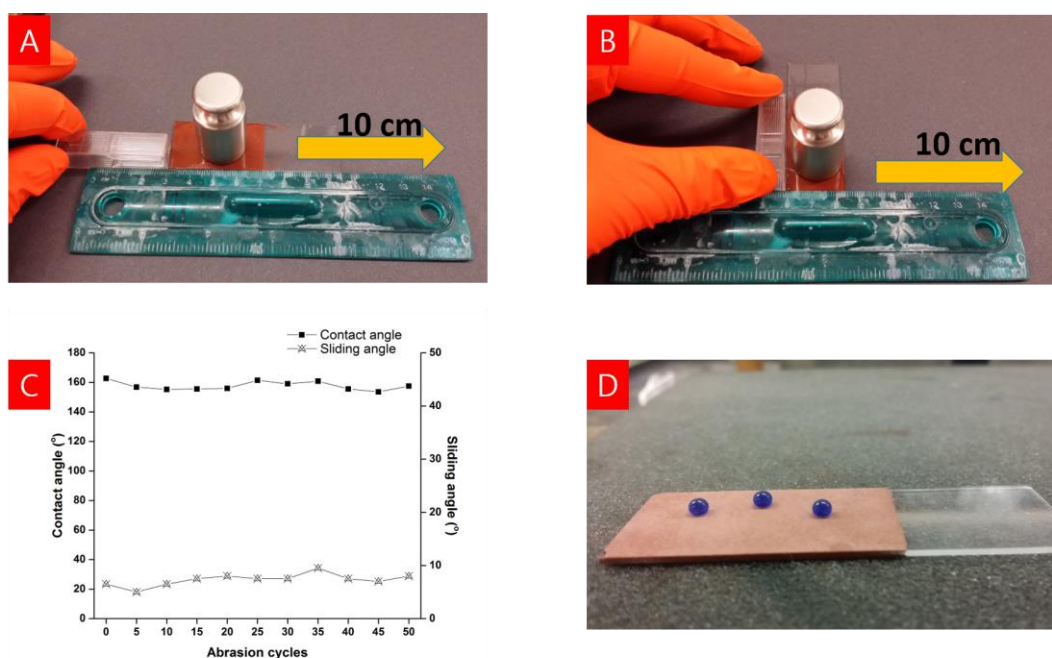
Fig. 5.12 (A) and (B) Illustration of one cycle of the sandpaper abrasion test for the PDMS-coated superhydrophobic glass surface. (C) CA and SA change of the superhydrophobic surface with abrasion cycles, (D) photograph of water droplets on the coating after 50 cycles of abrasion test.

Furthermore, the morphology of the coating was examined upon cyclic sand abrasion using SEM. As shown in **Fig. 5.13 (a and b)**, it is apparent that the original coating is a homogenous particle packing structure with PDMS as particle interconnection covering the Cu particles. Even after 50 cycles of sand abrasion, no obvious difference could be

111

observed on the surface and the micro/nano-roughness features were similar to the non-abraded surface (**Fig. 5.13 (c and d)**). It has been demonstrated that smooth hydrophobic Teflon (CA = 103˚) can be converted to superhydrophobic after roughening using sandpaper.[352] Similarly, PDMS is also hydrophobic and the surface shows excellent abrasion resistance since the fresh exposed surface is still rough with low surface energy.
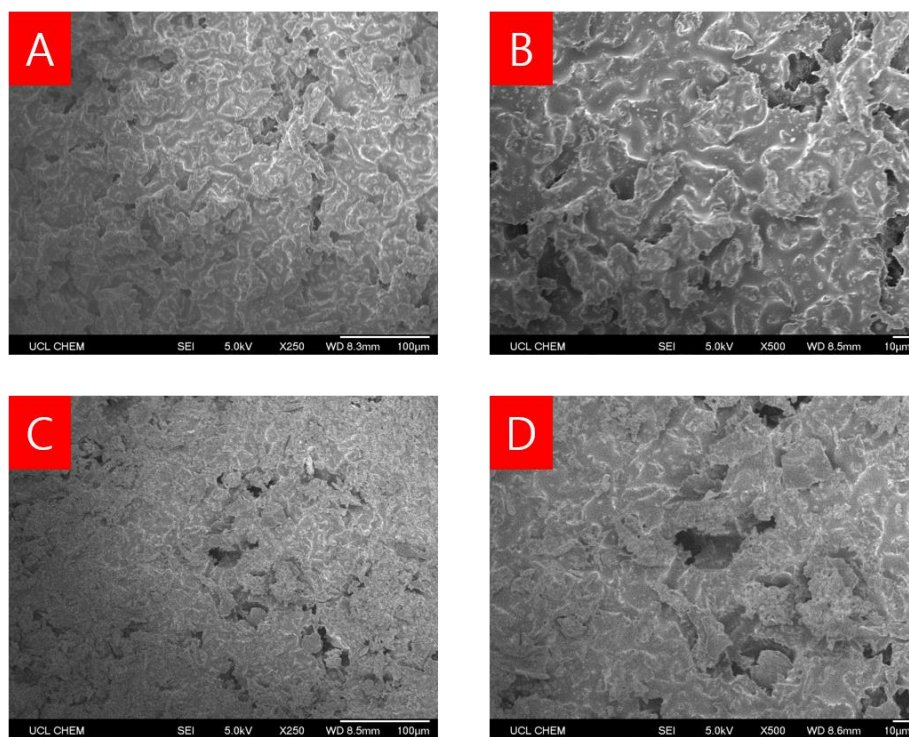
Fig. 5.13 SEM images of the superhydrophobic coating (A, B) before abrasion; (C, D) after 50 cyclic sand abrasion.

The mechanical stability of the coatings was also investigated using finger-wipe and knife-scratch tests. As demonstrated in **Fig. 5.14 and 5.15** upon being scratched by a scalpel and being pressed by finger, the surfaces retained their superhydrophobicity and water droplets could easily roll off the damaged surfaces. The damaged areas caused by the knife cutting or the finger-wiping can be clearly seen. The methylene blue labeled water could still readily slide down or across the damaged coating at a TA of 10˚ without leaving any traces behind (**Fig. 14**).

	After scratching	Water dropping	Water dropping	After dropping
Glass				
Silicone				
Paper				
Steel				
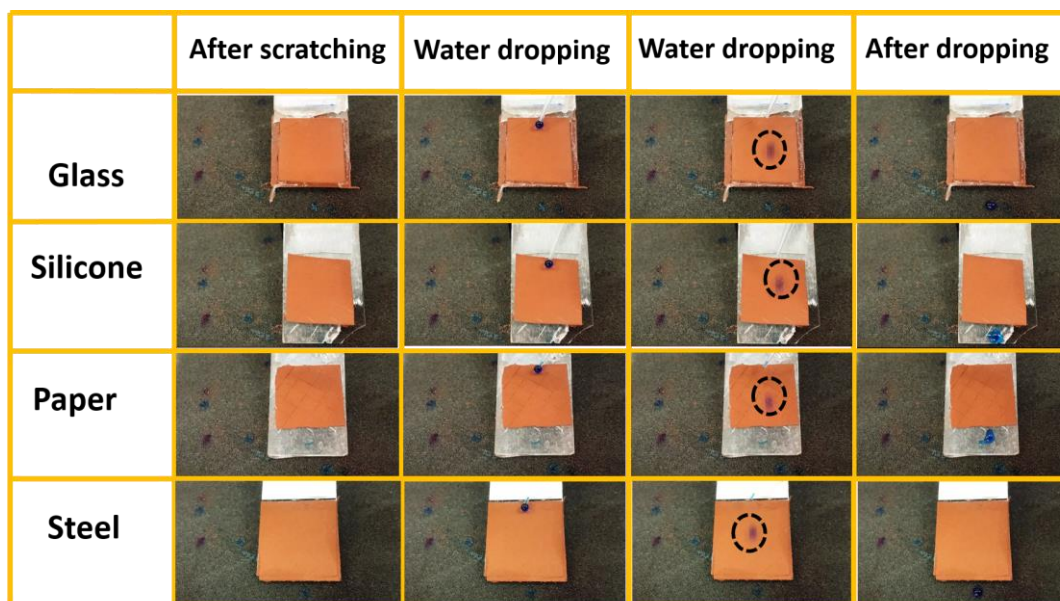
Fig. 5.14 Knife-scratch tests on the superhydrophobic glass, silicone, paper and steel substrates.

	Before wiping	**After wiping**
Glass		

Fig. 5.15 Finger-wipe tests on uncoated SH-Cu, plain and coated SH-Cu glass substrates, respectively (from left to right). The coating without PDMS was partly removed by a finger wife while the superhydrophobic glass with PDMS coating sustained water proofing properties, indicating the coating becomes more robust.

5.3.2: Antifouling activity

More than 60% of HAIs worldwide are attributed to bacteria forming biofilms on medical devices.[353,354] The biofouling process is complicated but it starts with spontaneous non-specific adsorption of organic molecules on to the surface followed by colonization by microorganisms.[355] In order to decrease HAIs cases and associated hospitalization costs, it

is essential to fabricate surfaces that inhibit bacterial attachment and subsequent biofilm formation.

In this work, the antifouling properties of the following samples were investigated using two model hospital-associated pathogens[356]; a Cu-deposited glass as a low-adhesive SH surface (SH-Cu) and a Cu-coated glass infused with silicone oil formed a slippery material (SLIP-Cu).

The anti-fouling properties of the samples was examined using overnight bacterial cultures in order to initiate biofilm formation under static conditions. Over this growth period (48 h), there was noticeable bacterial growth on all the samples. However, when the samples were washed with deionized-water, the attached biofilms were spontaneously delaminated resulting in clean surfaces (**Fig. 5.16**). This was attributed to the poor attachment of the bacteria to the samples.
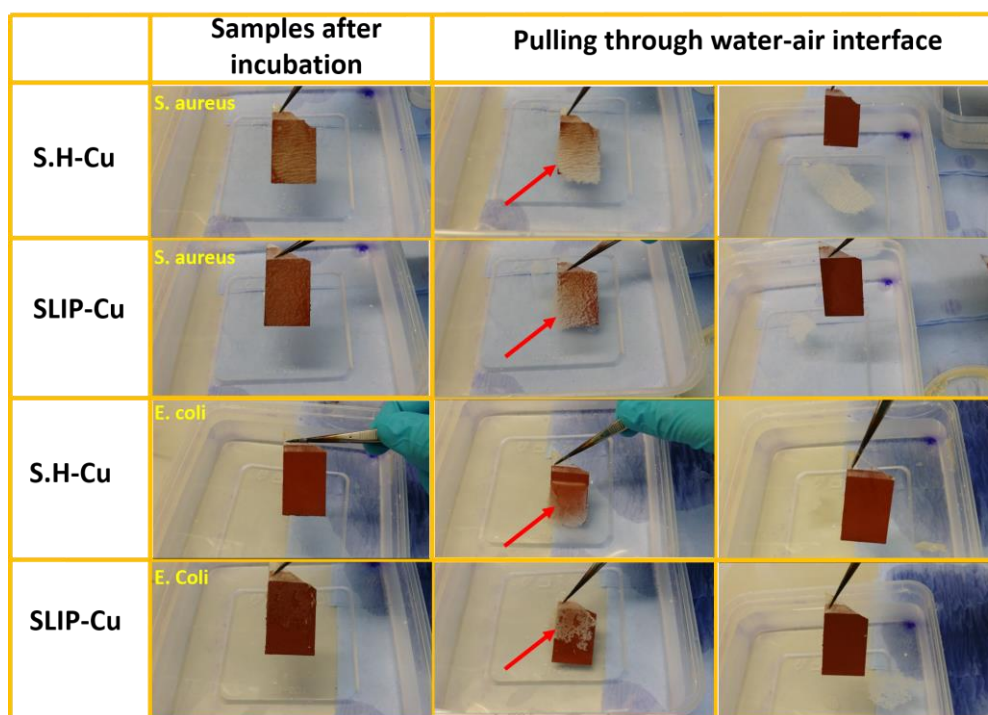
Fig. 5.16 Snapshots taken before and in the course of pulling of the samples from the media through the air-water interface after being exposed to either *S. aureus* or *E. coli* cultures for 2 days to grow biofilm.

114

In order to quantify the adherent bacteria, the attached biomass was washed and then stained with crystal violet. Measurement of the absorbance of the solubilized CV demonstrated a 99.3% reduction in *S. aureus* biofilm on SLIP-Cu compared with S.H-Cu over a 2-day growth period (**Fig.5.17 (a)**). Antifouling activity was also apparent in experiments with *E. coli*. The amount of *E. coli* attachment on SLIP-Cu was decreased by 88.9% compared to S.H-Cu under the same conditions (**Fig. 5.17 (b)**).

It is important to note that many environmental conditions where biofilm inhibition is essential are not static. Most submerged biofilm formation takes place under different flow conditions such as in plumbing, catheters, ship hulls and so on.[357,358] Therefore, slippery surfaces on which biofilm attachment is significantly reduced is expected to promote easy removal of the attached cells by even gentle flow leading to a persistent antifouling strategy which is superior to bactericidal and chemical methods.

There might be two possible reasons for this low attachment. First, the bacteria could not penetrate through the lubricant layer to make contact with the solid surface since the bacterial suspension and the lubricant is immiscible. Second, bacteria cannot anchor onto a lubricant surface through pili and other cellular mechanics as would be possible on a solid surface.[359,360] Hence, any bacteria contact with the lubricant layer can be easily removed by even a gentle water rinse.
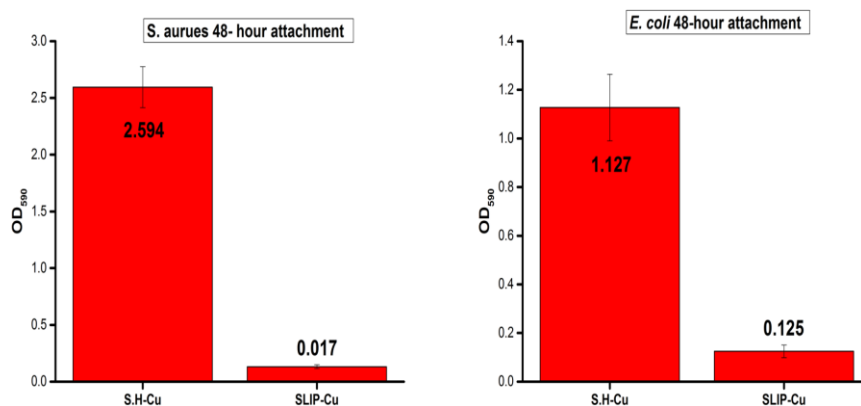
Fig. 5.17 Comparison of the attachment of biofilm-forming *S. aureus* (on the left) and *E. coli* (on the right) to S.H-Cu and SLIP-Cu.

The antifouling performance of the samples was also qualitatively investigated using SEM. It was apparent that after 2 days of incubation, a larger number of both *S. aureus* (**Fig. 5.18**) and *E. coli* (**Fig. 5.20**) cells have colonized the S.H-Cu surface, indicating its low antifouling efficiency despite its low surface energy. On the other hand, no biofouling caused by *S. aureus* (**Fig. 5.19**) or *E.coli* (**Fig. 5.21**) can be seen on SLIP surface indicating that the bacteria were not capable of sensing and adhering to the surface.[361]
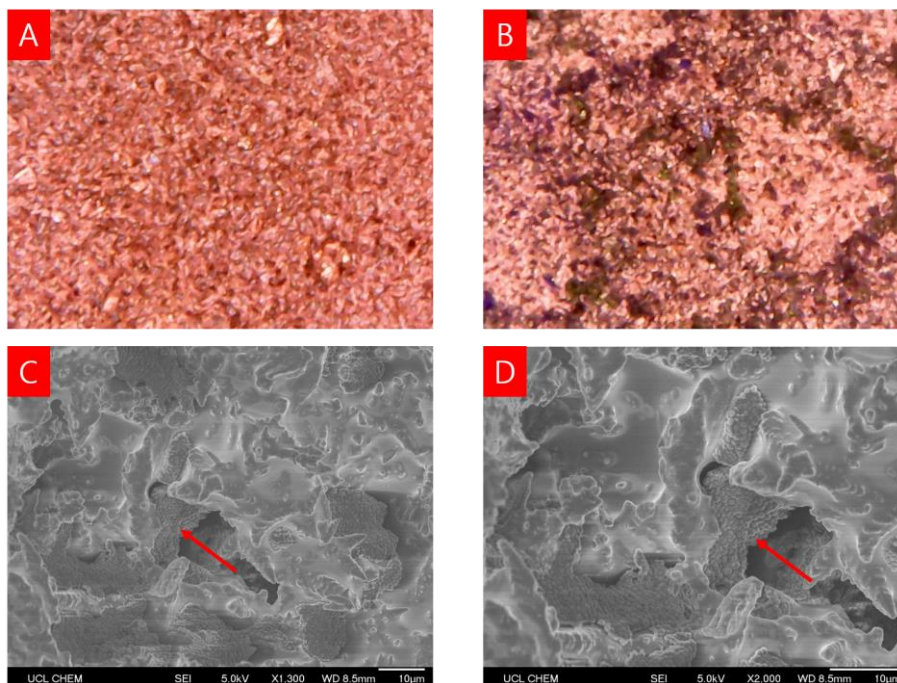
Fig. 5.18 Optical and SEM images of SH-Cu (A) before and (B, C, and D) after being exposed to *S. Aureus* culture for 2 days to grow biofilm. The magnifications are x1300 and x2000 for the inset images. The arrows show the bacterial colonies. The purple colour (B) indicates that the colonies were stained with crystal violet.
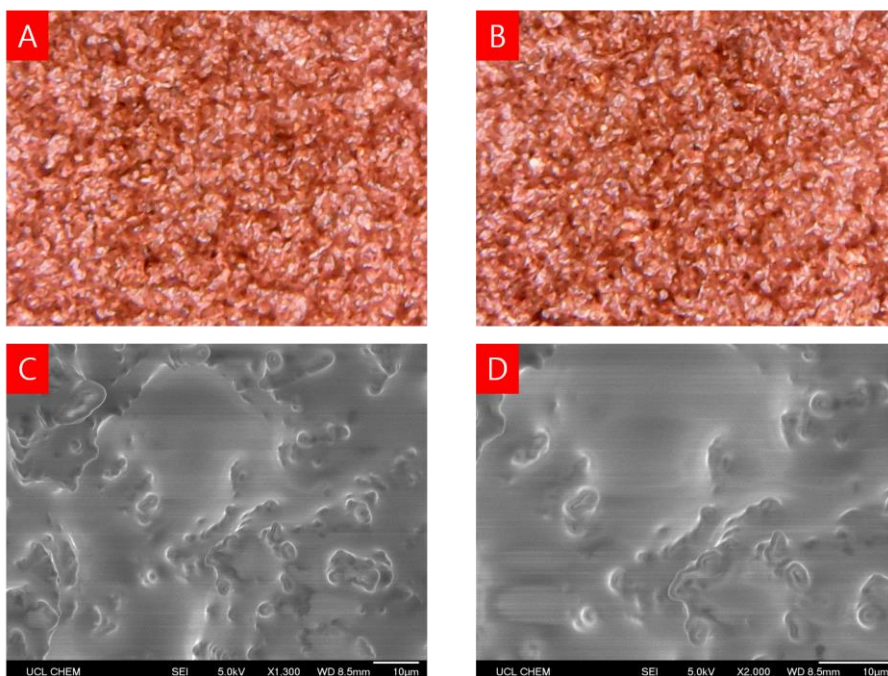
Fig. 5.19 Optical and SEM images of SLIP-Cu (A) before and (B, C, and D) after being exposed to *S. Aureus* culture for 2 days to grow biofilm. The magnifications are x1300 and x2000 for the inset images.
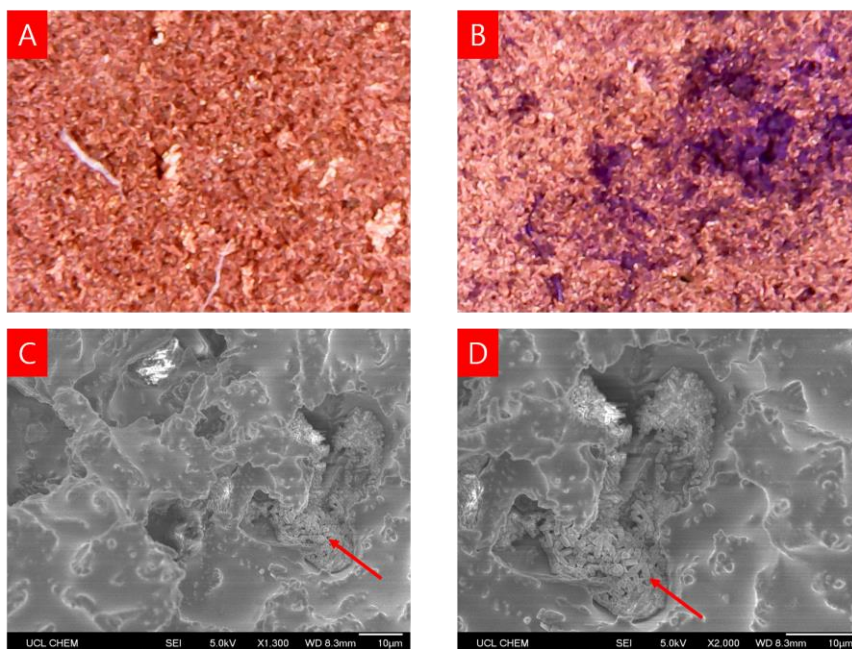
Fig. 5.20 Optical and SEM images of SH-Cu (A) before and (B, C, and D) after being exposed to *E. coli* culture for 2 days to grow biofilm. The magnifications are x1300 and x2000 for the inset images. The arrows show the bacterial colonies. The purple colour (B) indicates that the colonies were stained with violet.
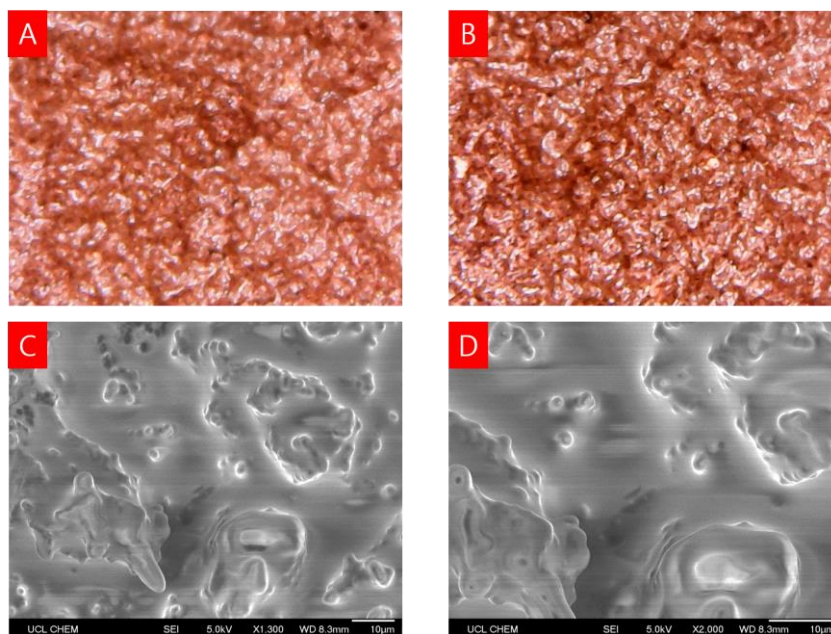
Fig. 5.21 Optical and SEM images of SLIP-Cu (A) before and (B, C, and D) after being exposed to *E. coli* culture for 2 days to grow biofilm. The magnifications are x1300 and x2000 for the inset images. The arrows show the bacterial colonies.

This performance difference between the SH and SLIP can be attributed to the instability of the air layer trapped in the SH-Cu surface under immersed conditions, in contrast with the stability of the lubricant over layer in the SLIP-CU surface under the same conditions. Superhydrophobic surfaces in the Cassie (trapped air) state are prone to irreversible wetting (Wenzel state), particularly when bacteria produce surfactants, seriously hindering their lifetime in submerged environments.[362] In addition, bacteria have been demonstrated to utilize their flagella to displace the trapped air layer from the superhydrophobic surface to provide new favorable sites for bacterial attachment.[363]

5.4: CONCLUSION

Mechanically durable Cu-based substrates with different surface properties (i.e. superhydrophobic and slippery) have been developed without the need for any expensive chemicals (e.g. fluorinated compounds) or further complex post-treatments (e.g. plasma modification and chemical grafting).

118

The main advantages of the as-prepared Cu coatings can be summarized as follows; (i) A facile, simple, inexpensive, scalable method fabricates exceptionally mechanically durable Cu films on different substrates including glass, silicone, paper, steel and so on. (ii) Robust superhydrophobic coatings with CAs of >155˚maintained their anti-wetting performance after various kinds of damage such as finger-wipe, knife-scratch and multiple abrasion cycles with sandpaper, validating their outstanding mechanical durability. (iii) When converted to the SLIP, they can repel even low-surface-tension liquids (e.g. glycerol) as well as complex fluids (e.g. blood) and considerably reduce attachment of pathogenic microorganisms without toxic effects. Consequently, these surfaces with extreme mechanical robustness and anti-fouling properties can offer numerous potential applications that require prolonged biofilm resistance even under harsh environmental and fouling conditions.

Chapter 6: CONCLUSIONS

The increasing incidence of HAIs often caused by antibiotic resistant pathogens highlights the importance of the development of efficacious infection-prevention approaches. One way of decreasing the spread of infection is the utilization of self-sterilizing surfaces to help both reduce the risk of infection upon use of medical devices (e.g. catheters) and also disrupt the cycle of person-person transmission of pathogenic bacteria in healthcare environments. In this thesis, various antibacterial surfaces have been fabricated that destroy colonising bacteria in the dark or light.

Chapter 2 and 3 outlined the development of potent antibacterial surfaces that show an enhanced activity triggered by a light-activated bactericidal mechanism. A novel method was employed, exploiting the concept of PDT. The advantage of this method for use in biomedical applications is two-fold. Firstly, these polymers eradicate bacterial cells through production of a broad range of ROS that show a non-site specific and multi-site attack mechanism against bacteria in the vicinity, reducing the likelihood of the emergence of bacterial resistance. Secondly, while other bactericidal surfaces lose their biocidal efficacy because of the build-up of dirt masking the antibacterial properties, it is assumed that the ROS produced by these samples can oxidize organic matter contaminating the polymer surface, hence sustaining the antibacterial properties.

In Chapter 2, the photo-active dye, crystal violet, was successfully incorporated into a non-toxic polymer, PDMS, using a facile ''swell-encapsulation-shrink'' method for potential use in hospital touch surface applications. The antibacterial activity was activated using a white hospital light source. This CV-embedded polymer was able to kill *S. aureus* in 2 hours and *E. coli* in 4 hours, with bacteria numbers reduced below the detection limit upon white-light illumination.

Further work highlighted the fabrication of materials that induced a dual-mechanism bacterial kill approach, through the incorporation of both photo-active crystal violet and intrinsically antibacterial Zinc Oxide NPs, for the development of self-sterilizing surfaces (Chapter 3). The results revealed that further enhancement of antibacterial efficacy of the

dye incorporated polymer was observed upon the introduction of ZnO NPs. ZnO/CV composites induced the lethal photosensitization of both *S. aureus* and *E. coli* in just 45 min and 90 min, respectively, with a minimum of a 4-log reduction in the numbers of both bacteria.

Next, Chapter 4 and 5, focused on the development of materials that not only kill the bacteria without any white light activation or a photosensitizer, but also reduce the attachment of bacteria. A two-step deposition process was employed to coat 3-5 nm copper nanoparticles (Cu NPs) onto a curable silicone polymer, polydimethylsiloxane (PDMS) using aerosol assisted chemical vapour deposition (AACVD) (Chapter 4). Cu particles adherent to the PDMS surfaces were expected to destroy the contacted pathogenic bacteria while the low surface energy could significantly reduce the number of adhered bacteria and subsequent biofilm formation. The modified samples showed superhydrophobicity with a water contact angle of 151° as well as remarkable water bouncing properties. Also, they demonstrated rapid, potent biocidal activity under dark conditions when tested against both *E. coli* and *S. aureus* (>4 log reduction in bacterial numbers) in 15 min and 60 min, respectively. Furthermore, the CVD treated superhydrophobic surfaces considerably prevented the attachment of both types of bacteria in contrast with uncoated glass samples following 1 h period of incubation.

However, superhydrophobic surfaces should possess a mico-/nano surface roughness and a low-surface-energy layer, which are essential for superhydrophobicity. Hence, such surfaces are susceptible to mechanical abrasion, limiting their use in real-world applications because of the fragile surface micro/nano structures and fast degradation or removal of low-surface-energy species.

To overcome this problem, in Chapter 5, mechanically stable antifouling coatings on different substrates (e.g. glass, metal, silicone) were fabricated by incorporating PDMS and commercially available hydrophobic copper particles. The resultant materials showed superhydrophobicity with high water contact angle values (CA, > 155˚) and very low sliding angle (SA, < 5˚). These coatings also demonstrated resilience and sustained its performance after different types of physical damage including finger-wipe, knife-scratch

and multiple abrasion cycles with sandpaper. However, superhydrophobic surfaces in the Cassie (trapped air) state are prone to irreversible wetting (Wenzel state), particularly when bacteria produce surfactants, seriously hindering their lifetime in submerged environments On the other hand, Xiao *et al.* has shown that different bacteria types including *Pseudomonas aeruginosa, E. coli* and *S. aureus* do not form biofilms on slippery liquid-infused porous surfaces (SLIPS).[364] In addition, SLIPS have demonstrated a reduction in settlement of various marine organisms such as Ulva linza zoospores and Balanus Amphitrite larvae.[364] Inspired by these works, slippery surfaces were obtained by infusion of a silicone oil lubricant on the robust superhydrophobic surfaces *via* capillary effect.

The anti-biofouling properties of the samples were examined using high density cultures of *S. aureus* and *E. coli*. They were immersed in growth media containing app. 10^8 CFU mL^{-1} for 2 days under static conditions. The results demonstrated that the superhydrophobic surfaces were significantly fouled. On the other hand, no biofouling was observed on the slippery surfaces. Based on CV absorbance, these slippery surfaces inhibited 88.9% and 99.3% of *E. coli* and *S. aureus*, respectively.

Future work should focus on an investigation into the photochemical mechanisms for the antibacterial activity of photo-activated CV-coated samples using EPR spectroscopy that can determine whether Type 1 or Type 2 pathways are responsible for the destruction of bacteria. This should be carried out in the presence and absence of ZnO NPs to detect any differences. ICP-OES should be performed for quantification and analysis of nanoparticle that might leach from the nanoparticle-doped polymer samples fabricated in this thesis. This would give valuable information on how the leaching of nanoparticles from the polymers influence the viability of bacteria.

Also, the stability and longevity of the modified samples should be investigated over a longer period of time (e.g. months/years) under various conditions (e.g. with routine cleaning, organic contamination and without coverslip and light). Moreover, the effects of environmental factors including organic contamination, humidity, and temperature on the bactericidal activity of the samples should be investigated.

Since some discrepancies between the efficacy of the modified samples against Gram-positive bacteria and Gram-negative bacteria were observed, testing different types of bacteria would help identify a pattern. Moreover, further investigation on the interaction of bacterial cells with both superhydrophobic and slippery materials fabricated in this thesis should be performed in order to elucidate the mechanism of observed anti-adhesion activity, i.e. AFM to measure the interaction force of bacteria with the modified sample.

References

1.   Health and Social Care Act London: Parliament of the United Kingdom; 2008.

2.   Leape, L. L. *et al.* The Nature of Adverse Events in Hospitalized Patients. *N. Engl. J. Med.* **324,** 377–384 (1991).

3.   Abreu, A. C., Tavares, R. R., Borges, A., Mergulhão, F. & Simões, M. Current and emergent strategies for disinfection of hospital environments. *J. Antimicrob. Chemother.* **68,** 2718–32 (2013).

4.   Pan, S.-C. *et al.* Assessing the thoroughness of hand hygiene: "seeing is believing". *Am. J. Infect. Control* **42,** 799–801 (2014).

5.   Hawkey, P. M. The growing burden of antimicrobial resistance. *J. Antimicrob. Chemother.* **62 Suppl 1,** i1-9 (2008).

6.   Lesprit, P. & Brun-Buisson, C. Hospital antibiotic stewardship. *Curr. Opin. Infect. Dis.* **21,** 344–9 (2008).

7.   World Health Organization: Antimicrobial Resistance, 2015.

8.   Healthy Lifestyle: Consumer Health: Mayo Clinic, 2014. [cited 2016 15/03/2016] Available from: http://www.mayoclinic.org/healthy--- lifestyle/consumer---health/in---depth/antibiotics/art---20045720.

9.   Gold, H. S. & Moellering, R. C. Antimicrobial-drug resistance. *N. Engl. J. Med.* **335,** 1445–53 (1996).

10.   Cohen, M. L. Changing patterns of infectious disease. *Nature* **406,** 762–767 (2000).

11.   Antibiotic Resistance Threats in the United States, 2013 | Antibiotic/Antimicrobial Resistance | CDC. at <http://www.cdc.gov/drugresistance/threat-report-2013/>

12.   Metz, M. & Shlaes, D. M. Eight more ways to deal with antibiotic resistance.

Antimicrob. Agents Chemother. **58,** 4253–6 (2014).

13. Antibiotic resistance threats in the United States, 2013. Centers for Disease Control and Prevention, US Department of Health and Human Services, Atlanta, GA." In: Centers for Disease Control and Prevention (2013).

14. Garner, J. S. Guideline for isolation precautions in hospitals. The Hospital Infection Control Practices Advisory Committee. *Infect. Control Hosp. Epidemiol.* **17,** 53–80 (1996).

15. NHS National Patient Safety Agency. (2004). NHS National Patient Safety Agency cleanyourhands campaign [Online]. Available: http://www.npsa.nhs.uk/cleanyourhands.

16. Casewell, M. & Phillips, I. Hands as route of transmission for Klebsiella species. *Br. Med. J.* **2,** 1315–7 (1977).

17. Hayden, M. K. *et al.* Reduction in acquisition of vancomycin-resistant enterococcus after enforcement of routine environmental cleaning measures. *Clin. Infect. Dis.* **42,** 1552–60 (2006).

18. Pittet, D., Allegranzi, B., Boyce, J. & World Health Organization World Alliance for Patient Safety First Global Patient Safety Challenge Core Group of Experts. The World Health Organization Guidelines on Hand Hygiene in Health Care and their consensus recommendations. *Infect. Control Hosp. Epidemiol.* **30,** 611–22 (2009).

19. Samore, M. H., Venkataraman, L., DeGirolami, P. C., Arbeit, R. D. & Karchmer, A. W. Clinical and molecular epidemiology of sporadic and clustered cases of nosocomial Clostridium difficile diarrhea. *Am. J. Med.* **100,** 32–40 (1996).

20. Weber, D. J. & Rutala, W. A. Role of environmental contamination in the transmission of vancomycin-resistant enterococci. *Infect. Control Hosp. Epidemiol.* **18,** 306–9 (1997).

21. Devine, J., Cooke, R. P. & Wright, E. P. Is methicillin-resistant Staphylococcus aureus (MRSA) contamination of ward-based computer terminals a surrogate marker for nosocomial MRSA transmission and handwashing compliance? *J. Hosp. Infect.* **48,** 72–5 (2001).

22. Dancer, S. J. Importance of the environment in meticillin-resistant Staphylococcus aureus acquisition: the case for hospital cleaning. *Lancet. Infect. Dis.* **8,** 101–13 (2008).

23. Pittet, D., Allegranzi, B., Boyce, J. & World Health Organization World Alliance for Patient Safety First Global Patient Safety Challenge Core Group of Experts. The World Health Organization Guidelines on Hand Hygiene in Health Care and their consensus recommendations. *Infect. Control Hosp. Epidemiol.* **30,** 611–22 (2009).

24. Dancer, S. J. *et al.* Mopping up hospital infection. *J. Hosp. Infect.* **43,** 85–100 (1999).

25. Falagas, M. E. *et al.* Airborne hydrogen peroxide for disinfection of the hospital environment and infection control: a systematic review. *J. Hosp. Infect.* **78,** 171–7 (2011).

26. Talon, D. *et al.* The role of the hospital environment in the epidemiology of multi-resistant bacteria. *J. Hosp. Infect.* **43,** 13–7 (1999).

27. Zollfrank, C., Gutbrod, K., Wechsler, P. & Guggenbichler, J. P. Antimicrobial activity of transition metal acid MoO3 prevents microbial growth on material surfaces. *Mater. Sci. Eng. C* **32,** 47–54 (2012).

28. Boyce, J. M. Environmental contamination makes an important contribution to hospital infection. *J. Hosp. Infect.* **65 Suppl 2,** 50–4 (2007).

29. Dancer, S. J. The role of environmental cleaning in the control of hospital-acquired infection. *J. Hosp. Infect.* **73,** 378–85 (2009).

30. Wood, M. W., Lund, R. C. & Stevenson, K. B. Bacterial contamination of stethoscopes with antimicrobial diaphragm covers. *Am. J. Infect. Control* **35,** 263–6 (2007).

31. Berendt, A. E., Turnbull, L., Spady, D., Rennie, R. & Forgie, S. E. Three swipes and you're out: how many swipes are needed to decontaminate plastic with disposable wipes? *Am. J. Infect. Control* **39,** 442–3 (2011).

32. Kramer, A., Schwebke, I. & Kampf, G. How long do nosocomial pathogens persist on inanimate surfaces? A systematic review. *BMC Infect. Dis.* **6,** 130 (2006).

33. Hota, B. Contamination, disinfection, and cross-colonization: are hospital surfaces reservoirs for nosocomial infection? *Clin. Infect. Dis.* **39,** 1182–9 (2004).

34. Otter, J. A., Yezli, S. & French, G. L. The role played by contaminated surfaces in the transmission of nosocomial pathogens. *Infect. Control Hosp. Epidemiol.* **32,** 687–99 (2011).

35. Schmid-Hempel, P. & Frank, S. A. Pathogenesis, Virulence, and Infective Dose. *PLoS Pathog.* **3,** e147 (2007).

36. Schmidt, M. G. *et al.* Patient environment microbial burden reduction: a pilot study comparison of 2 terminal cleaning methods. *Am. J. Infect. Control* **40,** 559–61 (2012).

37. Rzezutka, A. & Cook, N. Survival of human enteric viruses in the environment and food. *FEMS Microbiol. Rev.* **28,** 441–53 (2004).

38. Barrett, F. F., McGehee, R. F. & Finland, M. Methicillin-Resistant *Staphylococcus aureus* at Boston City Hospital. *N. Engl. J. Med.* **279,** 441–448 (1968).

39. Rocha, L. A., Marques Ribas, R., da Costa Darini, A. L. & Gontijo Filho, P. P. Relationship between nasal colonization and ventilator-associated pneumonia and the role of the environment in transmission of Staphylococcus aureus in intensive care units. *Am. J. Infect. Control* **41,** 1236–40 (2013).

40. Mulvey, D. *et al.* Finding a benchmark for monitoring hospital cleanliness. *J. Hosp. Infect.* **77,** 25–30 (2011).

41. Mermel, L. A., Cartony, J. M., Covington, P., Maxey, G. & Morse, D. Methicillin-resistant Staphylococcus aureus colonization at different body sites: a prospective, quantitative analysis. *J. Clin. Microbiol.* **49,** 1119–21 (2011).

42. Roisin, S. *et al.* Impact of rapid molecular screening at hospital admission on nosocomial transmission of methicillin-resistant Staphylococcus aureus: cluster randomised trial. *PLoS One* **9,** e96310 (2014).

43. Jarvis, W. R., Schlosser, J., Chinn, R. Y., Tweeten, S. & Jackson, M. National prevalence of methicillin-resistant Staphylococcus aureus in inpatients at US health care facilities, 2006. *Am. J. Infect. Control* **35,** 631–7 (2007).

44. Fuller, C. *et al.* The national one week prevalence audit of universal meticillin-resistant Staphylococcus aureus (MRSA) admission screening 2012. *PLoS One* **8,** e74219 (2013).

45. Uhlemann, A.-C. *et al.* The environment as an unrecognized reservoir for community-associated methicillin resistant Staphylococcus aureus USA300: a case-control study. *PLoS One* **6,** e22407 (2011).

46. Escherichiacoli:TheRoyalChildrensHospitalMelbourne,2016.[cited201615/03/16]; Availableon:http://www.rch.org.au/washup/for_health_professionals/Escherichia_coli.

47. Peleg, A. Y. & Hooper, D. C. Hospital-acquired infections due to gram-negative bacteria. *N. Engl. J. Med.* **362,** 1804–13 (2010).

48. Hodges, K. & Gill, R. Infectious diarrhea: Cellular and molecular mechanisms. *Gut Microbes* **1,** 4–21 (2010).

49. Jacobsen, S. M., Stickler, D. J., Mobley, H. L. T. & Shirtliff, M. E. Complicated

catheter-associated urinary tract infections due to Escherichia coli and Proteus mirabilis. *Clin. Microbiol. Rev.* **21,** 26–59 (2008).

50.

  HemolyticUremicSyndroneinChildren:NationalInstituteofDiabetesandDigestiveandKidneyDiseases2015.[cited201615/03/2016];Availablefrom:http://www.niddk.nih.gov/health---information/health---topics/kidney---disease/hemolytic---uremic---syndrome---in---children.

51. Abstracts from the 37th Annual Meeting of the Society of General Internal Medicine. Journal of General Internal Medicine. 2014;29(Suppl 1):1---545. doi:10.1007/s11606---014---2834---9.

52.

  EnglishSurveillanceProgrammeforAntimicrobialUtilisationandResistanceannualreport;PublicHealthEngland,2015.[cited201615/03/16];Availablefrom:https://www.gov.uk/government/publications/health---protection---report---volume---9---2015/hpr---volume---9---issu.

53. Coureuil, M. *et al.* Mechanism of meningeal invasion by Neisseria meningitidis. *Virulence* **3,** 164–72

54. Oie, S., Hosokawa, I. & Kamiya, A. Contamination of room door handles by methicillin-sensitive/methicillin-resistant Staphylococcus aureus. *J. Hosp. Infect.* **51,** 140–143 (2002).

55. French, G. L. *et al.* Tackling contamination of the hospital environment by methicillin-resistant Staphylococcus aureus (MRSA): a comparison between conventional terminal cleaning and hydrogen peroxide vapour decontamination. *J. Hosp. Infect.* **57,** 31–7 (2004).

56. National audit office, The management and control of hospital acquired infection in acute NHS trusts in England, http://www.nao.org.uk/wp-content/uploads/2000/02/9900230.pdf, accessed: Feb, 2000.

57. National audit office, Improving patient care by reducing the risk of hospital acquired infection: A progress report, http://www.nao.org.uk/wp-content/uploads/2004/07/0304876.pdf, accessed: July, 2004.

58. House of commons, Reducing healthcare associated infection in hospitals in England, http://www.publications.parliament.uk/pa/cm200809/cmselect/cmpubacc/812/812.pdf, accessed: July, 2009.

59. Bourn J. The Management and Control of Hospital Acquired Infection In Acute NHS Trusts in England. *Natl. Audit Off.* (2000).

60. Alanis, A. J. Resistance to antibiotics: are we in the post-antibiotic era? *Arch. Med. Res.* **36,** 697–705 (2005).

61. Riley, M. A. *et al.* Resistance is futile: the bacteriocin model for addressing the antibiotic resistance challenge. *Biochem. Soc. Trans.* **40,** (2012).

62. Levy, S. B. & Marshall, B. Antibacterial resistance worldwide: causes, challenges and responses. (2004).

63. Davies, J. & Davies, D. Origins and evolution of antibiotic resistance. *Microbiol. Mol. Biol. Rev.* **74,** 417–33 (2010).

64. Huh, A. J. & Kwon, Y. J. 'Nanoantibiotics': a new paradigm for treating infectious diseases using nanomaterials in the antibiotics resistant era. *J. Control. Release* **156,** 128–45 (2011).

65. Huh, A. J. & Kwon, Y. J. 'Nanoantibiotics': a new paradigm for treating infectious diseases using nanomaterials in the antibiotics resistant era. *J. Control. Release* **156,** 128–45 (2011).

66. Zhang, L., Pornpattananangku, D., Hu, C.-M. J. & Huang, C.-M. Development of nanoparticles for antimicrobial drug delivery. *Curr. Med. Chem.* **17,** 585–94 (2010).

67. Huang, C.-M. *et al.* Eradication of drug resistant Staphylococcus aureus by liposomal oleic acids. *Biomaterials* **32,** 214–21 (2011).

68. Hajipour, M. J. *et al.* Antibacterial properties of nanoparticles. *Trends Biotechnol.* **30,** 499–511 (2012).

69. Weir, E., Lawlor, A., Whelan, A. & Regan, F. The use of nanoparticles in anti-microbial materials and their characterization. *Analyst* **133,** 835–45 (2008).

70. Friedman, A. J. *et al.* Antimicrobial and anti-inflammatory activity of chitosan-alginate nanoparticles: a targeted therapy for cutaneous pathogens. *J. Invest. Dermatol.* **133,** 1231–9 (2013).

71. Chopra, I. The increasing use of silver-based products as antimicrobial agents: a useful development or a cause for concern? *J. Antimicrob. Chemother.* **59,** 587–90 (2007).

72. Taubes, G. The bacteria fight back. *Science* **321,** 356–61 (2008).

73. Monteiro, D. R. *et al.* The growing importance of materials that prevent microbial adhesion: antimicrobial effect of medical devices containing silver. *Int. J. Antimicrob. Agents* **34,** 103–10 (2009).

74. Yuan Gao, Y. & Cranston, R. Recent Advances in Antimicrobial Treatments of Textiles. *Text. Res. J.* **78,** 60–72 (2008).

75. Blecher, K., Nasir, A. & Friedman, A. The growing role of nanotechnology in combating infectious disease. *Virulence* **2,** 395–401 (2011).

76. Huh, A. J. & Kwon, Y. J. 'Nanoantibiotics': A new paradigm for treating infectious diseases using nanomaterials in the antibiotics resistant era. *J. Control. Release* **156,** 128–145 (2011).

77. Hindi, K. M. *et al.* The antimicrobial efficacy of sustained release silver-carbene complex-loaded L-tyrosine polyphosphate nanoparticles: characterization, in vitro

and in vivo studies. *Biomaterials* **30,** 3771–9 (2009).

78. Knetsch, M. L. W. & Koole, L. H. New Strategies in the Development of Antimicrobial Coatings: The Example of Increasing Usage of Silver and Silver Nanoparticles. *Polymers (Basel).* **3,** 340–366 (2011).

79. Lara, H. H., Ayala-Núñez, N. V., Ixtepan Turrent, L. del C. & Rodríguez Padilla, C. Bactericidal effect of silver nanoparticles against multidrug-resistant bacteria. *World J. Microbiol. Biotechnol.* **26,** 615–621 (2010).

80. Brown, A. N. *et al.* Nanoparticles functionalized with ampicillin destroy multiple-antibiotic-resistant isolates of Pseudomonas aeruginosa and Enterobacter aerogenes and methicillin-resistant Staphylococcus aureus. *Appl. Environ. Microbiol.* **78,** 2768–74 (2012).

81. Huang, L., Dai, T., Xuan, Y., Tegos, G. P. & Hamblin, M. R. Synergistic combination of chitosan acetate with nanoparticle silver as a topical antimicrobial: efficacy against bacterial burn infections. *Antimicrob. Agents Chemother.* **55,** 3432–8 (2011).

82. Raimondi, F., Scherer, G. G., Kötz, R. & Wokaun, A. Nanoparticles in energy technology: examples from electrochemistry and catalysis. *Angew. Chem. Int. Ed. Engl.* **44,** 2190–209 (2005).

83. Sondi, I. & Salopek-Sondi, B. Silver nanoparticles as antimicrobial agent: a case study on E. coli as a model for Gram-negative bacteria. *J. Colloid Interface Sci.* **275,** 177–82 (2004).

84. Pal, S., Tak, Y. K. & Song, J. M. Does the antibacterial activity of silver nanoparticles depend on the shape of the nanoparticle? A study of the Gram-negative bacterium Escherichia coli. *Appl. Environ. Microbiol.* **73,** 1712–20 (2007).

85. Rai, M., Yadav, A. & Gade, A. Silver nanoparticles as a new generation of antimicrobials. *Biotechnol. Adv.* **27,** 76–83 (2009).

86. Shahverdi, A. R., Fakhimi, A., Shahverdi, H. R. & Minaian, S. Synthesis and effect of silver nanoparticles on the antibacterial activity of different antibiotics against Staphylococcus aureus and Escherichia coli. *Nanomedicine* **3,** 168–71 (2007).

87. Fayaz, A. M. *et al.* Biogenic synthesis of silver nanoparticles and their synergistic effect with antibiotics: a study against gram-positive and gram-negative bacteria. *Nanomedicine* **6,** 103–9 (2010).

88. Drake, P. L. & Hazelwood, K. J. Exposure-related health effects of silver and silver compounds: a review. *Ann. Occup. Hyg.* **49,** 575–85 (2005).

89. Johnston, H. J. *et al.* A review of the in vivo and in vitro toxicity of silver and gold particulates: particle attributes and biological mechanisms responsible for the observed toxicity. *Crit. Rev. Toxicol.* **40,** 328–46 (2010).

90. Oberdörster, G., Oberdörster, E. & Oberdörster, J. Nanotoxicology: an emerging discipline evolving from studies of ultrafine particles. *Environ. Health Perspect.* **113,** 823–39 (2005).

91. Grass, G., Rensing, C. & Solioz, M. Metallic copper as an antimicrobial surface. *Appl. Environ. Microbiol.* **77,** 1541–7 (2011).

92. Usman, M., Ibrahim, N., Shameli, K., Zainuddin, N. & Yunus, W. Copper Nanoparticles Mediated by Chitosan: Synthesis and Characterization via Chemical Methods. *Molecules* **17,** 14928–14936 (2012).

93. UMER, A., NAVEED, S., RAMZAN, N. & RAFIQUE, M. S. SELECTION OF A SUITABLE METHOD FOR THE SYNTHESIS OF COPPER NANOPARTICLES. *Nano* **7,** 1230005 (2012).

94. Tran, Q. H., Nguyen, V. Q. & Le, A.-T. Silver nanoparticles: synthesis, properties, toxicology, applications and perspectives. *Adv. Nat. Sci. Nanosci. Nanotechnol.* **4,** 33001 (2013).

95.   Wu, W., He, Q. & Jiang, C. Magnetic iron oxide nanoparticles: synthesis and surface functionalization strategies. *Nanoscale Res. Lett.* **3,** 397–415 (2008).

96.   Worthington, K. L. S. *et al.* Chitosan coating of copper nanoparticles reduces *in vitro* toxicity and increases inflammation in the lung. *Nanotechnology* **24,** 395101 (2013).

97.   Barthel, M. J. *et al.* Synthesis of Highly Fluorescent Copper Clusters Using Living Polymer Chains as Combined Reducing Agents and Ligands. *ACS Nano* **9,** 11886–11897 (2015).

98.   Gawande, M. B. *et al.* Cu and Cu-Based Nanoparticles: Synthesis and Applications in Catalysis. *Chem. Rev.* **116,** 3722–3811 (2016).

99.   Prado, V. *et al.* Effectiveness of copper contact surfaces in reducing the microbial burden (MB) in the intensive care unit (ICU) of hospital del Cobre, Calama, Chile. *Int. J. Infect. Dis.* **14,** e268 (2010).

100.   Schmidt, M. & Initiative, C. T. S. Copper surfaces in the ICU reduced the relative risk of acquiring an infection while hospitalized. *BMC Proc.* **5,** O53 (2011).

101.   Warnes, S. L. & Keevil, C. W. Mechanism of copper surface toxicity in vancomycin-resistant enterococci following wet or dry surface contact. *Appl. Environ. Microbiol.* **77,** 6049–59 (2011).

102.   Casey, A. L. *et al.* Role of copper in reducing hospital environment contamination. *J. Hosp. Infect.* **74,** 72–77 (2010).

103.   Yoshida, Y., Furuta, S. & Niki, E. Effects of metal chelating agents on the oxidation of lipids induced by copper and iron. *Biochim. Biophys. Acta* **1210,** 81–8 (1993).

104.   Noyce, J. O., Michels, H. & Keevil, C. W. Potential use of copper surfaces to reduce survival of epidemic meticillin-resistant Staphylococcus aureus in the healthcare environment. *J. Hosp. Infect.* **63,** 289–297 (2006).

105. Weaver, L., Noyce, J. O., Michels, H. T. & Keevil, C. W. Potential action of copper surfaces on meticillin-resistant Staphylococcus aureus. *J. Appl. Microbiol.* **109,** 2200–2205 (2010).

106. Jiang, P., Zhou, J.-J. & Fang, H.-F. Hierarchical shelled ZnO structures made of bunched nanowire arrays. **17,** 1303–1310 (2007).

107. Zhou, J., Xu, N. S. & Wang, Z. L. Dissolving Behavior and Stability of ZnO Wires in Biofluids: A Study on Biodegradability and Biocompatibility of ZnO Nanostructures. *Adv. Mater.* **18,** 2432–2435 (2006).

108. Dibrov, P., Dzioba, J., Gosink, K. K. & Häse, C. C. Chemiosmotic mechanism of antimicrobial activity of Ag(+) in Vibrio cholerae. *Antimicrob. Agents Chemother.* **46,** 2668–70 (2002).

109. Brayner, R. *et al.* Toxicological impact studies based on Escherichia coli bacteria in ultrafine ZnO nanoparticles colloidal medium. *Nano Lett.* **6,** 866–70 (2006).

110. Roselli, M., Finamore, A., Garaguso, I., Britti, M. S. & Mengheri, E. Zinc oxide protects cultured enterocytes from the damage induced by Escherichia coli. *J. Nutr.* **133,** 4077–82 (2003).

111. Dastjerdi, R. & Montazer, M. A review on the application of inorganic nano-structured materials in the modification of textiles: focus on anti-microbial properties. *Colloids Surf. B. Biointerfaces* **79,** 5–18 (2010).

112. Huang, Z. *et al.* Toxicological effect of ZnO nanoparticles based on bacteria. *Langmuir* **24,** 4140–4 (2008).

113. Liu, Y. *et al.* Antibacterial activities of zinc oxide nanoparticles against Escherichia coli O157:H7. *J. Appl. Microbiol.* **107,** 1193–201 (2009).

114. van Grieken, R., Marugán, J., Sordo, C., Martínez, P. & Pablos, C. Photocatalytic inactivation of bacteria in water using suspended and immobilized silver-TiO2. *Appl. Catal. B Environ.* **93,** 112–118 (2009).

115. O'Neill, S. A., Parkin, I. P., Clark, R. J. H., Mills, A. & Elliott, N. Atmospheric pressure chemical vapour deposition of titanium dioxide coatings on glass. *J. Mater. Chem.* **13,** 56–60 (2003).

116. Paz, Y. *et al.* Photooxidative self-cleaning transparent titanium dioxide films on glass. *J. Mater. Res.* **10,** 2842–2848 (1995).

117. Paz, Y. *et al.* Photo-oxidatively self-cleaning transparent titanium dioxide films on soda lime glass: The deleterious effect of sodium contamination and its prevention. *J. Mater. Res.* **12,** 2759–2766 (1997).

118. and, T. N., Fujishima*, A., Sawunyama, P. & Hashimoto, K. Photocatalytic Degradation of Gaseous Formaldehyde Using TiO2 Film. (1998). doi:10.1021/ES980299+

119. Watanabe, T. *et al.* Photocatalytic activity and photoinduced hydrophilicity of titanium dioxide coated glass. *Thin Solid Films* **351,** 260–263 (1999).

120. Meilert, K. T., Laub, D. & Kiwi, J. Photocatalytic self-cleaning of modified cotton textiles by TiO2 clusters attached by chemical spacers. *J. Mol. Catal. A Chem.* **237,** 101–108 (2005).

121. Qi, K. *et al.* Self-cleaning cotton. *J. Mater. Chem.* **16,** 4567 (2006).

122. Ohko, Y. *et al.* Self-sterilizing and self-cleaning of silicone catheters coated with TiO(2) photocatalyst thin films: a preclinical work. *J. Biomed. Mater. Res.* **58,** 97–101 (2001).

123. Photoelectrochemical sterilization of microbial cells by semiconductor powders. *en.wikipedia.org/wiki/Polydimethylsiloxane* at <en.wikipedia.org/wiki/Polydimethylsiloxane>

124. Rehman, S., Ullah, R., Butt, A. M. & Gohar, N. D. Strategies of making TiO2 and ZnO visible light active. *J. Hazard. Mater.* **170,** 560–9 (2009).

125. Krishna, V. *et al.* Photocatalytic Disinfection with Titanium Dioxide Coated Multi-Wall Carbon Nanotubes. *Process Saf. Environ. Prot.* **83,** 393–397 (2005).

126. Amin, S. A., Pazouki, M. & Hosseinnia, A. Synthesis of TiO2–Ag nanocomposite with sol–gel method and investigation of its antibacterial activity against E. coli. *Powder Technol.* **196,** 241–245 (2009).

127. Kubacka, A., Ferrer, M., Martínez-Arias, A. & Fernández-García, M. Ag promotion of TiO2-anatase disinfection capability: Study of Escherichia coli inactivation. *Appl. Catal. B Environ.* **84,** 87–93 (2008).

128. Akhavan, O. Lasting antibacterial activities of Ag–TiO2/Ag/a-TiO2 nanocomposite thin film photocatalysts under solar light irradiation. *J. Colloid Interface Sci.* **336,** 117–124 (2009).

129. Zhang, W., Chen, Y., Yu, S., Chen, S. & Yin, Y. Preparation and antibacterial behavior of Fe3+-doped nanostructured TiO2 thin films. *Thin Solid Films* **516,** 4690–4694 (2008).

130. Skorb, E. V. *et al.* Antibacterial activity of thin-film photocatalysts based on metal-modified TiO2 and TiO2:In2O3 nanocomposite. *Appl. Catal. B Environ.* **84,** 94–99 (2008).

131. Chung, C.-J. *et al.* Photocatalytic TiO2 on copper alloy for antimicrobial purposes. *Appl. Catal. B Environ.* **85,** 103–108 (2008).

132. Yuan, W., Ji, J., Fu, J. & Shen, J. A facile method to construct hybrid multilayered films as a strong and multifunctional antibacterial coating. *J. Biomed. Mater. Res. Part B Appl. Biomater.* **85B,** 556–563 (2008).

133. Wu, P., Xie, R., Imlay, J. A. & Shang, J. K. Visible-light-induced photocatalytic inactivation of bacteria by composite photocatalysts of palladium oxide and nitrogen-doped titanium oxide. *Appl. Catal. B Environ.* **88,** 576–581 (2009).

134. Fujishima, A., Zhang, X. & Tryk, D. A. TiO2 photocatalysis and related surface

phenomena. *Surf. Sci. Rep.* **63,** 515–582 (2008).

135. Ireland, J. C., Klostermann, P., Rice, E. W. & Clark, R. M. Inactivation of Escherichia coli by titanium dioxide photocatalytic oxidation. *Appl. Envir. Microbiol.* **59,** 1668–1670 (1993).

136. Bonnett, R. *et al.* Photosensitizers of the porphyrin and phthalocyanine series for photodynamic therapy. *Chem. Soc. Rev.* **24,** 19 (1995).

137. Dolmans, D. E. J. G. J., Fukumura, D. & Jain, R. K. Photodynamic therapy for cancer. *Nat. Rev. Cancer* **3,** 380–7 (2003).

138. Wainwright, M. Photodynamic antimicrobial chemotherapy (PACT). *J. Antimicrob. Chemother.* **42,** 13–28 (1998).

139. Usuda, J. *et al.* Photodynamic Therapy (PDT) for Lung Cancers. *J. Thorac. Oncol.* **1,** 489–493 (2006).

140. Fien, S. M. & Oseroff, A. R. Photodynamic therapy for non-melanoma skin cancer. *J. Natl. Compr. Canc. Netw.* **5,** 531–40 (2007).

141. Bressler, N. M. *et al.* Verteporfin therapy for subfoveal choroidal neovascularization in age-related macular degeneration: four-year results of an open-label extension of 2 randomized clinical trials: TAP Report No. 7. *Arch. Ophthalmol. (Chicago, Ill. 1960)* **123,** 1283–5 (2005).

142. Hamblin, M. R. & Hasan, T. Photodynamic therapy: a new antimicrobial approach to infectious disease? *Photochem. Photobiol. Sci.* **3,** 436–50 (2004).

143. Raab & Raab, O. Effect of fluorescent substances on Infusoria. *Z. Biol.* **39,** 524–546 (1900).

144. Von Tappeiner H. and Jodlbauer A (1904). Uber wirkung der photodynamischen (fluorieszierenden) stoffe auf protozoan und enzyme. Dtsch Arch Klin Med 80: 427- 487. in

145. Von Tappeiner H and Jodlbauer A (1907). Die sensibilisierende wirkung fluorieszierender substanzer. Gesammte untersuchungen uber die photodynamische Erscheinung. Leipzig: F. C. W. Vogel.

146. Wilson, M. Light-activated antimicrobial coating for the continuous disinfection of surfaces. *Infect. Control Hosp. Epidemiol.* **24,** 782–4 (2003).

147. Bamfield, P. & Bamfield, P. *Chromic Phenomena*. (Royal Society of Chemistry, 2010). doi:10.1039/9781849731034

148. Green, T. J., Wilson, D. F., Vanderkooi, J. M. & DeFeo, S. P. Phosphorimeters for analysis of decay profiles and real time monitoring of exponential decay and oxygen concentrations. *Anal. Biochem.* **174,** 73–79 (1988).

149. Ochsner, M. Photophysical and photobiological processes in the photodynamic therapy of tumours. *J. Photochem. Photobiol. B.* **39,** 1–18 (1997).

150. Luksiene, Z. Photodynamic therapy: mechanism of action and ways to improve the efficiency of treatment. *Medicina (Kaunas).* **39,** 1137–50 (2003).

151. MacRobert AJ, Bown SG, Phillips D. What are the ideal photo properties for a sensitizer? In Bock G, Harnett S, editors. Photosensitizing compounds: their chemistry, biology and clinical use. Ciba Foundation Symposium; 2007. p. 146.

152. O'Riordan, K., Akilov, O. E. & Hasan, T. The potential for photodynamic therapy in the treatment of localized infections. *Photodiagnosis Photodyn. Ther.* **2,** 247–262 (2005).

153. Stenstrøm, A. G., Moan, J., Brunborg, G. & Eklund, T. Photodynamic inactivation of yeast cells sensitized by hematoporphyrin. *Photochem. Photobiol.* **32,** 349–52 (1980).

154. Wainwright, M., Byrne, M. N. & Gattrell, M. A. Phenothiazinium-based photobactericidal materials. *J. Photochem. Photobiol. B.* **84,** 227–30 (2006).

155. Takahashi, P. K., Toups, H. J., Greenberg, D. B., Dimopoullos, G. T. & Rusoff, L. L. Irradiation of Escherichia coli in the visible spectrum with a tunable organic-dye laser energy source. *Appl. Microbiol.* **29,** 63–7 (1975).

156. Jori, G., Galiazzo, G. & Scoffone, E. Photodynamic action of porphyrins on amino acids and proteins. I. Selective photooxidation of methionine in aqueous solution. *Biochemistry* **8,** 2868–2875 (1969).

157. Schäfer, M. *et al.* Systematic study of parameters influencing the action of Rose Bengal with visible light on bacterial cells: comparison between the biological effect and singlet-oxygen production. *Photochem. Photobiol.* **71,** 514–23 (2000).

158. Harris, F., Chatfield, L. K. & Phoenix, D. A. Phenothiazinium based photosensitisers--photodynamic agents with a multiplicity of cellular targets and clinical applications. *Curr. Drug Targets* **6,** 615–27 (2005).

159. Dougherty, T. J. *et al.* Photodynamic therapy. *J. Natl. Cancer Inst.* **90,** 889–905 (1998).

160. Hamblin, M. R. & Hasan, T. Photodynamic therapy: a new antimicrobial approach to infectious disease? *Photochem. Photobiol. Sci.* **3,** 436–50 (2004).

161. Huang, Z. A review of progress in clinical photodynamic therapy. *Technol. Cancer Res. Treat.* **4,** 283–93 (2005).

162. Naik, A. J. T., Ismail, S., Kay, C., Wilson, M. & Parkin, I. P. Antimicrobial activity of polyurethane embedded with methylene blue, toluidene blue and gold nanoparticles against Staphylococcus aureus; illuminated with white light. *Mater. Chem. Phys.* **129,** 446–450 (2011).

163. Perni, S. *et al.* Toluidine blue-containing polymers exhibit potent bactericidal activity when irradiated with red laser light. *J. Mater. Chem.* **19,** 2715 (2009).

164. Perni, S. *et al.* Antibacterial Activity of Light-Activated Silicone Containing Methylene Blue and Gold Nanoparticles of Different Sizes. *J. Clust. Sci.* **21,** 427–

438 (2010).

165. Perni, S. *et al.* The antimicrobial properties of light-activated polymers containing methylene blue and gold nanoparticles. *Biomaterials* **30,** 89–93 (2009).

166. Perni, S. *et al.* Antimicrobial properties of light-activated polyurethane containing indocyanine green. *J. Biomater. Appl.* **25,** 387–400 (2011).

167. Naik, A. J. T., Ismail, S., Kay, C., Wilson, M. & Parkin, I. P. Antimicrobial activity of polyurethane embedded with methylene blue, toluidene blue and gold nanoparticles against Staphylococcus aureus; illuminated with white light. *Mater. Chem. Phys.* **129,** 446–450 (2011).

168. Hamblin, M. R. & Hasan, T. Photodynamic therapy: a new antimicrobial approach to infectious disease? *Photochem. Photobiol. Sci.* **3,** 436–50 (2004).

169. Li, H. *et al.* A series of meso-tris(N-methyl-pyridiniumyl)-(4-alkylamidophenyl) porphyrins: Synthesis, interaction with DNA and antibacterial activity. *Biochim. Biophys. Acta - Gene Struct. Expr.* **1354,** 252–260 (1997).

170. Imray, F. P. & MacPhee, D. G. The role of DNA polymerase I and the rec system in survival of bacteria and bacteriophages damaged by the photodynamic action of acridine orange. *MGG Mol. Gen. Genet.* **123,** 289–298 (1973).

171. Schäfer, M., Schmitz, C. & Horneck, G. High sensitivity of Deinococcus radiodurans to photodynamically-produced singlet oxygen. *Int. J. Radiat. Biol.* **74,** 249–53 (1998).

172. Lauro, F. M., Pretto, P., Covolo, L., Jori, G. & Bertoloni, G. Photoinactivation of bacterial strains involved in periodontal diseases sensitized by porphycene–polylysine conjugates. *Photochem. Photobiol. Sci.* **1,** 468–470 (2002).

173. Pedigo, L. A., Gibbs, A. J., Scott, R. J. & Street, C. N. <title>Absence of bacterial resistance following repeat exposure to photodynamic therapy</title>. in *12th World Congress of the International Photodynamic Association* (ed. Kessel, D. H.)

73803H–73803H–7 (International Society for Optics and Photonics, 2009). doi:10.1117/12.822834

174. Costerton, J. W., Stewart, P. S. & Greenberg, E. P. Bacterial biofilms: a common cause of persistent infections. *Science* **284,** 1318–22 (1999).

175. Costerton, J. W., Lewandowski, Z., Caldwell, D. E., Korber, D. R. & Lappin-Scott, H. M. Microbial biofilms. *Annu. Rev. Microbiol.* **49,** 711–45 (1995).

176. Davies, D. Understanding biofilm resistance to antibacterial agents. *Nat. Rev. Drug Discov.* **2,** 114–22 (2003).

177. Costerton, J. W. *et al.* Bacterial biofilms in nature and disease. *Annu. Rev. Microbiol.* **41,** 435–64 (1987).

178. Hancock, R. E. W. & Speert, D. P. Antibiotic resistance in Pseudomonas aeruginosa: mechanisms and impact on treatment. *Drug Resist. Updat.* **3,** 247–255 (2000).

179. Anderson, R. L., Holland, B. W., Carr, J. K., Bond, W. W. & Favero, M. S. Effect of disinfectants on pseudomonads colonized on the interior surface of PVC pipes. *Am. J. Public Health* **80,** 17–21 (1990).

180. Boe-Hansen, R., Martiny, A. & Arvin, E. Monitoring biofilm formation and activity in drinking water distribution networks under oligotrophic conditions. **47,**

181. Donlan, R. & Costerton, J. Biofilms: Survival mechanisms of clinically relevant microorganisms. **15,**

182. Costerton, J. & Stewart, P. Battling biofilms - The war is against bacterial colonies that cause some of the most tenacious infections known. The weapon is knowledge of the enemy's communication system. *Sci. Am.* **285,** 74–81 (2001).

183. Chauhan, A. *et al.* Preventing biofilm formation and associated occlusion by biomimetic glycocalyxlike polymer in central venous catheters. *J. Infect. Dis.* **210,**

1347–56 (2014).

184.   Wu, D. *et al.* Substrate-anchored and degradation-sensitive anti-inflammatory coatings for implant materials. *Sci. Rep.* **5,** 11105 (2015).

185.   Chen, X. *et al.* Choline phosphate functionalized surface: protein-resistant but cell-adhesive zwitterionic surface potential for tissue engineering. *Chem. Commun. (Camb).* **51,** 487–90 (2015).

186.   The Direct Medical Costs of Healthcare-Associated Infections in U.S. Hospitals and the Benefits of Prevention - scott_costpaper.pdf. at <http://www.cdc.gov/hai/pdfs/hai/scott_costpaper.pdf>

187.   Designing surfaces that kill bacteria on contact. *Natl. Audit Off. Reducing Healthc. Assoc. Infect. Hosp. Engl.* (2009).

188.   Ivanova, E. P. *et al.* Natural bactericidal surfaces: mechanical rupture of Pseudomonas aeruginosa cells by cicada wings. *Small* **8,** 2489–94 (2012).

189.   Chuang, H. F., Smith, R. C. & Hammond, P. T. Polyelectrolyte multilayers for tunable release of antibiotics. **9,**

190.   Wu, P. & Grainger, D. W. Drug/device combinations for local drug therapies and infection prophylaxis. *Biomaterials* **27,** 2450–67 (2006).

191.   Zodrow, K. R., Schiffman, J. D. & Elimelech, M. Biodegradable polymer (PLGA) coatings featuring cinnamaldehyde and carvacrol mitigate biofilm formation. *Langmuir* **28,** 13993–9 (2012).

192.   Heinlaan, M., Ivask, A., Blinova, I., Dubourguier, H.-C. & Kahru, A. Toxicity of nanosized and bulk ZnO, CuO and TiO2 to bacteria Vibrio fischeri and crustaceans Daphnia magna and Thamnocephalus platyurus. *Chemosphere* **71,** 1308–16 (2008).

193.   Sapkota, A., Anceno, A. J., Baruah, S., Shipin, O. V & Dutta, J. Zinc oxide

nanorod mediated visible light photoinactivation of model microbes in water. *Nanotechnology* **22,** 215703 (2011).

194. Jones, N., Ray, B., Ranjit, K. T. & Manna, A. C. Antibacterial activity of ZnO nanoparticle suspensions on a broad spectrum of microorganisms. *FEMS Microbiol. Lett.* **279,** 71–6 (2008).

195. Banerjee, I., Pangule, R. C. & Kane, R. S. Antifouling coatings: recent developments in the design of surfaces that prevent fouling by proteins, bacteria, and marine organisms. *Adv. Mater.* **23,** 690–718 (2011).

196. Silver, S. Bacterial silver resistance: molecular biology and uses and misuses of silver compounds. *FEMS Microbiol. Rev.* **27,** 341–353 (2003).

197. Scardino, A. J. & de Nys, R. Mini review: Biomimetic models and bioinspired surfaces for fouling control. *Biofouling* **27,** 73–86 (2011).

198. Yoon, S. H., Rungraeng, N., Song, W. & Jun, S. Superhydrophobic and superhydrophilic nanocomposite coatings for preventing Escherichia coli K-12 adhesion on food contact surface. *J. Food Eng.* **131,** 135–141 (2014).

199. Hu, C. *et al.* Micro-/Nanometer Rough Structure of a Superhydrophobic Biodegradable Coating by Electrospraying for Initial Anti-Bioadhesion. *Adv. Healthc. Mater.* **2,** 1314–1321 (2013).

200. Zhang, X., Wang, L. & Levänen, E. Superhydrophobic surfaces for the reduction of bacterial adhesion. *RSC Adv.* **3,** 12003 (2013).

201. Shirtcliffe, N. J., McHale, G. & Newton, M. I. Wet adhesion and adhesive locomotion of snails on anti-adhesive non-wetting surfaces. *PLoS One* **7,** e36983 (2012).

202. Jin, C. *et al.* Cellulose-based material with amphiphobicity to inhibit bacterial adhesion by surface modification. *J. Mater. Chem.* **22,** 12562 (2012).

203. Roosjen, A., van der Mei, H. C., Busscher, H. J. & Norde, W. Microbial Adhesion to Poly(ethylene oxide) Brushes: Influence of Polymer Chain Length and Temperature. *Langmuir* **20,** 10949–10955 (2004).

204. Ostuni, E. *et al.* Self-Assembled Monolayers That Resist the Adsorption of Proteins and the Adhesion of Bacterial and Mammalian Cells. *Langmuir* **17,** 6336–6343 (2001).

205. Park, K. D. *et al.* Bacterial adhesion on PEG modified polyurethane surfaces. *Biomaterials* **19,** 851–859 (1998).

206. Kingshott, P., Wei, J., Bagge-Ravn, D., Gadegaard, N. & Gram, L. Covalent Attachment of Poly(ethylene glycol) to Surfaces, Critical for Reducing Bacterial Adhesion. *Langmuir* **19,** 6912–6921 (2003).

207. Kane, R. S., Deschatelets, P. & Whitesides, G. M. Kosmotropes Form the Basis of Protein-Resistant Surfaces. *Langmuir* **19,** 2388–2391 (2003).

208. Cheng, G., Xue, H., Zhang, Z., Chen, S. & Jiang, S. A Switchable Biocompatible Polymer Surface with Self-Sterilizing and Nonfouling Capabilities. *Angew. Chemie Int. Ed.* **47,** 8831–8834 (2008).

209. Att, W. *et al.* The effect of UV-photofunctionalization on the time-related bioactivity of titanium and chromium–cobalt alloys. *Biomaterials* **30,** 4268–4276 (2009).

210. Barthlott, W. & Neinhuis, C. Purity of the sacred lotus, or escape from contamination in biological surfaces. *Planta* **202,** 1–8 (1997).

211. Barthlott, W. & Neinhuis, C. Purity of the sacred lotus, or escape from contamination in biological surfaces. *Planta* **202,** 1–8 (1997).

212. Zhang, X., Liu, X., Laakso, J., Levänen, E. & Mäntylä, T. Easy-to-clean property and durability of superhydrophobic flaky γ-alumina coating on stainless steel in field test at a paper machine. *Appl. Surf. Sci.* **258,** 3102–3108 (2012).

213. Tang, P. *et al.* Effect of Superhydrophobic Surface of Titanium on *Staphylococcus aureus* Adhesion. *J. Nanomater.* **2011,** 1–8 (2011).

214. Privett, B. J. *et al.* Antibacterial fluorinated silica colloid superhydrophobic surfaces. *Langmuir* **27,** 9597–601 (2011).

215. Crick, C. R., Ismail, S., Pratten, J. & Parkin, I. P. An investigation into bacterial attachment to an elastomeric superhydrophobic surface prepared via aerosol assisted deposition. *Thin Solid Films* **519,** 3722–3727 (2011).

216. Freschauf, L. R., McLane, J., Sharma, H. & Khine, M. Shrink-induced superhydrophobic and antibacterial surfaces in consumer plastics. *PLoS One* **7,** e40987 (2012).

217. Fadeeva, E. *et al.* Bacterial Retention on Superhydrophobic Titanium Surfaces Fabricated by Femtosecond Laser Ablation. *Langmuir* **27,** 3012–3019 (2011).

218. Sousa, C. *et al.* Superhydrophobic poly(L-lactic acid) surface as potential bacterial colonization substrate. *AMB Express* **1,** 34 (2011).

219. Genzer, J. & Efimenko, K. Recent developments in superhydrophobic surfaces and their relevance to marine fouling: a review. *Biofouling* **22,** 339–60 (2006).

220. Berendjchi, A. *et al.* Fabrication of superhydrophobic and antibacterial surface on cotton fabric by doped silica-based sols with nanoparticles of copper. *Nanoscale Res. Lett.* **6,** 594 (2011).

221. Stallard, C. P., McDonnell, K. A., Onayemi, O. D., O'Gara, J. P. & Dowling, D. P. Evaluation of Protein Adsorption on Atmospheric Plasma Deposited Coatings Exhibiting Superhydrophilic to Superhydrophobic Properties. *Biointerphases* **7,** 1–12 (2012).

222. Roach, P., Shirtcliffe, N. J., Farrar, D. & Perry, C. C. Quantification of surface-bound proteins by fluorometric assay: Comparison with quartz crystal microbalance and amido black assay. *J. Phys. Chem. B* **110,** 20572–9 (2006).

223. Koc, Y. *et al.* Nano-scale superhydrophobicity: suppression of protein adsorption and promotion of flow-induced detachment. *Lab Chip* **8,** 582 (2008).

224. Pernites, R. B. *et al.* Tunable Protein and Bacterial Cell Adsorption on Colloidally Templated Superhydrophobic Polythiophene Films. *Chem. Mater.* **24,** 870–880 (2012).

225. Ling, X. *et al.* Superhydrophobic Modification of Hydroxyapatite Decreased in vitro Streptococcus mutans Adhesion and Calcium Dissolution.

226. Truong, V. K. *et al.* Air-directed attachment of coccoid bacteria to the surface of superhydrophobic lotus-like titanium. *Biofouling* **28,** 539–550 (2012).

227. Lafuma, A. & Quéré, D. Superhydrophobic states. *Nat. Mater.* **2,** 457–60 (2003).

228. Shafrin, E. G. & Zisman, W. A. CONSTITUTIVE RELATIONS IN THE WETTING OF LOW ENERGY SURFACES AND THE THEORY OF THE RETRACTION METHOD OF PREPARING MONOLAYERS [1]. *J. Phys. Chem.* **64,** 519–524 (1960).

229. Poetes, R., Holtzmann, K., Franze, K. & Steiner, U. Metastable Underwater Superhydrophobicity. *Phys. Rev. Lett.* **105,** 166104 (2010).

230. Moran, J. A. Pitcher Dimorphism, Prey Composition and the Mechanisms of Prey Attraction in the Pitcher Plant Nepenthes Rafflesiana in Borneo. *J. Ecol.* **84,** 515 (1996).

231. Bohn, H. F. & Federle, W. Insect aquaplaning: Nepenthes pitcher plants capture prey with the peristome, a fully wettable water-lubricated anisotropic surface. *Proc. Natl. Acad. Sci. U. S. A.* **101,** 14138–43 (2004).

232. Bauer, U. & Federle, W. The insect-trapping rim of Nepenthes pitchers. *Plant Signal. Behav.* **4,** 1019–1023 (2009).

233. Chen, H. *et al.* Continuous directional water transport on the peristome surface of

Nepenthes alata. *Nature* **532,** 85–9 (2016).

234. Wong, T.-S. *et al.* Bioinspired self-repairing slippery surfaces with pressure-stable omniphobicity. *Nature* **477,** 443–7 (2011).

235. Li, J. *et al.* Hydrophobic liquid-infused porous polymer surfaces for antibacterial applications. *ACS Appl. Mater. Interfaces* **5,** 6704–11 (2013).

236. Xiao, L. *et al.* Slippery liquid-infused porous surfaces showing marine antibiofouling properties. *ACS Appl. Mater. Interfaces* **5,** 10074–80 (2013).

237. Kim, P. *et al.* Liquid-infused nanostructured surfaces with extreme anti-ice and anti-frost performance. *ACS Nano* **6,** 6569–77 (2012).

238. Chen, J. *et al.* Robust Prototypical Anti-icing Coatings with a Self-lubricating Liquid Water Layer between Ice and Substrate. *ACS Appl. Mater. Interfaces* 130510105547001 (2013). doi:10.1021/am401004t

239. Epstein, A. K., Wong, T.-S., Belisle, R. A., Boggs, E. M. & Aizenberg, J. Liquid-infused structured surfaces with exceptional anti-biofouling performance. *Proc. Natl. Acad. Sci.* **109,** 13182–13187 (2012).

240. Anand, S., Paxson, A. T., Dhiman, R., Smith, J. D. & Varanasi, K. K. Enhanced Condensation on Lubricant-Impregnated Nanotextured Surfaces. *ACS Nano* **6,** 10122–10129 (2012).

241. Yao, X. *et al.* Adaptive fluid-infused porous films with tunable transparency and wettability. *Nat. Mater.* **12,** 529–534 (2013).

242. Wei, Q. *et al.* Supramolecular Polymers as Surface Coatings: Rapid Fabrication of Healable Superhydrophobic and Slippery Surfaces. *Adv. Mater.* **26,** 7358–7364 (2014).

243. Liu, H., Zhang, P., Liu, M., Wang, S. & Jiang, L. Organogel-based thin films for self-cleaning on various surfaces. *Adv. Mater.* **25,** 4477–81 (2013).

244. Epstein, A. K., Wong, T.-S., Belisle, R. A., Boggs, E. M. & Aizenberg, J. Liquid-infused structured surfaces with exceptional anti-biofouling performance. *Proc. Natl. Acad. Sci. U. S. A.* **109,** 13182–7 (2012).

245. Epstein, A. K., Wong, T.-S., Belisle, R. A., Boggs, E. M. & Aizenberg, J. Liquid-infused structured surfaces with exceptional anti-biofouling performance. *Proc. Natl. Acad. Sci. U. S. A.* **109,** 13182–7 (2012).

246. Vazquez JA (2006) The Emerging Problem of Infectious Diseases: The Impact of Antimicrobial Resistance in Wound Care. Wounds supplement November: 1-9. Available at: http://www.woundsresearch.com/files/docs/SN_WOUNDS_1106.pdf.

247. Taylor, P. W., Stapleton, P. D. & Paul Luzio, J. New ways to treat bacterial infections. *Drug Discov. Today* **7,** 1086–91 (2002).

248. Hwang, G. B., Allan, E. & Parkin, I. P. White light-activated antimicrobial paint using crystal violet. *ACS Appl. Mater. Interfaces* (2015). doi:10.1021/acsami.5b06927

249. Noimark, S. *et al.* Dual-Mechanism Antimicrobial Polymer-ZnO Nanoparticle and Crystal Violet-Encapsulated Silicone. *Adv. Funct. Mater.* **25,** 1367–1373 (2015).

250. Tanaka, Y. *et al.* Demonstration of a PDMS-based bio-microactuator using cultured cardiomyocytes to drive polymer micropillars. *Lab Chip* **6,** 230 (2006).

251. Park, K.-I. *et al.* Flexible nanocomposite generator made of $BaTiO_3$ nanoparticles and graphitic carbons. *Adv. Mater.* **24,** 2999–3004, 2937 (2012).

252. Lee, J. N., Park, C. & Whitesides, G. M. Solvent compatibility of poly(dimethylsiloxane)-based microfluidic devices. *Anal. Chem.* **75,** 6544–54 (2003).

253. No Title. *Natl. Biochem. Corp., Cryst. Violet., http//www.nationalbiochem.com/pdf/pis/MC3886%20PS.pdf, accessed 22 May*

2014

254. Seethapathy, S. & Górecki, T. Applications of polydimethylsiloxane in analytical chemistry: a review. *Anal. Chim. Acta* **750,** 48–62 (2012).

255. Perni, S. *et al.* The antimicrobial properties of light-activated polymers containing methylene blue and gold nanoparticles. *Biomaterials* **30,** 89–93 (2009).

256. Noimark, S. *et al.* Incorporation of methylene blue and nanogold into polyvinyl chloride catheters; a new approach for light-activated disinfection of surfaces. *J. Mater. Chem.* **22,** 15388 (2012).

257. Castano, A. P., Demidova, T. N. & Hamblin, M. R. Mechanisms in photodynamic therapy: part one-photosensitizers, photochemistry and cellular localization. *Photodiagnosis Photodyn. Ther.* **1,** 279–93 (2004).

258. Chatterjee, D. K., Fong, L. S. & Zhang, Y. Nanoparticles in photodynamic therapy: An emerging paradigm. *Adv. Drug Deliv. Rev.* **60,** 1627–1637 (2008).

259. Decraene, V., Pratten, J. & Wilson, M. Cellulose acetate containing toluidine blue and rose bengal is an effective antimicrobial coating when exposed to white light. *Appl. Environ. Microbiol.* **72,** 4436–9 (2006).

260. Noimark, S. *et al.* Photobactericidal polymers; the incorporation of crystal violet and nanogold into medical grade silicone. *RSC Adv.* **3,** 18383 (2013).

261. Noimark, S., Allan, E. & Parkin, I. P. Light-activated antimicrobial surfaces with enhanced efficacy induced by a dark-activated mechanism. *Chem. Sci.* **5,** 2216 (2014).

262. Noimark, S. *et al.* Incorporation of methylene blue and nanogold into polyvinyl chloride catheters; a new approach for light-activated disinfection of surfaces. *J. Mater. Chem.* **22,** 15388 (2012).

263. Komerik, N. & Wilson, M. Factors influencing the susceptibility of Gram-negative

bacteria to toluidine blue O-mediated lethal photosensitization. *J. Appl. Microbiol.* **92,** 618–623 (2002).

264. Souza, R. C. *et al.* Comparison of the photodynamic fungicidal efficacy of methylene blue, toluidine blue, malachite green and low-power laser irradiation alone against Candida albicans. *Lasers Med. Sci.* **25,** 385–389 (2010).

265. Naik, A. J. T., Ismail, S., Kay, C., Wilson, M. & Parkin, I. P. Antimicrobial activity of polyurethane embedded with methylene blue, toluidene blue and gold nanoparticles against Staphylococcus aureus; illuminated with white light. *Mater. Chem. Phys.* **129,** 446–450 (2011).

266. Noimark, S. *et al.* Photobactericidal polymers; the incorporation of crystal violet and nanogold into medical grade silicone. *RSC Adv.* **3,** 18383 (2013).

267. Sehmi, S. K. *et al.* Lethal photosensitisation of Staphylococcus aureus and Escherichia coli using crystal violet and zinc oxide-encapsulated polyurethane. *J. Mater. Chem. B* **3,** 6490–6500 (2015).

268. Sehmi, S. K. *et al.* Enhancing the Antibacterial Activity of Light-Activated Surfaces Containing Crystal Violet and ZnO Nanoparticles: Investigation of Nanoparticle Size, Capping Ligand, and Dopants. *ACS omega* **1,** 334–343 (2016).

269. Brock Biology of Microorganisms. *CIBSE, Chart. Inst. Build. Serv. Eng. Light. Guid. LG2 Hosp. Healthc. Build. Chart. Inst. Build. Serv. Eng. London, United Kingdom., 1989.*

270. Dunnill, C. W. *et al.* Nanoparticulate silver coated-titania thin films—Photo-oxidative destruction of stearic acid under different light sources and antimicrobial effects under hospital lighting conditions. *J. Photochem. Photobiol. A Chem.* **220,** 113–123 (2011).

271. Gong, P. *et al.* Preparation and antibacterial activity of Fe 3 O 4 @Ag nanoparticles. *Nanotechnology* **18,** 285604 (2007).

272. Raghupathi, K. R., Koodali, R. T. & Manna, A. C. Size-Dependent Bacterial Growth Inhibition and Mechanism of Antibacterial Activity of Zinc Oxide Nanoparticles. *Langmuir* **27,** 4020–4028 (2011).

273. and, N. L. R. & Mirkin*, C. A. Nanostructures in Biodiagnostics. (2005). doi:10.1021/CR030067F

274. Raghupathi, K. R., Koodali, R. T. & Manna, A. C. Size-Dependent Bacterial Growth Inhibition and Mechanism of Antibacterial Activity of Zinc Oxide Nanoparticles. *Langmuir* **27,** 4020–4028 (2011).

275. Applerot, G. *et al.* Enhanced Antibacterial Activity of Nanocrystalline ZnO Due to Increased ROS-Mediated Cell Injury. *Adv. Funct. Mater.* **19,** 842–852 (2009).

276. Li, M., Zhu, L. & Lin, D. Toxicity of ZnO nanoparticles to Escherichia coli: mechanism and the influence of medium components. *Environ. Sci. Technol.* **45,** 1977–83 (2011).

277. Brayner, R. *et al.* Toxicological impact studies based on Escherichia coli bacteria in ultrafine ZnO nanoparticles colloidal medium. *Nano Lett.* **6,** 866–70 (2006).

278. Li, Y., Niu, J., Zhang, W., Zhang, L. & Shang, E. Influence of aqueous media on the ROS-mediated toxicity of ZnO nanoparticles toward green fluorescent protein-expressing Escherichia coli under UV-365 irradiation. *Langmuir* **30,** 2852–62 (2014).

279. Li, Y., Zhang, W., Niu, J. & Chen, Y. Mechanism of photogenerated reactive oxygen species and correlation with the antibacterial properties of engineered metal-oxide nanoparticles. *ACS Nano* **6,** 5164–73 (2012).

280. Tam, K. H. *et al.* Antibacterial activity of ZnO nanorods prepared by a hydrothermal method. *Thin Solid Films* **516,** 6167–6174 (2008).

281. Kitching, H. *et al.* The interaction of gold and silver nanoparticles with a range of anionic and cationic dyes. *Phys. Chem. Chem. Phys.* **16,** 6050 (2014).

282. Sehmi, S. K. *et al.* Potent Antibacterial Activity of Copper Embedded into Silicone and Polyurethane. *ACS Appl. Mater. Interfaces* **7,** 22807–22813 (2015).

283. Li, Q. *et al.* Antimicrobial nanomaterials for water disinfection and microbial control: potential applications and implications. *Water Res.* **42,** 4591–602 (2008).

284. Hirota, K. *et al.* Preparation of zinc oxide ceramics with a sustainable antibacterial activity under dark conditions. *Ceram. Int.* **36,** 497–506 (2010).

285. Joshi, P. *et al.* Role of surface adsorbed anionic species in antibacterial activity of ZnO quantum dots against Escherichia coli. *J. Nanosci. Nanotechnol.* **9,** 6427–33 (2009).

286. Sawai, J. & Yoshikawa, T. Quantitative evaluation of antifungal activity of metallic oxide powders (MgO, CaO and ZnO) by an indirect conductimetric assay. *J. Appl. Microbiol.* **96,** 803–9 (2004).

287. Premanathan, M., Karthikeyan, K., Jeyasubramanian, K. & Manivannan, G. Selective toxicity of ZnO nanoparticles toward Gram-positive bacteria and cancer cells by apoptosis through lipid peroxidation. *Nanomedicine* **7,** 184–92 (2011).

288. Li, M. *et al.* Stability, bioavailability, and bacterial toxicity of ZnO and iron-doped ZnO nanoparticles in aquatic media. *Environ. Sci. Technol.* **45,** 755–61 (2011).

289. Jones, N., Ray, B., Ranjit, K. T. & Manna, A. C. Antibacterial activity of ZnO nanoparticle suspensions on a broad spectrum of microorganisms. *FEMS Microbiol. Lett.* **279,** 71–6 (2008).

290. Yin, H., Casey, P. S., McCall, M. J. & Fenech, M. Effects of surface chemistry on cytotoxicity, genotoxicity, and the generation of reactive oxygen species induced by ZnO nanoparticles. *Langmuir* **26,** 15399–408 (2010).

291. Perelshtein, I. *et al.* Antibacterial properties of an in situ generated and simultaneously deposited nanocrystalline ZnO on fabrics. *ACS Appl. Mater. Interfaces* **1,** 361–6 (2009).

292. Lakshmi Prasanna, V. & Vijayaraghavan, R. Insight into the Mechanism of Antibacterial Activity of ZnO: Surface Defects Mediated Reactive Oxygen Species Even in the Dark. *Langmuir* **31,** 9155–62 (2015).

293. Gracanin, M., Hawkins, C. L., Pattison, D. I. & Davies, M. J. Singlet-oxygen-mediated amino acid and protein oxidation: formation of tryptophan peroxides and decomposition products. *Free Radic. Biol. Med.* **47,** 92–102 (2009).

294. Kohanski, M. A., Dwyer, D. J., Hayete, B., Lawrence, C. A. & Collins, J. J. A common mechanism of cellular death induced by bactericidal antibiotics. *Cell* **130,** 797–810 (2007).

295. Sehmi, S. K. *et al.* Lethal photosensitisation of Staphylococcus aureus and Escherichia coli using crystal violet and zinc oxide-encapsulated polyurethane. *J. Mater. Chem. B* **3,** 6490–6500 (2015).

296. Kawamoto, K. *et al.* Antibacterial Effect of Yellow He-Ne Laser Irradiation with Crystal Violet Solution on Porphyromonas gingivalis: An Evaluation Using Experimental Rat Model Involving Subcutaneous Abscess. *Lasers Med. Sci.* **15,** 257–262 (2000).

297. Saji, M. *et al.* Efficacy of gentian violet in the eradication of methicillin-resistant Staphylococcus aureus from skin lesions. *J. Hosp. Infect.* **31,** 225–228 (1995).

298. Hong, T.-K. *et al.* A comprehensive in vitro and in vivo study of ZnO nanoparticles toxicity. *J. Mater. Chem. B* **1,** 2985 (2013).

299. Reddy, K. M. *et al.* Selective toxicity of zinc oxide nanoparticles to prokaryotic and eukaryotic systems. *Appl. Phys. Lett.* **90,** 2139021–2139023 (2007).

300. Joshi, S. G. *et al.* Control of methicillin-resistant Staphylococcus aureus in planktonic form and biofilms: a biocidal efficacy study of nonthermal dielectric-barrier discharge plasma. *Am. J. Infect. Control* **38,** 293–301 (2010).

301. Olson, M. E., Ceri, H., Morck, D. W., Buret, A. G. & Read, R. R. Biofilm bacteria:

formation and comparative susceptibility to antibiotics. *Can. J. Vet. Res. = Rev. Can. Rech. vétérinaire* **66,** 86–92 (2002).

302. Bazaka, K., Jacob, M. V, Crawford, R. J. & Ivanova, E. P. Efficient surface modification of biomaterial to prevent biofilm formation and the attachment of microorganisms. *Appl. Microbiol. Biotechnol.* **95,** 299–311 (2012).

303. Arciola, C. R., Campoccia, D., Speziale, P., Montanaro, L. & Costerton, J. W. Biofilm formation in Staphylococcus implant infections. A review of molecular mechanisms and implications for biofilm-resistant materials. *Biomaterials* **33,** 5967–82 (2012).

304. Salwiczek, M. *et al.* Emerging rules for effective antimicrobial coatings. *Trends Biotechnol.* **32,** 82–90 (2014).

305. Magin, C. M., Cooper, S. P. & Brennan, A. B. Non-toxic antifouling strategies. *Mater. Today* **13,** 36–44 (2010).

306. Majumdar, P., Stafslien, S., Daniels, J. & Webster, D. C. High throughput combinatorial characterization of thermosetting siloxane–urethane coatings having spontaneously formed microtopographical surfaces. *J. Coatings Technol. Res.* **4,** 131–138 (2007).

307. Genzer, J. & Efimenko, K. Recent developments in superhydrophobic surfaces and their relevance to marine fouling: a review. *Biofouling* **22,** 339–60 (2006).

308. Feng, L. *et al.* Super-Hydrophobic Surfaces: From Natural to Artificial. *Adv. Mater.* **14,** 1857–1860 (2002).

309. Arima, Y. & Iwata, H. Effect of wettability and surface functional groups on protein adsorption and cell adhesion using well-defined mixed self-assembled monolayers. *Biomaterials* **28,** 3074–82 (2007).

310. Wu, H.-Q., Wei, X.-W., Shao, M.-W., Gu, J.-S. & Qu, M.-Z. Synthesis of copper oxide nanoparticles using carbon nanotubes as templates. *Chem. Phys. Lett.* **364,**

155

152–156 (2002).

311. Jia, B., Mei, Y., Cheng, L., Zhou, J. & Zhang, L. Preparation of copper nanoparticles coated cellulose films with antibacterial properties through one-step reduction. *ACS Appl. Mater. Interfaces* **4,** 2897–902 (2012).

312. Klein, T. Y., Wehling, J., Treccani, L. & Rezwan, K. Effective bacterial inactivation and removal of copper by porous ceramics with high surface area. *Environ. Sci. Technol.* **47,** 1065–72 (2013).

313. Harrison, J. J., Ceri, H., Stremick, C. A. & Turner, R. J. Biofilm susceptibility to metal toxicity. *Environ. Microbiol.* **6,** 1220–7 (2004).

314. Ruparelia, J. P., Chatterjee, A. K., Duttagupta, S. P. & Mukherji, S. Strain specificity in antimicrobial activity of silver and copper nanoparticles. *Acta Biomater.* **4,** 707–16 (2008).

315. Hassan, I. A., Parkin, I. P., Nair, S. P. & Carmalt, C. J. Antimicrobial activity of copper and copper(i) oxide thin films deposited via aerosol-assisted CVD. *J. Mater. Chem. B* **2,** 2855 (2014).

316. Decraene, V., Pratten, J. & Wilson, M. Cellulose acetate containing toluidine blue and rose bengal is an effective antimicrobial coating when exposed to white light. *Appl. Environ. Microbiol.* **72,** 4436–9 (2006).

317. Dunnill, C. W. *et al.* Nanoparticulate silver coated-titania thin films—Photo-oxidative destruction of stearic acid under different light sources and antimicrobial effects under hospital lighting conditions. *J. Photochem. Photobiol. A Chem.* **220,** 113–123 (2011).

318. Moniz, S. J. A. *et al.* MOCVD of crystalline Bi2O3 thin films using a single-source bismuth alkoxide precursor and their use in photodegradation of water. *J. Mater. Chem.* **20,** 7881 (2010).

319. Blackman, C. S. *et al.* Single-source CVD routes to titanium phosphide. *J. Chem.*

Soc. Dalt. Trans. **4,** 2702–2709 (2002).

320. Choy, K. L. Chemical vapour deposition of coatings. *Prog. Mater. Sci.* **48,** 57–170 (2003).

321. Marchand, P., Hassan, I. A., Parkin, I. P. & Carmalt, C. J. Aerosol-assisted delivery of precursors for chemical vapour deposition: expanding the scope of CVD for materials fabrication. *Dalton Trans.* **42,** 9406–22 (2013).

322. Xiong, J., Wang, Y., Xue, Q. & Wu, X. Synthesis of highly stable dispersions of nanosized copper particles using l-ascorbic acid. *Green Chem.* **13,** 900 (2011).

323. Izuka, A., Winter, H. H. & Hashimoto, T. Molecular weight dependence of viscoelasticity of polycaprolactone critical gels. *Macromolecules* **25,** 2422–2428 (1992).

324. Macomber, L., Rensing, C. & Imlay, J. A. Intracellular copper does not catalyze the formation of oxidative DNA damage in Escherichia coli. *J. Bacteriol.* **189,** 1616–26 (2007).

325. Shi, M., Kwon, H. S., Peng, Z., Elder, A. & Yang, H. Effects of surface chemistry on the generation of reactive oxygen species by copper nanoparticles. *ACS Nano* **6,** 2157–64 (2012).

326. Gunawan, C., Teoh, W. Y., Marquis, C. P. & Amal, R. Cytotoxic origin of copper(II) oxide nanoparticles: comparative studies with micron-sized particles, leachate, and metal salts. *ACS Nano* **5,** 7214–25 (2011).

327. Espírito Santo, C. *et al.* Bacterial killing by dry metallic copper surfaces. *Appl. Environ. Microbiol.* **77,** 794–802 (2011).

328. Molteni, C., Abicht, H. K. & Solioz, M. Killing of bacteria by copper surfaces involves dissolved copper. *Appl. Environ. Microbiol.* **76,** 4099–101 (2010).

329. Wenzel, R. Resistance of solid surfaces to wetting by water. **28,** 988–994 (1936).

330. Zhang, X., Shi, F., Niu, J., Jiang, Y. & Wang, Z. Superhydrophobic surfaces: from structural control to functional application. *J. Mater. Chem.* **18,** 621 (2008).

331. Ostuni, E., Chen, C. & Ingber, D. Selective deposition of proteins and cells in arrays of microwells. **17,** 2828–2834 (2001).

332. Song, W., Gaware, V. S. & Runarsson, O. V. Functionalized superhydrophobic biomimetic chitosan-based films. **81,** 140–144 (2010).

333. Antimicrobial Activity in Thin Films of Pseudobrookite-Structured Titanium Oxynitride under UV Irradiation Observed for Escherichia coli. *ASTM Ann. B. ASTM Stand.*

334. Yamada, T. *et al.* A stretchable carbon nanotube strain sensor for human-motion detection. *Nat. Nanotechnol.* **6,** 296–301 (2011).

335. Lu, Y. *et al.* Robust self-cleaning surfaces that function when exposed to either air or oil. *Science (80-.).* **347,** (2015).

336. Wang, P. *et al.* Transparent and abrasion-resistant superhydrophobic coating with robust self-cleaning function in either air or oil. *J. Mater. Chem. A* **4,** 7869–7874 (2016).

337. Zhou, H. *et al.* Fluoroalkyl Silane Modified Silicone Rubber/Nanoparticle Composite: A Super Durable, Robust Superhydrophobic Fabric Coating. *Adv. Mater.* **24,** 2409–2412 (2012).

338. Chen, K., Zhou, S. & Wu, L. Self-Healing Underwater Superoleophobic and Antibiofouling Coatings Based on the Assembly of Hierarchical Microgel Spheres. *ACS Nano* **10,** 1386–1394 (2016).

339. Puretskiy, N., Chanda, J., Stoychev, G., Synytska, A. & Ionov, L. Anti-Icing Superhydrophobic Surfaces Based on Core-Shell Fossil Particles. *Adv. Mater. Interfaces* **2,** 1500124 (2015).

340. Zhang, J. & Seeger, S. Polyester Materials with Superwetting Silicone Nanofilaments for Oil/Water Separation and Selective Oil Absorption. *Adv. Funct. Mater.* **21,** 4699–4704 (2011).

341. Ellinas, K. *et al.* Superamphiphobic polymeric surfaces sustaining ultrahigh impact pressures of aqueous high- and low-surface-tension mixtures, tested with laser-induced forward transfer of drops. *Adv. Mater.* **27,** 2231–5 (2015).

342. Callow, J. A., Callow, M. E. & Callow, M. E. Trends in the development of environmentally friendly fouling-resistant marine coatings. *Nat. Commun.* **2,** 244 (2011).

343. Rosenhahn, A., Ederth, T., Pettitt, M. E. & Pettitt, M. E. Advanced nanostructures for the control of biofouling: The FP6 EU Integrated Project AMBIO. *Biointerphases* **3,** IR1-5 (2008).

344. Leslie, D. C. *et al.* A bioinspired omniphobic surface coating on medical devices prevents thrombosis and biofouling. *Nat. Biotechnol.* **32,** 1134–1140 (2014).

345. Cheng, M., Song, M., Dong, H. & Shi, F. Surface Adhesive Forces: A Metric Describing the Drag-Reducing Effects of Superhydrophobic Coatings. *Small* **11,** 1665–1671 (2015).

346. Boinovich, L., Emelyanenko, A. M. & Pashinin, A. S. Analysis of Long-Term Durability of Superhydrophobic Properties under Continuous Contact with Water. *ACS Appl. Mater. Interfaces* **2,** 1754–1758 (2010).

347. Cassie, A. B. D. & Baxter, S. Wettability of porous surfaces. *Trans. Faraday Soc.* **40,** 546 (1944).

348. Vogel, N., Belisle, R. A., Hatton, B., Wong, T.-S. & Aizenberg, J. Transparency and damage tolerance of patternable omniphobic lubricated surfaces based on inverse colloidal monolayers. *Nat. Commun.* **4,** 988–994 (2013).

349. Rousseau, A. F. *et al.* Microstructural and tribological characterisation of a

nitriding/TiAlN PVD coating duplex treatment applied to M2 High Speed Steel tools. *Surf. Coatings Technol.* **272,** 403–408 (2015).

350. Chen, Q. & Thouas, G. A. Metallic implant biomaterials. *Mater. Sci. Eng. R Reports* **87,** 1–57 (2015).

351. Su, C. *et al.* The abrasion resistance of a superhydrophobic surface comprised of polyurethane elastomer. *Soft Matter* **6,** 6068 (2010).

352. Nilsson, M. A., Daniello, R. J. & Rothstein, J. P. A novel and inexpensive technique for creating superhydrophobic surfaces using Teflon and sandpaper. *J. Phys. D. Appl. Phys.* **43,** 45301 (2010).

353. Lichter, J. A., Van Vliet, K. J. & Rubner, M. F. Design of Antibacterial Surfaces and Interfaces: Polyelectrolyte Multilayers as a Multifunctional Platform. *Macromolecules* **42,** 8573–8586 (2009).

354. Campoccia, D., Montanaro, L. & Arciola, C. R. The significance of infection related to orthopedic devices and issues of antibiotic resistance. *Biomaterials* **27,** 2331–2339 (2006).

355. Hochbaum, A. I. & Aizenberg, J. Bacteria Pattern Spontaneously on Periodic Nanostructure Arrays. *Nano Lett.* **10,** 3717–3721 (2010).

356. Laupland, K. B., Gregson, D. B., Church, D. L., Ross, T. & Pitout, J. D. D. Incidence, risk factors and outcomes of Escherichia coli bloodstream infections in a large Canadian region. *Clin. Microbiol. Infect.* **14,** 1041–7 (2008).

357. Tsai, Y.-P. Impact of flow velocity on the dynamic behaviour of biofilm bacteria. *Biofouling* **21,** 267–277 (2005).

358. Purevdorj, B., Costerton, J. W. & Stoodley, P. Influence of hydrodynamics and cell signaling on the structure and behavior of Pseudomonas aeruginosa biofilms. *Appl. Environ. Microbiol.* **68,** 4457–64 (2002).

359. O'Toole, G. A. & Kolter, R. Flagellar and twitching motility are necessary for Pseudomonas aeruginosa biofilm development. *Mol. Microbiol.* **30,** 295–304 (1998).

360. Gibiansky, M. L. *et al.* Bacteria Use Type IV Pili to Walk Upright and Detach from Surfaces. *Science (80-.).* **330,** 197–197 (2010).

361. Busscher, H. J. & Mei, H. C. van der. How Do Bacteria Know They Are on a Surface and Regulate Their Response to an Adhering State? *PLoS Pathog.* **8,** (2012).

362. Xue, C.-H., Bai, X., Jia, S.-T., Zhou, F. & Xue, Q. Robust, Self-Healing Superhydrophobic Fabrics Prepared by One-Step Coating of PDMS and Octadecylamine. *Sci. Rep.* **6,** 27262 (2016).

363. MacCallum, N. *et al.* Liquid-Infused Silicone As a Biofouling-Free Medical Material. *ACS Biomater. Sci. Eng.* **1,** 43–51 (2015).

364. Xiao, L. *et al.* Slippery Liquid-Infused Porous Surfaces Showing Marine Antibiofouling Properties. *ACS Appl. Mater. Interfaces* **5,** 10074–10080 (2013).